Tampere University

Roman Chalabov

OPERATION OF STATCOM CONNECTED TO A WEAK GRID

Faculty of Information Technology
and Communication Sciences
Master of Science Thesis
September 2019

ABSTRACT

Roman Chalabov: Operation of STATCOM connected to a weak grid
Master of Science Thesis, 83 pages
Tampere University
Master's Degree Programme in Electrical Engineering
September 2019

The purpose of this thesis was to investigate the operational possibility of MMC STATCOM in weak grid conditions. Weak grid is a power system which has low short circuit capacity, high equivalent grid impedance, high dV/dQ sensitivity and higher volatility to voltage instability. Hence integration of power electronics based equipment due to their fast response is a big challenge in weak grid. Interaction with high grid impedance of weak grid leads to loss of synchronization and consequently unstable operation of VSC connected to weak grid.

In this thesis first, the effects of high grid impedance on the PLL synchronization was investigated. It was observed that high grid impedance has high impact on PLL dynamics and introduces self-synchronization. However, it was noticed that the PLL remains stable if there is no power exchange between grid and VSC. Therefore, STATCOM performance is not deteriorated by the weak grid conditions. STATCOM model connected to weak grid was simulated in Matlab/Simulink environment to study the impact of the weak grid on STATCOM control system.

Initially STATCOM was simulated as a constant current source to investigate the factors that impacts STATCOM stability. It was found that STATCOM operation in weak and very weak grid conditions is limited due to some factors that affects STATCOM stability. In capacitive mode the amount of the DC link voltage is main limiting factor and insufficient amount of DC link voltage results in the harmonic injection by STATCOM. In inductive mode high reactive power absorption results in high frequency oscillations in grid voltage which leads to loss of synchronization. Making PLL slower improves the synchronization with the grid; however, this modification deteriorates the DC link voltage performance which requires DC link voltage controller retuning.

Second, STATCOM was simulated in the voltage regulation mode and it was noticed that STATCOM operation introduces high frequency ripple to grid voltage. The ripple frequency changes with the grid strengths and at very low short circuit levels system becomes unstable. To improve the system stability a notch filter tuned to the ripple frequency was added. Notch filter significantly improved STATCOM performance and extended the operational limits of STATCOM. However, it was noticed that at some short circuit levels resonance happens and in inductive mode high inductive current absorption makes system unstable. Further elaborations showed that interaction with the HF filter cause the system instability and reduction of the HF filter rating improves the system stability.

Finally, STATCOM performance was tested under symmetrical and asymmetrical fault conditions. In case of asymmetrical fault due to unbalanced grid voltages part of the current is used to balance DC link voltage waveforms and the output current of the STATCOM was reduced.

Keywords: FACTS, MMC, PLL, reactive power compensation, STATCOM, synchronization, VSC, weak grid

PREFACE

This thesis work was carried out at GE Grid Solutions Oy between November 2018 and June 2019

I want to express my deepest gratitude to Dr Anssi Mäkinen for offering me this thesis position and supervising me throughout the thesis period. I would like to thank Adjunct Professor Tuomas Messo for his assistance, guidance and help during the final stages of the thesis and helped me to finish thesis on time. Also, I would like to thank MSc Järi Lavapuro and MSc Juha Hälli for helping me with Matlab simulations.

I would like to thank Professor Sami Repo and Dr Tuomas Rauhala for examining my thesis. Also, I am thankful to Dr Jenni Rekola for her recommendations, support and mentorship during my studies at university.

Finally, I am very grateful to my parents for their love and support throughout my life.

Tampere, 6 September 2019

Roman Chalabov

CONTENTS

LIST OF SYMBOLS AND ABBREVIATIONS

AC	Alternative Current
CHB	Cascaded H-bridge
DC	Direct Current
DCC	Diode Clamped Converter
DDSRF	Double Decoupled SRF
DS-FB	Double-Star Full-Bridge
DS-HB	Double-Star Half-Bridge
FACTS	Flexible AC Transmission System
FCC	Flying Capacitor Converter
HF	High Frequency
HVDC	High Voltage DC
IEA	International Energy Agency
IGBT	Insulated Gate Bipolar Transistor
MMC	Modular Multilevel Converter
NLM	Nearest Level Modulation
NL-PWM	Nearest Level PWM
NPCC	Neutral Point Clamped Converter
PCC	Point of Common Coupling
PED	Power Electronic Device
PI	Proportional Integral
PLL	Phase Locked Loop
PR	Proportional Resonant
pu	Per Unit
PWM	Pulse Width Modulation
SCC	Short Circuit Capacity
SCL	Short Circuit Level
SCR	Short Circuit Ratio
SD-CHB	Single-Delta CHB
SRF	Synchronous Reference Frame
SS-CHB	Single-Star CHB
SVC	Static Var Compensator
STATCOM	STATic synchronous COMpensator
VR	Voltage Regulation
VSC	Voltage Source Converter
ZSCI	Zero Sequence Current Injection

C_{dc}	Submodule capacitance
i_a	Instantaneous line current phase a
i_{ab}	Instantaneous phase current between phases a and b
i_b	Instantaneous line current phase b
i_{bc}	Instantaneous phase current between phases b and c
i_c	Instantaneous line current phase c
$\boldsymbol{I}_c$	Converter current vector
i_{ca}	Instantaneous phase current between phases c and a
i_{cd}^*	d-component of converter current reference value
i_{cq}^*	q-component of converter current reference value
$\vec{I}_{st}$	STATCOM current RMS value
i_{Yd}	Instantaneous line current d-component
i_{Yq}	Instantaneous line current q-component
$i_{\Delta d}$	Instantaneous phase current d-component
$i_{\Delta q}$	Instantaneous phase current q-component

$\hat{I}$	RMS magnitude of phase current
k	Safety factor coefficient
k_{ipcc}	Integral gain of voltage controller
k_{ilf}	Integral gain of loop filter
k_{pdc}	Proportional gain of DC voltage controller
k_{pi}	Proportional gain of current controller
k_{plf}	Proportional gain of loop filter
k_{ri}	Resonant gain of current controller
L_f	Filter reactor inductance
L_g	Grid inductance
L_l	Line equivalent inductance
m	Modulation index
m_c	Single submodule modulation signal
m_d	Modulation signal d-component
m_q	Modulation signal q-component
n	Number of submodules per phase
P	Active power
p_{ac}	STATCOM AC side instantaneous active power
p_{dc}	STATCOM DC side instantaneous active power
p_{loss}	Instantaneous active power loss between AC and DC
Q	Reactive power
R_{dc}	Capacitor equivalent parasitic resistance
R_f	Filter reactor equivalent parasitic resistance
R_g	Grid resistance
R_l	Line equivalent resistance
s	Laplace transform variable
s_c	Converter switching function
S	Apparent power
S_{SC}	Short circuit capacity
Superscript “0”	Refers to zero sequence component
Superscript “+”	Refers to positive sequence component
Superscript “−”	Refers to negative sequence component
Superscript “a”	Denotes phase a
Superscript “b”	Denotes phase b
Superscript “c”	Denotes phase c
Superscript “$*$”	Reference value for a parameter
t	Time
V	Voltage magnitude
V_{dc}	Total DC link voltage
V_{DES}	Desired VSC output voltage
v_{dc}	Submodule capacitor voltage
v_{ga}	Instantaneous grid voltage phase a
$\boldsymbol{V}_g$	Grid voltage vector
$\boldsymbol{v}_{dq}$	Voltage vector in synchronous reference frame
v_{gd}	d-component of grid phase voltage
v_{gq}	q-component of grid phase voltage
v_{PCCa}	Instantaneous voltage at PCC phase a
v_{PCCab}	Instantaneous voltage at PCC between phases a and b
v_{PCCbc}	Instantaneous voltage at PCC between phases b and c
v_{PCCb}	Instantaneous voltage at PCC phase b
v_{PCCca}	Instantaneous voltage at PCC between phases c and a
v_{PCCc}	Instantaneous voltage at PCC phase c

$v_{PCC\Delta}$	Amplitude of instantaneous PCC phase to phase voltage
V_S	Source voltage
$\boldsymbol{V}_t$	Terminal voltage vector
V_{tq}^c	PLL sensed terminal voltage
V_{VSC}	VSC output voltage
$\hat{V}$	RMS magnitude of STATCOM voltage
$\overline{v}_{dc}$	Average submodule capacitor voltage
$\vec{V}_{gr}$	Grid voltage RMS value
$\vec{V}_{st}$	STATCOM voltage RMS value
v_{Yd}	d-component of PCC phase voltage
v_{Yq}	q-component of PCC phase voltage
$\boldsymbol{v}_{\alpha\beta}$	Voltage vector in stationary reference frame
$v_{\Delta d}$	d-component of PCC phase to phase voltage
$v_{\Delta q}$	q-component of PCC phase to phase voltage
X_{tr}	Transmission line reactance
Z_g	Grid impedance
Z_{th}	Thevenin equivalent impedance
α_{dc}	DC voltage controller bandwidth
α_i	Current controller bandwidth
α_f	Low pass filter bandwidth
α_{PR}	PR controller bandwidth
α_{pcc}	Voltage controller bandwidth
α_{pll}	PLL bandwidth
α_0	Zero sequence current phase angle
δ	Phase difference between grid voltage and STATCOM voltage
δ_i	STATCOM current phase angle
φ	Voltage initial phase angle
θ	Grid voltage angle
θ_g	Grid voltage angle
θ_{pll}	PLL measured angle
θ_v	STATCOM voltage phase angle
$\hat{\theta}$	PLL estimated grid angle
ω	Angular frequency
ω_0	Grid angular frequency
ω_1	Fundamental angular frequency
ω_{pll}	PLL angular frequency

1. INTRODUCTION

1.1 Power system in future

Electrical power transmission system introduced more than a century ago is currently undergoing tremendous change due to growing penetration of renewables and increasing demand for electricity. Transmission systems needs to be more flexible to be able to provide secure system operation and high reliability of supply of electricity.

The International Energy Agency (IEA) expects that by 2030 global electricity production will be more than 33 000 TWh [1]. The environmental concerns and feasibility of the new technologies shift the traditional electricity generation from fossil fuels towards renewable energy resources. The share of renewables in electricity production will rise from current 18.2% in 2016 to 35% in 2030, and the primary energy sources for the new renewable generation will be solar and wind [1][2]. Therefore, the power system in the future will have reduced share of fossil fuel and nuclear power plants with high and steady power generation capacity, and increased number of the renewable generation stations installed in remote locations and have volatile power generation capacity. The intermittent power generation, weak and aging grids, as well as little space for building new installations are limiting transmission system development. The application of High Voltage DC (HVDC) and Flexible AC Transmission Systems (FACTS) can improve the voltage support and capabilities of the existing transmission systems to a large extent.

1.2 Overview of shunt FACTS Devices

Recent developments in power electronic devices made FACTS more feasible and achievable for transmission system improvement [3][4], and the role of FACTS will be significant in the future power systems [3][5][6].

Figure 1 shows FACTS devices based on power electronics devices utilized and connection configuration. Shunt connected FACTS devices are the most common in the current market [6]. There are two types of shunt connected FACTS Device: Static Var Compensator (SVC) based on thyristor-based technology and Static Synchronous Compensator (STATCOM) based on Voltage Source Converter (VSC).

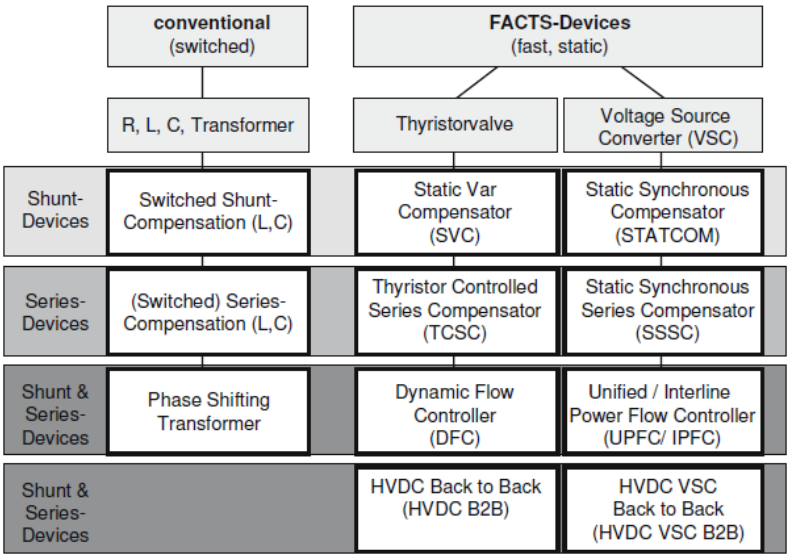

Figure 1.*Overview of major FACTS-Devices [6].*

For quite a long time rotating synchronous condenser and fixed or mechanically switched capacitors and inductors were the main reactive power compensating devices. However, since 1980s FACTS devices have been applied for reactive power compensation. In utility grid applications reactive power compensation and voltage control are mostly commonly used FACTS device is SVC with the first commercial utility SVC installed in 1979 [6]. SVC consists of Thyristor Controlled Reactors (TCR) and Thyristor Switched Capacitors (TSC). The basic operating principle of the SVC based on the control of shunt susceptance by varying thyristor firing angles of the TCR and switching on/off TSC. Main advantages of the SVC are fast dynamic response, high voltage and power ratings.

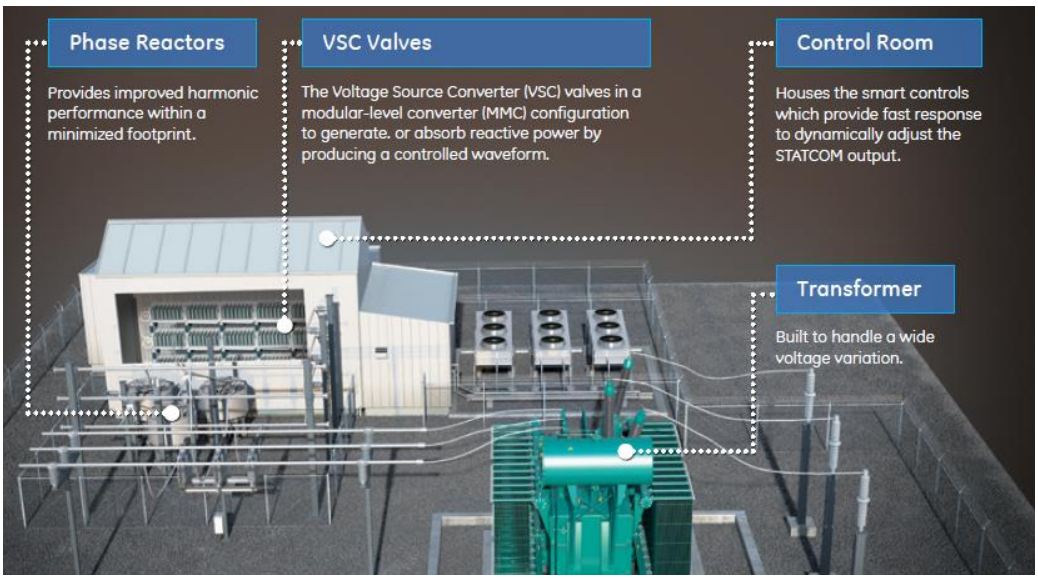

Figure 2.*Basic STATCOM Configuration and Main Components [7].*

Another main shunt reactive power compensating FACTS device is STATCOM. The developments in power electronics made the VSC technology applicable, and now it is replacing the thyristor based current switched converters. STATCOM is the FACTS device that utilizes VSC technology. Just like the SVC, its primary function is to keep the voltage at the specified voltage magnitude by supplying/absorbing reactive power. Figure 2 depicts the basic configuration and main components of the STATCOM. Compared to SVC STATCOM has shorter response time due to VSC's fast switching. The operation principle of the STATCOM in contrast to the SVC's variable susceptance, based on variable and controlled voltage source [4]. Compared to SVC STATCOM has the following advantages faster dynamic response, less space requirement, current injection is independent of line voltage.

1.3 Thesis objective

The primary goals for this thesis are listed below:

- In-depth understanding of the mathematical modelling, operating principles and control of the Modular Multilevel Converter (MMC) STATCOM
- Investigate the issues that affects the VSC operation in weak grid
- Study the STATCOM operation possibility in weak grid, obtain the limiting factors that restrict the operation in weak grid and propose solution if any found.
- Simulate STATCOM with the proposed improvements and compare the results.

1.4 Thesis outline

Chapter 2 gives an overview of the various reactive power compensation techniques and devices. It describes the reactive power compensation principle of STATCOM. Further, this chapter briefly introduces various multilevel topologies and their configuration.

Chapter 3 explains the mathematical modelling and steady-state operation principle of MMC STATCOM and based on this model the control design process of MMC STATCOM is provided. Next, it explains synchronization technique, modulation and, finally, control design for unbalanced cases.

Chapter 4 provides the information regarding power system strength and challenges of the VSC integration to the weak grid. Theoretical analysis of the PLL self-synchronization in the weak grid is provided and possible effects of self-synchronization on STATCOM is explained. Finally, this chapter presents the simulation model and simulation parameters.

Chapter 5 provides the simulation results for given theoretical approach. Initially possible issues due to STATCOM operation as a constant current source are identified and solution to improve the operation is provided. Next, it investigates STATCOM operation in voltage regulation mode and possible consequences of this operation. Finally, it presents the results of the fault simulations.

Finally, Chapter 6 concludes the key findings from this thesis study and summary of the obtained simulation and experimental results.

2. STATCOM REACTIVE POWER COMPENSATION

2.1 Reactive power compensation

Power system consists of generation, transmission and distribution of the electrical energy from the source to the customers. Apparent power consists of two components: active and reactive power. Active power is a part of the apparent power that is consumed by load and does actual work; whereas, reactive power is a part of the apparent power related to energy exchange between source and reactive component on the load side. Reactive power oscillates between source and load with frequency two times the rated value. Even though the net effect of the reactive power is zero, its imbalance has significant impact on system voltage.

In real power system loads are mostly inductive and they require sufficient amount of reactive power for normal operation. The direct transfer of the reactive power from the source to the load over long distances has many drawbacks such as overloading of the power system generators and equipment, reduced power transfer capability, voltage drop over transmission line and, increased power losses. In power system, the power generation and load must balance all the times. In case of disturbance by changing system voltage and frequency system can regulate itself to some extent. However, this self-regulation is within limited margin of few percent. The violation of the real power balance causes frequency instability; whereas, violating the reactive power balance will lead to voltage instability [8].

Usually reactive power compensating devices are connected in series or in shunt. Shunt compensator is usually installed in parallel with the load at the load side or midpoint of the line and changes the load impedance, effectively bringing the power factor at the load side to unity. Since the main purpose of series compensator, in contrast to shunt, is to reduce the transmission line reactance, series compensator's location in contrast to shunt compensator is not limited and can be installed anywhere in between source and load. Hence, by varying transmission line reactance, power transfer capability of the transmission line enhanced.

Depending on the controllability and dynamic response reactive power compensators can be divided into two groups: conventional and FACTS devices. Examples of the conventional compensators are fixed capacitors/inductors and synchronous condenser. These compensators are very limited in terms of flexibility and controllability, making the respond to any changes in power flow or voltage very poor in terms of accuracy and

smoothness. FACTS devices in contrast to conventional power compensators are built on power electronic devices; hence, have very quick respond to any changes in the system providing improved system flexibility. Examples of the FACTS devices are SVC, STATCOM etc. Figure 1 depicts main compensating devices based on dynamic response and connection scheme.

Reactive power flow in shunt compensation is controlled by installing compensating device at the load side or mid-point of the line and reducing reactive component of the source current. Thus, voltage drop and power losses over the transmission line decreases.

A simple system consisting of source, transmission line and inductive load without reactive compensation device connected is depicted in Figure 3. For normal operation load requires reactive power that is supplied by the source which results in large current flow. High current flow from source to load causes high voltage drop and power losses over transmission line as it is shown in the phasor diagram in Figure 3.

Figure 4 depicts the same system with current-source device added as a reactive compensator at load side. This compensator supplies all the reactive current required by the load effectively reducing the reactive component of the source current to zero as seen from the phasor diagram in Figure 4.

Shunt reactive power compensation improves the system voltage regulation and helps the nearby generators to operate at unity power factor. Majority of the loads are inductive thus the capacitive reactive power compensation is required. However, in some cases reactive power needs to be absorbed by the system to limit the voltage rise due to light load operation of the system. Hence, a compensator with capability also for inductive reactive power compensation is needed. Synchronous condenser, SVC and STATCOM

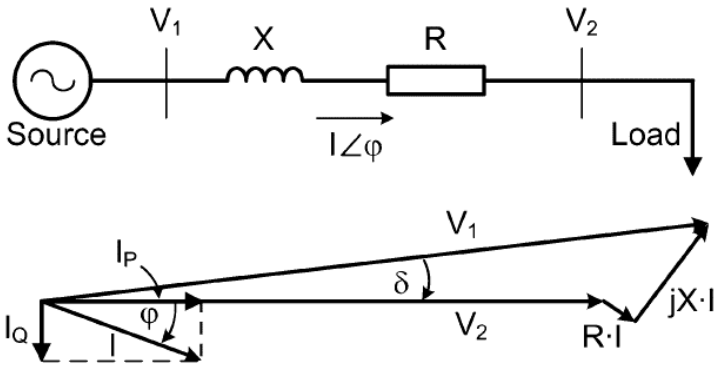

Figure 3.*Single line diagram of AC transmission line without compensation and its phasor diagram [9].*

are examples of shunt connected reactive power compensators, that can compensate both inductive and capacitive reactive power.

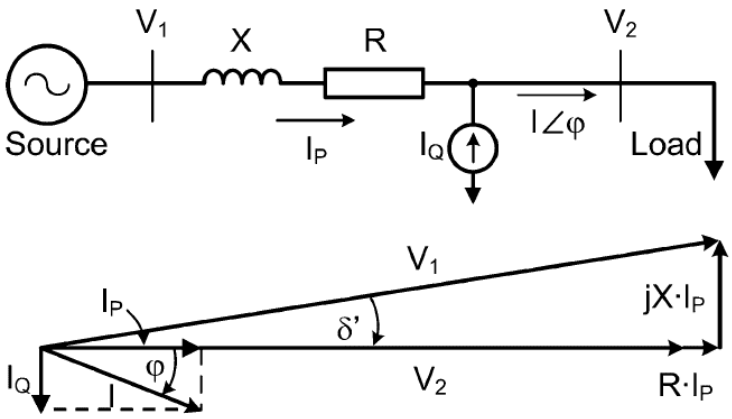

Figure 4. *Single line diagram of AC transmission line with shunt compensation and its phasor diagram [9].*

2.2 STATCOM operating principle

STATCOM is shunt connected device of FACTS family that is based on VSC technology. First installed in 1999, STATCOM since then has been widely used for the system voltage control and reactive power compensation. Figure 5 represents simple structural diagram showing main components of STATCOM, which consists of a step-down transformer, smoothing inductor, IGBT switches, DC side capacitor and dedicated control system. Main function of STATCOM is to supply/absorb the reactive power to/from the grid to support the voltage at Point of Common Coupling (PCC). Since DC side capacitor is relatively small there is only reactive power exchange between STATCOM and grid. However, by connecting the energy storage like battery, STATCOM is capable to supply also the active power [10][11].

The reactive power is compensated by STATCOM by controlling the amplitude and the phase of the voltage at the converter output, Figure 6 presents the simplified single-line diagram of STATCOM connected to the grid. For simplicity resistance is omitted and equivalent impedance of the line is equal to X_{tr}.

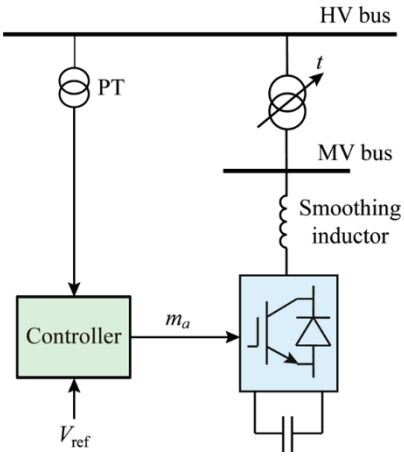

Figure 5. *STATCOM configuration diagram [4].*

The phase difference between STATCOM output voltage V_{st} and grid voltage V_{gr} is δ. The current flow I_{st} between STATCOM and the grid can be expressed with following equation:

$$\vec{I}_{st} = \frac{\vec{V}_{gr} - \vec{V}_{st}}{jX_{tr}} = \frac{V_{st}\sin\delta - j(V_{gr} - V_{st}\cos\delta)}{X_{tr}} \quad (1)$$

Hence the power flow S between STATCOM and grid can be calculated like this:

$$S = \vec{V}_{gr}\vec{I}_{st}^{*} = V_{gr} \times \left(\frac{V_{st}\sin\delta + j(V_{gr} - V_{st}\cos\delta)}{X_{tr}}\right) \quad (2)$$

The resulting active and reactive power equations of the STATCOM are the following:

$$P = \frac{V_{gr}V_{st}\sin\delta}{X_{tr}} \quad (3)$$

$$Q = \frac{V_{gr}^2 - V_{gr}V_{st}\cos\delta}{X_{tr}} \quad (4)$$

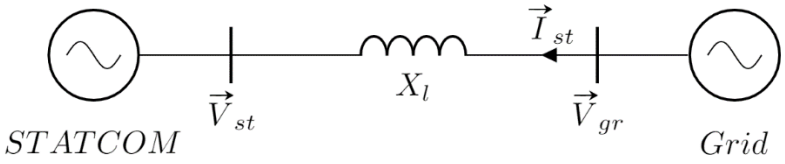

Figure 6. *STATCOM single-line diagram.*

From the equations (3) and (4) it can be concluded that by varying the amplitude and the phase angle of STATCOM output voltage, the active and reactive power can be separately controlled. Ideally STATCOM output voltage is in phase with grid side voltage and the reactive power equation (4) can be simplified:

$$Q = \frac{V_{gr} - V_{st}}{X_{tr}} V_{gr} \quad (5)$$

Therefore, by varying STATCOM output voltage amplitude the reactive power is controlled. In real case there will be a small phase difference between STATCOM and grid voltage to compensate active losses in STATCOM.

Figure 7 shows the operating modes STATCOM and corresponding voltage and current phasor diagrams. For inductive operation STATCOM voltage amplitude is lower than grid side voltage; hence, the reactive power is absorbed. Whereas, in capacitive mode the amplitude of the STATCOM voltage is higher than grid voltage and reactive current is supplied to the network. For standby mode the amplitude of the both voltages are equal and there is no current flow between grid and STATCOM.

In contrast to SVC, STATCOM reactive current injection is independent of system voltage as it can be observed from the Figure 8. Thus, the amount of the reactive power STATCOM capable to provide at low voltage is higher than SVC and it varies linearly. Moreover, STATCOM has better dynamic response, requires less space and has symmetrical inductive/capacitive reactive power range.

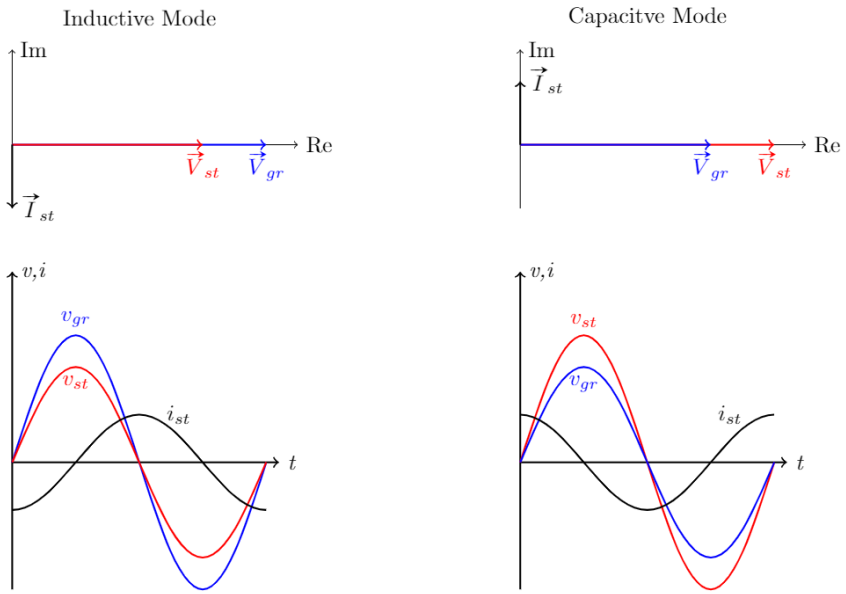

Figure 7. *STATCOM operating modes and corresponding voltage and current waveforms.*

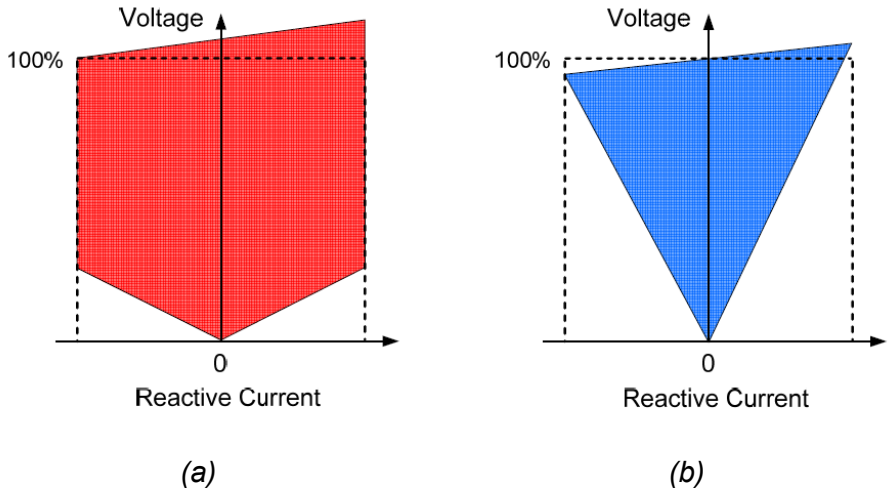

Figure 8. *Reactive current vs system voltage of a) STATCOM and b) SVC [12].*

2.3 MMC STATCOM

For low voltage and low power rating applications, two-level STATCOM is feasible solution. However, for applications requiring higher power and voltage ratings, this configuration is not a good choice. The following are main limitations of the two-level STATCOM:

- The main power electronic device (PED) used in VSCs is Insulated Gate Bipolar Transistor (IGBT); hence, in medium and high voltage grid applications IGBTs with high blocking ratings are required. The maximum blocking voltage of commercially available Si IGBTs is 6.5 kV and seems that in terms of voltage ratings this technology reached its limit [13]. IGBTs based on SiC technology are capable to block voltages up to 15 kV and look very promising for future application but their application for high voltage is still questionable [14][14].
- Switching of the converter creates the harmonics on AC-side voltage around multiples of the switching frequency. In low voltage applications high switching frequency is used for cheap and small harmonic filter design. In high voltage applications the high switching frequency will cause high switching power losses thus switching frequency is limited to 1 kHz which will result in more expensive and bulkier harmonic filter design.
- In high voltage application fast switching of the phase voltage between DC rails of two-level converter will result in high voltage slope. Due to this high voltage

slope, AC side connected equipment's insulation will be inflicted with very high burden [15].

Due to the abovementioned reasons, multilevel topologies are the most prominent solution for medium and high voltage applications [16]. MMC is the most prominent multilevel topology has the following advantages compared to two-level VSC:

- Low switching losses due to the lower switching frequency.
- Low voltage rating of the power electronic devices.
- Generated output voltage has a lower harmonic distortion and reduced dv/dt.
- Modularity makes it possible to replace faulty modules.
- Possible transformer-less installation

On the other hand, MMC has the following disadvantages:

- MMC consists of large number of switches which makes system expensive and complex.
- Large number of switches makes control of the system challenging.

2.4 Multilevel VSC topologies

The application of IGBT based VSC technology in medium and high voltages makes the utilization of simple two-level topologies almost impossible due to switching losses, harmonic distortion and PED ratings. To overcome these issues multilevel VSC has been used. Multilevel VSC consists of series connected PEDs and capacitors as voltage sources, the output of which generate voltages with stepped waveforms [16]. Multilevel VSC can generate more than two voltage levels, which helps to create output voltage very close to pure sinusoidal by stepping. This results in reduced harmonic content, lower switching frequency and consequently lower switching losses, less stress on switches and lower voltage rating requirements for the switches. Depending on the number of connected DC sources multilevel VSCs can be categorized into two groups [17][18][19]:

- Single DC source multilevel VSCs
- Multiple DC sources multilevel VSCs

2.4.1 Single DC source multilevel VSC

The most known single source multilevel converter topologies are Diode Clamped Converter (DCC) and Flying Capacitor Converter (FCC). These were the first introduced multilevel VSC topologies.

DCC uses series connected identical DC capacitors to create different voltage levels. Diodes inserted to clamp the blocking voltage of each switch. DCC that has only three levels is called Neutral Point Clamped Converter (NPCC). Figure 9 depicts the circuit diagrams of NPCC and five-level DCC converter. For DCC the blocking voltage of the switches does not change, whereas the reverse voltage blocking ratings of the diodes will be different. Hence, for high number of the voltage levels the DCC topology becomes impractical to implement due to increased number of components and component ratings, system and control complexities.

FCC was introduced to remove the drawbacks of DCC and its structure is identical to DCC; however, in this case instead of diodes, capacitors are clamped to evenly divide the blocking voltage between switches. The voltage difference between two adjacent legs defines the voltage steps of the output AC waveform. Figure 10 illustrates the circuit diagrams for three- and five-level FCCs. Like DCC, generation of voltage waveforms with high number of voltage steps would require large number of capacitors in each phase leg making the system bulky and unreliable. Moreover, for low switching frequency the size of the capacitors become large. All these makes it challenging and impractical to implement high level FCC.

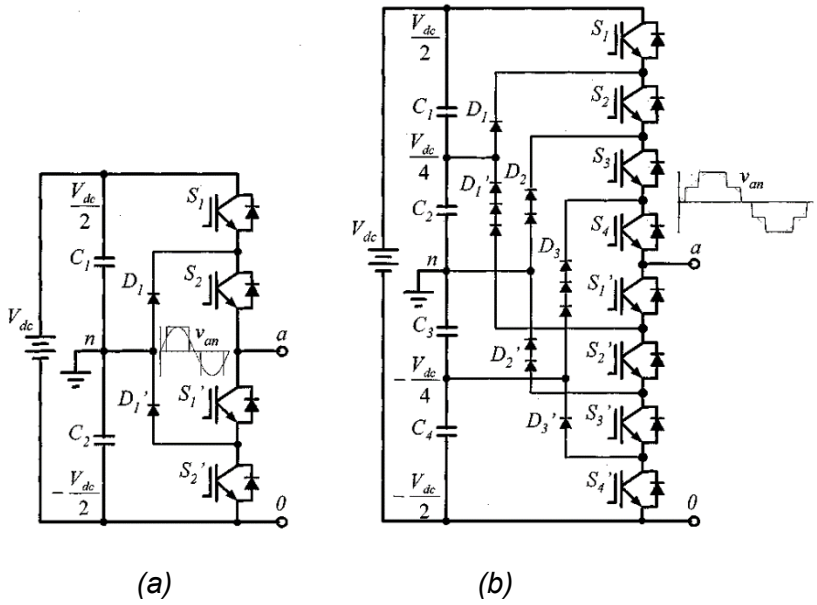

Figure 9. *DCC multilevel converter circuit. a) 3-level and b) 5-level [16].*

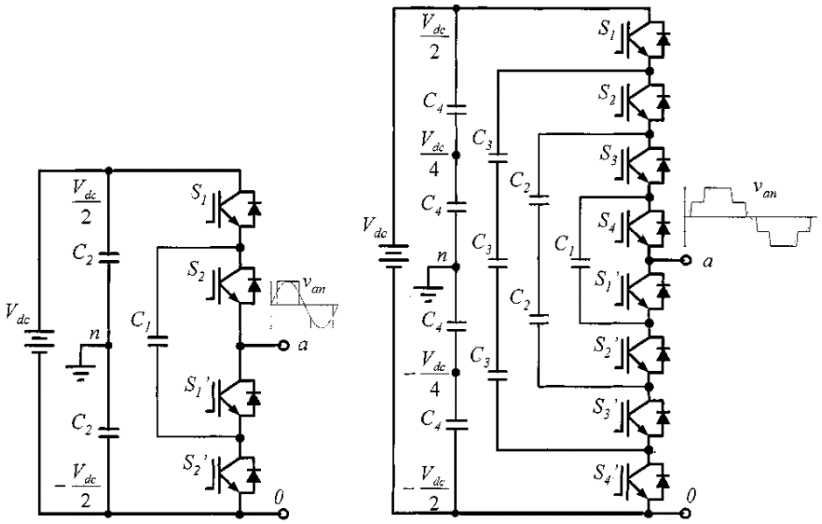

Figure 10. *FCC multilevel converter circuit. a) 3-level and b) 5-level [16].*

2.4.2 Multiple DC sources multilevel VSC

Another way to build multilevel converter is based on modularity, which is the combination of the system from smaller and identical subsystems. MMC consists of series connected small single-phase submodules with separate DC sources. There are several submodule configurations [17], the most commonly used configurations are Full-Bridge (FB) or H-Bridge and Half-Bridge. Figure 11 shows the schematics and the output voltage levels for these submodules. The addition of each submodule voltage connected in series will create the output phase voltage. Figure 12 represents one phase of nine-level Cascaded H-bridge converter and its associated output voltage waveform. Since in theory the number of submodules in MMC is not limited, the output AC waveform can be controlled with great precision and low harmonic content. Moreover, modular approach gives scalability and any desired ratings in terms of rated power and operating voltage can be achieved.

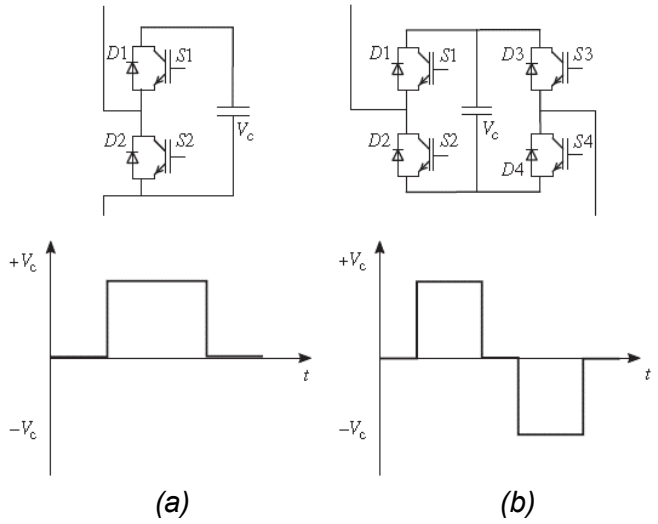

Figure 11. *Converter submodule topologies and corresponding output waveform. a) half-bridge and b) full-bridge [15].*

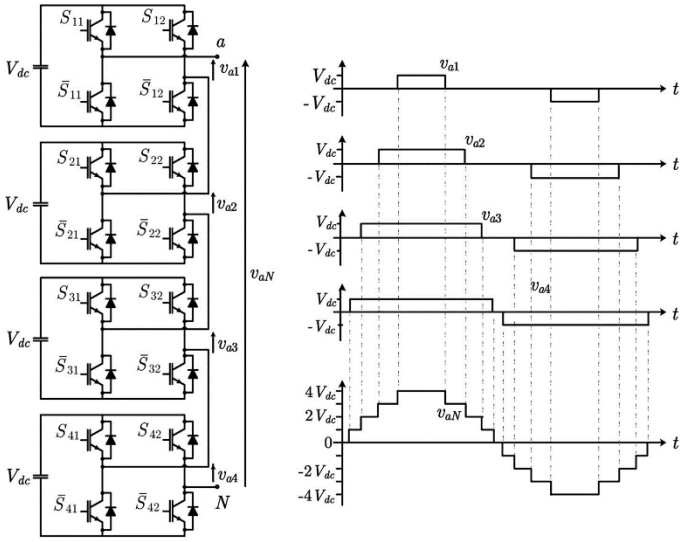

Figure 12. *Nine-level CHB converter and resulting output waveform [19].*

Depending on the connection and submodule configurations MMC is divided into 4 groups [20]:

- Single-Star Cascaded H-Bridge (SS-CHB)
- Single-Delta Cascaded H -Bridge (SD-CHB)
- Double-Star Half-Bridge (DS-HB)
- Double-Star Full-Bridge (DS-FB)

In literature the abovementioned topologies can be found under different naming; nevertheless, all these configurations are based on concepts of modularity and cascaded submodules. Therefore, in this thesis all STATCOMs based on modularity addressed as MMC.

Structure of Single-Star Cascaded H-Bridge is depicted in Figure 13-a. This configuration consists of chain connected H-Bridges in each of its phase legs that are connect-ed in star. An inductor is connected in series with each leg to limit harmonic currents and to allow for control of arm currents. Among all MMC configurations SS-CHB has the lowest submodule count and as result has the lowest cost. However, the major disadvantage of this configuration is inability to control negative-sequence reactive power under unbalanced conditions. To be able to generate negative-sequence current it has to add zero-sequence voltage equal to phase voltage regardless of the negative-sequence amplitude. This will lead to over-rated converter configuration. Therefore, STATCOM based on this configuration is mainly used for applications requiring positive reactive power compensation like voltage regulation [20].

The structure of the Single-Delta Cascaded H-Bridge is shown in Figure 13-b. In contrast to SS-CHB, phase legs consisting of series connected H-bridges are connected in delta and usually an inductor is connected inside delta branch of STATCOM, this results in √3 times higher phase voltage rating for SD-CHB compared to SS-CHB with the same number of submodules. On the other hand, SS-CHB has the √3 times higher phase current rating than SD-CHB. SD-CHB under unbalanced grid voltage is capable to circulate zero-sequence current that can be utilized for phase capacitor voltages balancing. Opposite

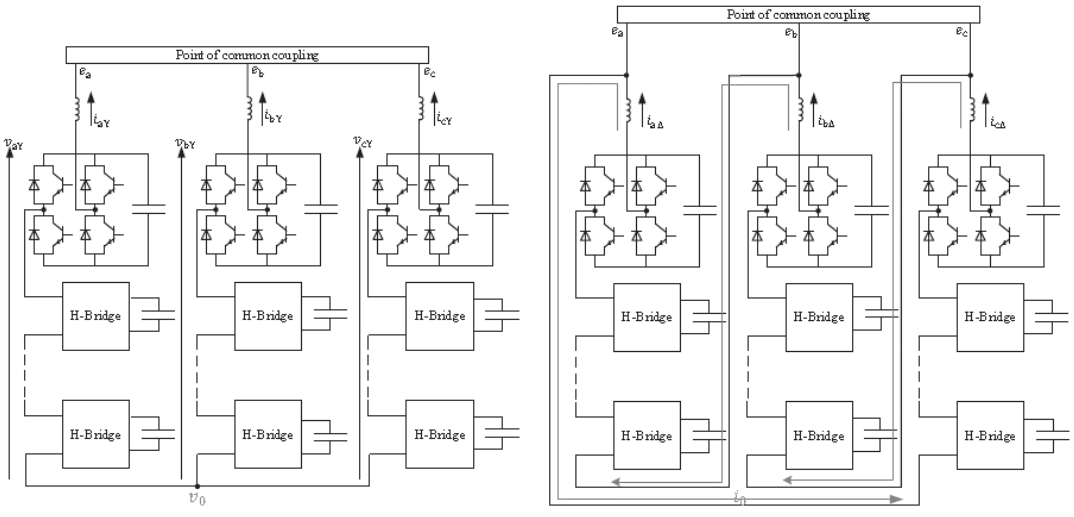

(a) *(b)*

Figure 13. *Cascaded H-Bridge converter topology [21].*

to star connected configuration, required zero-sequence current is proportional to the amplitude of negative sequence current. The capability to control negative-sequence reactive power makes STATCOM based on this configuration attractive solution for flicker compensation [20].

Figure 14 depicts the circuit configuration of Double-Star Half-Bridge. Each phase leg of DS-HB consists of two arms: upper and lower. Each arm composed of equal number of cascaded half-bridge inverter submodules and series connected inductor. AC output is connected to the midpoint of these arms. HB submodules generate only 2 voltage levels as depicted in Figure 11-a; therefore, the output AC waveform is the difference between upper and lower arm voltages as it is shown in Figure 14. Under unbalanced conditions, DS-HB's ability to control circulating current makes it possible to control negative-sequence current/power. In contrast to SD-CHB, DS-HB does not need to increase converter ratings. Compared to single star or delta configuration individual submodules requires lower device current ratings in double star configuration, due to current sharing between each arm. Main shortcomings of DS-HB configuration are higher cost due to increased number of switches and higher voltage rating compared to single star or delta.

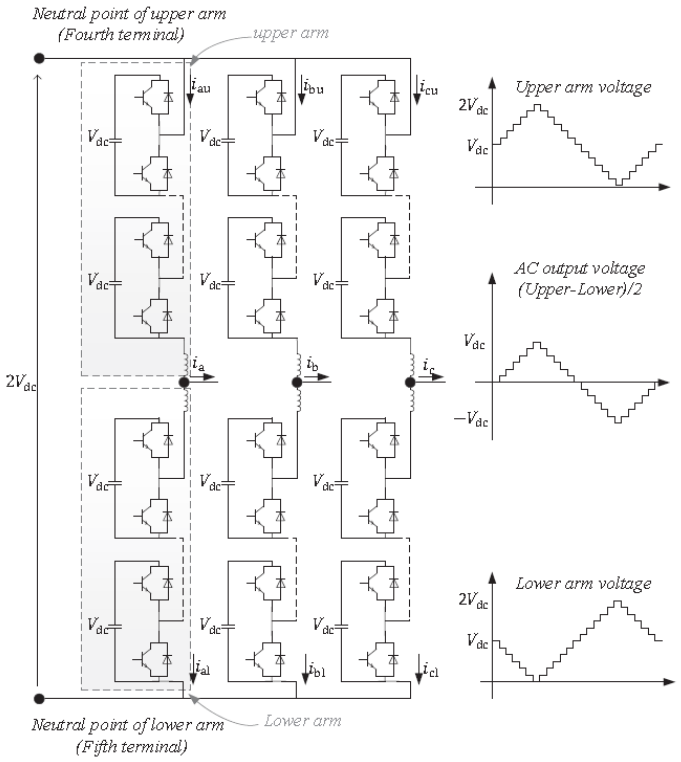

Figure 14. *DS-HB configuration and its associated output waveform [21].*

The last MMC converter topology is Double-Star Full-Bridge which has the same circuit topology as DS-HB with full-bridge inverters used as submodules. With DS-FB it is possible to achieve lower voltage rating of the converter with less submodules; however, due to full-bridge inverter-based submodules the quantity of required switches will be doubled compared to DS-HB with the same number of submodules [20][21].

The main difference between single-star, single-delta and double-star connected configurations is possibility to control active power through connected common DC-link on DC side. SS-CHB and SD-CHB are “three-terminal circuits” which means it is impossible to connect DC side of inverter to common DC link; hence, for these configurations the only possibility to control active power is by means of connecting isolated DC sources like battery packs to each submodule. On the other hand, DS-HB and DS-FB are called “five-terminal circuits” since it is possible to connect common DC link to their neutral points of the upper and lower arms. Therefore, there is no need for separate isolated DC sources to manipulate active power. This is the main advantage of the double-star configuration compared to the other two configurations. Possibility to connect common DC link makes double-star configurations very attractive for HVDC applications. In application that does not require only active power control like STATCOM, single star and delta connected configurations are preferred topologies[20][22].

3. MMC STATCOM MODELLING AND CONTROL DESIGN

3.1 Introduction

Compared to two or three-level converters, multilevel converters have much more complex internal dynamics due to presence of multiple submodules. Hence, control objective of the multilevel STATCOM can be divided into two parts: (i) overall control of reactive power for PCC voltage regulation or power factor correction and (ii) individual submodule capacitor voltage regulation and power balancing. The latter requires specially designed control strategy to fix the unbalanced power sharing between submodules in each leg of the multilevel STATCOM due to deviation of submodule parameters (like sizes of capacitors) from each other.

There are multiple control algorithms of STATCOM which can be implemented both in time and frequency domains, examples of these algorithms are instantaneous reactive power control (in *abc*- or *αβ*- domains), model predictive control, Fourier series theory, Kalman filter based control, synchronous reference frame (*dq*-domain). Among these control strategies *dq*-domain control is the simplest to implement because of straightforward application of the classical control theory and implementation of Proportional Integral (PI) controllers [15][23][24]. Use of PI controller provides good enough performance especially for controlled processes that have first-order dynamics or can be approximated so. On the other hand, this control method requires solid synchronization method to perform transformation of AC variables to DC [15][23][24].

In contrast to *dq*-domain control, stationary reference frame control does not require complex domain transform since the reference signals are generated in stationary frame. For linear control in stationary frame Proportional Resonant (PR) controller is used, its operation resembles the PI controller and can accurately track sinusoidal waveforms [15][24]. However, the disadvantage of the PR controller is that it can provide accurate reference tracking only for frequency it is tuned for. Hence, for multiple frequency signal tracking R part of PR controller needs to be tuned for each of the waveform frequency present [15].

Another aspect that must be considered during the selection of the control strategy is the amount of required computation burden by the selected strategy. For example, control strategy in frequency domain is slow and requires more computation burden compared

to the one implemented in time domain. Real devices used in practice for process control have limited amount of computation burden which puts restrictions in selection of the control method.

3.2 STATCOM modelling and steady-state analysis

In order to design proper control system, it is important to obtain the equations that determine STATCOM's behavior in dynamic and steady states. Figure 15 shows topology of SD-CHB MMC STATCOM with an arbitrary number of n H-bridge inverter-based submodules per phase connected to the grid that will be used to model the system behavior. A passive filter L_f between converter and grid is installed to filter out harmonics in the injected AC current and absorb instantaneous voltage difference between the STATCOM and grid.

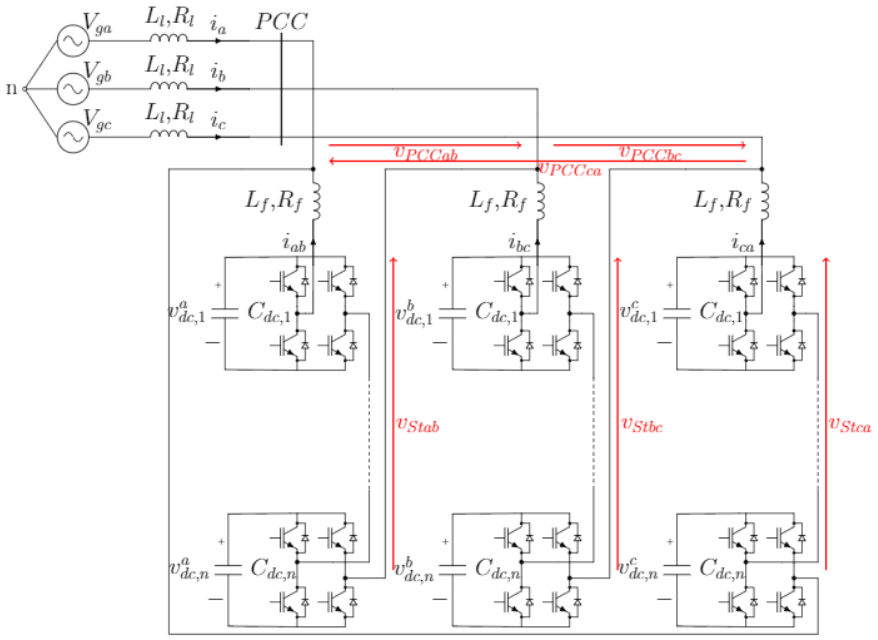

Figure 15. *SD-CHB MMC STATCOM configuration.*

Applying Kirchhoff's voltage law, the dynamic model for system in Figure 15 obtained. For modelling purpose, all submodules assumed to have identical DC capacitors precharged to same DC voltage and AC voltage is equally shared among each submodule. Hence, the dynamic equations for each phase on AC side expressed as:

$$ns_c^a v_{dc}^a - L_f \frac{di_{ab}}{dt} - R_f i_{ab} = v_{PCCab} \tag{6}$$

$$ns_c^b v_{dc}^b - L_f \frac{di_{bc}}{dt} - R_f i_{bc} = v_{PCCbc} \tag{7}$$

$$ns_c^c v_{dc}^c - L_f \frac{di_{ca}}{dt} - R_f i_{ca} = v_{PCCca} \quad (8)$$

where s_c^a, s_c^b, s_c^c are switching functions corresponding to each phase of STATCOM, R_f is the equivalent parasitic resistance of the L_f, v_{dc} is DC voltage of the single submodule capacitor and n is the number of submodules per phase.

DC side dynamic equation can be derived from the active power exchange between the grid and STATCOM, the total power on DC side expressed as:

$$p_{dc} = p_{ac} - p_{loss} \quad (9)$$

where p_{dc} is DC side power, p_{ac} is AC power of single phase, p_{loss} represents combined power losses on DC and AC sides. Therefore, the DC side dynamic equation for one submodule obtained as:

$$\frac{1}{2} C_{dc} \frac{dv_{dc}^2}{dt} = \frac{p_a - R_f |i_{ab}|^2}{n} - \frac{v_{dc}^2}{R_{dc}} \quad (10)$$

where C_{dc} is the submodule capacitor and R_{dc} represents the overall losses on DC side and connected in parallel with capacitor, p_a is total power transfered from grid to STATCOM in phase *a*. Equation (10) can be easily expanded to the remaining two phases.

The switching function for simplicity can be substituted with its fundamental component which is usually modulation index:

$$s_c^a \cong m_c^a \quad (11)$$

where m_c^a is modulation signal for single submodule in phase *a*.

Substituting (11) into (6-8) all dynamic model equations are expressed at fundamental frequency. Therefore, by applying Park's transform to these equations it is possible to obtain dynamic model of MMC STATCOM in synchronous reference frame. Corresponding STATCOM *dq*-domain equations are:

$$nm_d v_{dc} = v_{\Delta d} + L_f \frac{di_{\Delta d}}{dt} + R_f i_{\Delta d} - \omega L_f i_{\Delta q} \quad (12)$$

$$nm_q v_{dc} = v_{\Delta q} + L_f \frac{di_{\Delta q}}{dt} + R_f i_{\Delta q} + \omega L_f i_{\Delta d} \quad (13)$$

$$\frac{1}{2} C_{dc} \frac{dv_{dc}^2}{dt} = \frac{v_{\Delta d} i_{\Delta d} + v_{\Delta q} i_{\Delta q} - R_f (i_{\Delta d}^2 + i_{\Delta q}^2)}{2n} - \frac{v_{dc}^2}{R_{dc}} \quad (14)$$

where ω is the angular speed of rotating vectors.

Steady-state analysis required to evaluate the behavior of the STATCOM, modulating signals values and required compensating reactive power *Q* calculated by solving steady-state equations. In steady-state point transients die out; hence, derivatives are

equal to zero and state variables in steady-state can be expressed by corresponding capital letter.

Thus, the steady-state equations are:

$$M_d = \frac{V_{\Delta d}+R_f I_{\Delta d}-\omega L_f I_{\Delta q}}{nV_{dc}} \tag{15}$$

$$M_q = \frac{V_{\Delta q}+R_f I_{\Delta q}+\omega L_f I_{\Delta d}}{nV_{dc}} \tag{16}$$

$$0 = \frac{V_{\Delta d}I_{\Delta d}+V_{\Delta q}I_{\Delta q}-R_f(I_{\Delta d}^2+I_{\Delta q}^2)}{2n} - \frac{V_{dc}^2}{R_{dc}} \tag{17}$$

In *dq*-frame the power delivered by grid to STATCOM is calculated as:

$$S = \frac{3}{2}\underline{V}_{\Delta dq}\underline{I}^*_{\Delta dq} \rightarrow \begin{cases} P = \frac{3}{2}\left(V_{\Delta d}I_{\Delta d} + V_{\Delta q}I_{\Delta q}\right) \\ Q = \frac{3}{2}(-V_{\Delta d}I_{\Delta q} + V_{\Delta q}I_{\Delta d}) \end{cases} \tag{18}$$

Normally *dq*-reference frame synchronized with grid voltage and in steady-state the *q*-component of the voltage (i.e. $V_{\Delta q}$) is equal to zero. Thus, the power equation (18) simplified as:

$$P = \frac{3}{2}V_{\Delta d}I_{\Delta d} \quad \text{and} \quad Q = -\frac{3}{2}V_{\Delta d}I_{\Delta q} \tag{19}$$

It is obvious from equation (19) that active and reactive power can be controlled independently from each other by respectively varying *d*- and *q*-components of the current. Therefore, if Q^* is the amount of the required compensating reactive power desired value of the $I_{\Delta q}$ obtained as:

$$I_{\Delta q} = -\frac{2Q^*}{3V_{\Delta d}} \tag{20}$$

The values of the modulating signals equal to:

$$\begin{aligned} M_d &= \frac{V_{\Delta d}+R_f I_{\Delta d}-\omega L_f I_{\Delta q}}{nV_{dc}} \\ M_q &= \frac{R_f I_{\Delta q}+\omega L_f I_{\Delta d}}{nV_{dc}} \end{aligned} \tag{21}$$

where V_{dc} is the only unknown variable to calculate the values of the modulating signals.

The value of V_{dc} has to be selected so that the total sum of DC voltages of all submodules is higher than phase voltage amplitude:

$$nV_{dc} > \sqrt{V_{\Delta d}^2 + V_{\Delta q}^2} \rightarrow V_{dc} = \frac{kV_{\Delta d}}{n} \tag{22}$$

where k is the safety factor coefficient with a safety margin of 10% to 15%. Thus, substituting (22) into equation (21) and applying inverse Park's transform the modulation signals in *abc*-domain are obtained.

3.3 STATCOM overall control scheme

Control system design is based on cascaded loops, where the inner current control loop has highest bandwidth and fastest response of all control loops. The outer control loop feeds the reference signals to inner control loop. Figure 16 depicts the overall control block diagram of MMC STATCOM. STATCOM can operate in voltage regulation mode or reactive power compensation mode and depending on the mode selected Voltage controller or Q controller generates reference value of the current *q*-component. DC voltage controller maintains DC link voltage at desired level and produces reference value *d*-component of the current. The reference current in *dq*-domain is transformed to *abc*-domain and fed to current controller. Current controller supplies reference signals to Modulation and submodule balance block where individual submodule balancing happens and supplies firing pulses sent to switches. PLL is used to synchronize to the grid voltage and supply estimated grid angle θ for reference frame transformation. PLL synchronizes to the STATCOM branch voltage which is delta connected; hence, PCC line voltage due to phase displacement lags by $\frac{\pi}{6}$ and the grid angle will be $\theta - \frac{\pi}{6}$. Following subsections will provide controller design process explanation.

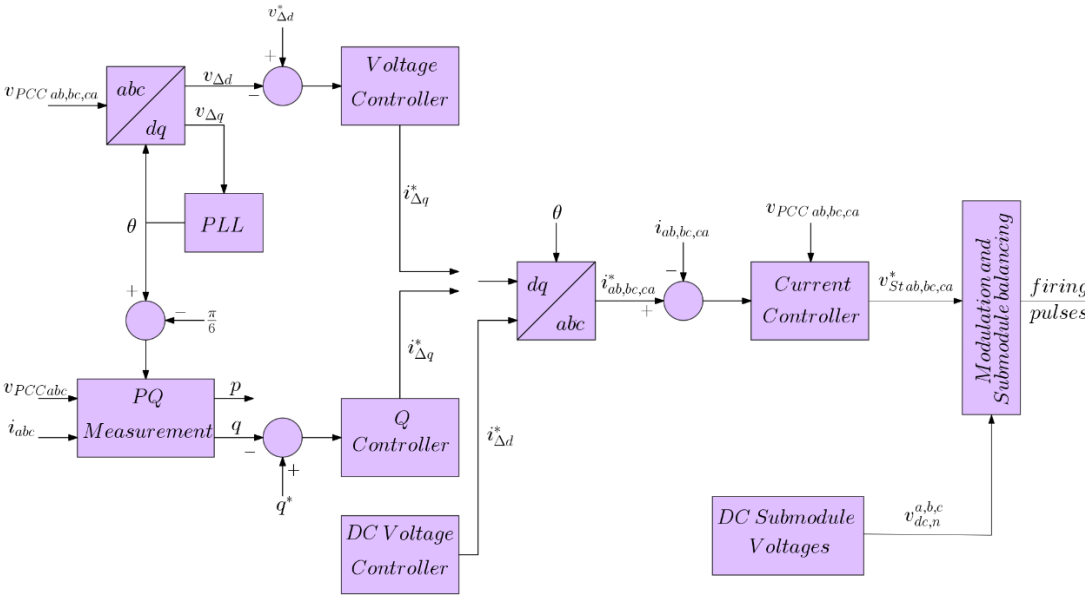

Figure 16. *Overall control block diagram of SD-CHB MMC STATCOM.*

3.4 Current controller

Current controller is implemented in abc-domain and the design of the current controller based on equations (6), (7) and (8). The design process here described for phase a which after Laplace transformation becomes as:

$$nm_a v_{dc} - v_{PCCab} = sL_f i_{ab} + R_f i_{ab} \tag{23}$$

the resulting equation can be easily expanded for the remaining two phases.

Figure 17 depicts overall block diagram of current controller that consists of PR controller which processes an error signal between the reference current and measured current and feedforward compensation. In order to reduce the effect of grid side disturbances on current control grid phase voltage is feedforwarded. The output of the current controller expressed by:

$$nm_a v_{dc} = \left(k_{pi} + \frac{k_{ri}s}{s^2+\omega_1^2}\right)(i_{ab}^* - i_{ab}) + v_{PCCab} \tag{24}$$

where k_{pi} and k_{ri} are proportional and resonant gains of PR controller, i_{ab}^* is the reference values of phase *a* current and ω_1 is the fundamental frequency.

To tune the PR controller parameters, it is necessary to obtain the closed loop transfer function of the current control process. The control process in Figure 17-a can be simplified as it is depicted in Figure 17-b and current-control loop transfer functions for the remaining two phases are identical; therefore, the same tuned parameters of PR controller will be applied for the other two phases. From Figure 17-b closed loop transfer function is:

$$G_{ci}(s) = \frac{i_{ab}}{i_{ab}^*} = \frac{k_{pi}(s^2+\omega_1^2)+k_{ri}s}{(s^2+\omega_1^2)(sL_f+R_f)+k_{pi}(s^2+\omega_1^2)+k_{ri}s} \tag{25}$$

PR controller parameters' tuning starts with the proportional gain since it will determine the system's dynamics with regarding to bandwidth, gain and phase margins. Therefore, first resonant gain k_{ri} is set to zero and since the equivalent series resistance R_f is very small it can be omitted for further calculations. Then, the closed loop transfer function $G_{ci}(s)$ can be expressed as a first-order transfer function:

$$G_{ci}(s) = \frac{{k_{pi}}/{L_f}}{s+{k_{pi}}/{L_f}} = \frac{\alpha_i}{s+\alpha_i} \tag{26}$$

from which the proportional gain value obtained as

$$k_{pi} = \alpha_i L_f \tag{27}$$

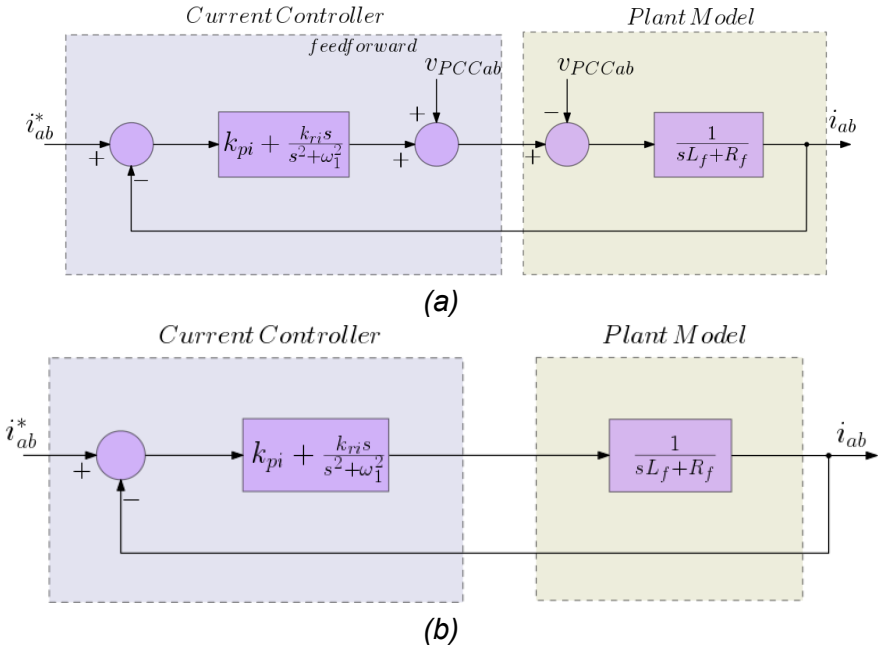

Figure 17. *Control block diagram of current controller a) overall and b) simplified.*

where α_i is the required bandwidth of the resulting closed loop system. Current controller has the highest bandwidth among the other controllers in STATCOM; however, when the time delay considered there is an upper bound due to stability. Hence, practically α_i selected to be not greater than one tenth of the angular sampling frequency [15].

The equation (25) after some manipulations can be expressed as:

$$G_{ci}(s) = \frac{\alpha_i}{s+\alpha_i} \cdot \frac{s^2+\frac{k_{ri}}{k_{pi}}s+\omega_1^2}{\left(s^2+\frac{k_{ri}}{k_{pi}}s+\omega_1^2\right)-\frac{k_{ri}}{k_{pi}}s^2} \tag{28}$$

it is obvious from this equation that if $k_{ri} \to 0$ resonant part of the PR controller would cause the issues with rejection of the signals that have small deviations from fundamental frequency it is tuned for. Hence, to be able to track signals with frequencies with slight variation from fundamental frequency, PR controller is chosen to be non-ideal with some bandwidth of α_{PR} , thus resonant gain k_{ri} can be expressed as:

$$k_{ri} = \alpha_{PR}k_{pi} = \alpha_{PR}\alpha_i L_f \tag{29}$$

By substituting (29) into equation (28) and considering that $\alpha_{PR} \ll \alpha_i$ the closed loop transfer function can be approximated as first-order transfer function:

$$G_{ci}(s) = \frac{\alpha_i}{s+\alpha_i} \cdot \frac{s^2+\alpha_{PR}s+\omega_1^2}{(s^2+\alpha_{PR}s+\omega_1^2)-\alpha_{PR}s^2} \approx \frac{\alpha_i}{s+\alpha_i} \tag{30}$$

3.5 DC voltage controller

DC voltage controller keeps the voltage of each branch at reference value and supplies the reference value of the *d*-component current. Figure 18 shows the equivalent single line circuit for phase *a*, capacitor equal to series connection of all submodule capacitors and summed up DC voltages. For given system if no loss system assumed the power balance equation DC and AC sides expressed as:

$$\begin{aligned} p_{dc} &= \frac{1}{2}\frac{C_{dc}}{n}\frac{d(\sum_{i=1}^{n} v_{dci}^{a})^2}{dt} = \frac{n}{2}C_{dc}\frac{d(\bar{v}_{dc}^{a})^2}{dt} \\ p_{ac} &= \frac{1}{2}v_{\Delta d}i_{\Delta d} \end{aligned} \tag{31}$$

where $\bar{v}_{dc}^{a}$ is DC mean capacitor voltage in phase *a*.

Since AC side and DC side powers are equal, the equation (31) in Laplace domain becomes:

$$snC_{dc}{\bar{v}_{dc}^{a}}^{2} = v_{\Delta d}i_{\Delta d} \tag{32}$$

thus, the plant transfer function of DC controller expressed as:

$$\frac{\bar{v}_{dc}^{2}}{i_{\Delta d}} = \frac{v_{\Delta d}}{snC_{dc}} \tag{33}$$

Since plant transfer function has a natural integrator, proportional controller is enough to achieve accurate control. The overall control block diagram is depicted in Figure 19.

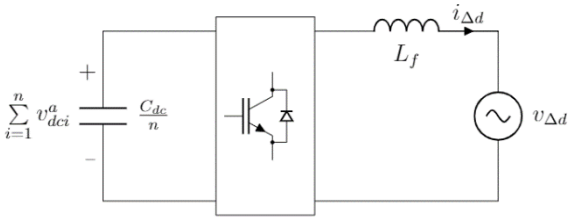

Figure 18. *Phase a equivalent single line circuit.*

Current controller is much faster than DC voltage controller; hence, the dynamics of DC voltage controller will not be affected by current controller and thus current assumed to be $i_{\Delta d}^{*} \approx i_{\Delta d}$. Therefore, the open loop transfer function of the controller is:

$$l_{dc}(s) = \frac{k_{pdc}v_{\Delta d}}{snC_{dc}} \tag{34}$$

where k_{pdc} is proportional gain of the controller. Then, closed-loop transfer function becomes a first-order transfer function and for a bandwidth of α_{dc} can be written as:

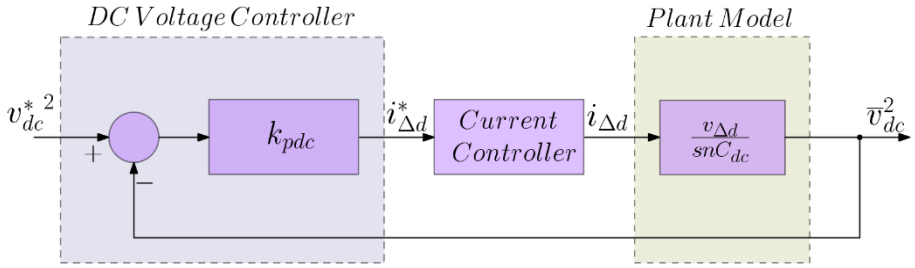

Figure 19. *Control block diagram of DC voltage controller.*

$$G_{cdc}(s) = \frac{v_{dc}^2}{v_{dc}^{*2}} = \frac{{}^{k_{pdc}v_{\Delta d}}/_{nC_{dc}}}{s+{}^{k_{pdc}v_{\Delta d}}/_{nC_{dc}}} = \frac{\alpha_{dc}}{s+\alpha_{dc}} \tag{35}$$

which is true for

$$k_{pdc} = \frac{\alpha_{dc} n C_{dc}}{v_{\Delta d}} \tag{36}$$

Normally the bandwidth α_{dc} of DC voltage controller is tuned to a value that is at least ten times smaller than the bandwidth of the current controller. This way it is possible for current controller to follow the current reference value generated by voltage controller.

3.6 Voltage controller

The reference value of the *q*-component current is provided depending on the operating mode of the STATCOM either by Q controller or voltage controller. The principle of the required reference value of the *q*-component current was explained before. Voltage controller maintains PCC voltage and Figure 20 shows simplified single line diagram of STATCOM phase *a* connected to grid through equivalent grid impedance $Z_g = L_g + R_g$. The dynamic equation for phase *a* is:

$$v_{PCCa} = L_g \frac{di_a}{dt} + R_g i_a + v_{ga} \tag{37}$$

where v_{PCCa} and v_{ga} respectively PCC and grid phase voltages, i_a is grid line current supplied by STATCOM. Equation can be expanded to the remaining two phases; hence, in *dq*-domain dynamic equations for PCC voltage will be:

$$v_{Yd} = L_g \frac{di_{Yd}}{dt} + R_g i_{Yd} - \omega L_g i_{Yq} + v_{gd} \tag{38}$$

$$v_{Yq} = L_g \frac{di_{Yq}}{dt} + R_g i_{Yq} + \omega L_g i_{Yd} + v_{gq} \tag{39}$$

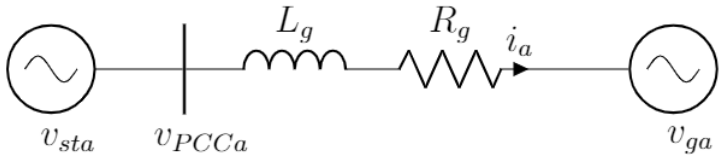

Figure 20. *Equivalent single line circuit of STATCOM phase a.*

where v_{Yd}, v_{Yq} are respectively *d*- and *q*-components of the phase voltage v_{PCC}, and i_{Yd}, i_{Yq} are respectively *d*- and *q*-components of the grid line current supplied by STATCOM.

In steady-state because of PLL synchronization v_{Yq} will be equal to zero, transients die out and if the voltage drop over R_g is neglected, it is obvious that v_{Yq} can be regulated by i_{Yq}. If PLL dynamics ignored, the equation (38) in Laplace domain approximated as:

$$v_{Yd} \approx v_{gd} - \omega L_g i_{Yq} \tag{40}$$

from which we can get the plant transfer function as:

$$\frac{v_{Yd}}{i_{Yq}} \approx -\omega L_g \tag{41}$$

Since the transfer function of the plant is a pure gain, integral control only for PI controller is sufficient to achieve good enough results. The overall control block diagram is depicted in Figure 21, from which first order closed loop transfer function obtained:

$$G_{pcc}(s) = \frac{v_{Yd}}{v_{Yd}^*} = \frac{k_{ipcc}\omega L_g}{s + k_{ipcc}\omega L_g} = \frac{\alpha_{pcc}}{s + \alpha_{pcc}} \tag{42}$$

which is true for integral gain k_{ipcc} equal to:

$$k_{ipcc} = \frac{\alpha_{pcc}}{\omega L_g} \tag{43}$$

where α_{pcc} is the bandwidth of the Voltage controller which is selected at least ten times less than current controller bandwidth.

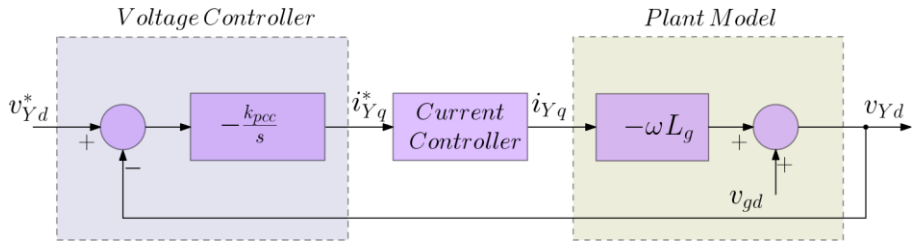

Figure 21. *Control block diagram of voltage controller.*

3.7 Synchronous Reference Frame Phase-Locked Loop (SRF-PLL)

STATCOM needs to be synchronized with grid voltages to perform the transformation of the measured signals from time domain to *dq*-domain. Figure 22-a shows the block diagram of the three-phase PLL used in STATCOM application. Clarke's and Park's transforms used to convert input grid voltages to stationary and synchronous reference frames, *q*-component of measured voltage fed to PI controller and the output of the PLL is fed back to Park's transform block. PI controller is used to adjust the PLL output angle $\hat{\theta}$ so that the sensed *q*-component of the grid voltage is equal to zero [25].The grid frequency is feedforwarded to accelerate the synchronization process.

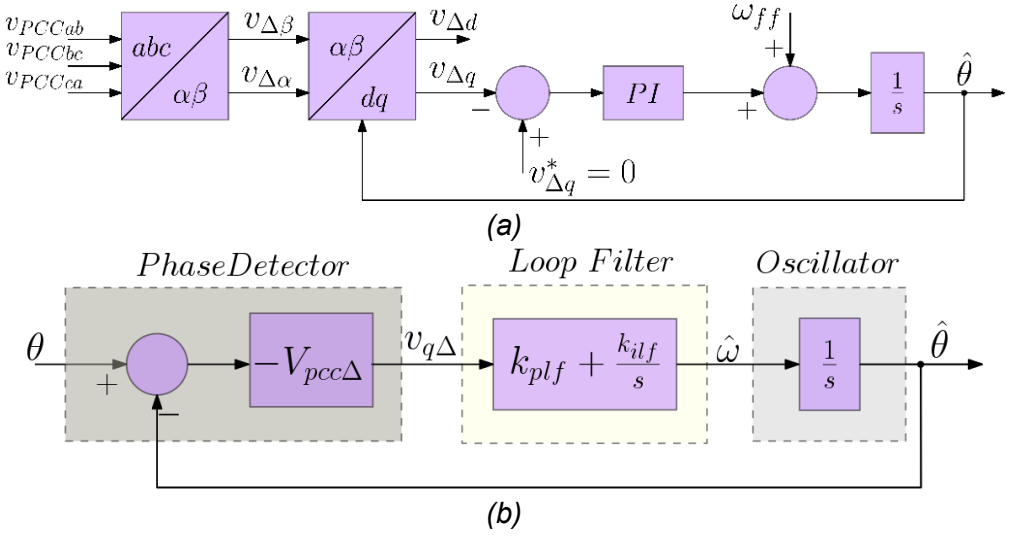

Figure 22. *a) Control block diagram and b) linearized block diagram of SRF-PLL*

The voltage at PCC is given by:

$$\begin{bmatrix} v_{PCCab} \\ v_{PCCbc} \\ v_{PCCca} \end{bmatrix} = \begin{bmatrix} V_{pcc\Delta} \cos\theta \\ V_{pcc\Delta} \cos(\theta - \frac{2\pi}{3}) \\ V_{pcc\Delta} \cos(\theta + \frac{2\pi}{3}) \end{bmatrix} \tag{44}$$

where $V_{PCC\Delta}$ is the amplitude and θ is the angle of the grid voltage. The grid voltages after Park's transformation becomes:

$$\begin{bmatrix} v_{\Delta d} \\ v_{\Delta q} \end{bmatrix} = V_{pcc\Delta} \begin{bmatrix} \cos(\theta - \hat{\theta}) \\ \sin(\theta - \hat{\theta}) \end{bmatrix} \tag{45}$$

where $\hat{\theta}$ is the sensed angle by PLL. Once PLL synchronized with the grid voltage the error between sensed and grid angle will be very small; hence, $v_{\Delta q}$ can be approximated as:

$$v_{\Delta q} \approx V_{pcc\Delta}(\theta - \hat{\theta}) \tag{46}$$

Based on (46) PLL can be linearized as it is depicted in Figure 22-b, where Loop Filter is PI controller with proportional and integral gain values of k_{plf} and k_{ilf} respectively.

Selection of the controller parameters based on closed loop transfer function of the PLL obtained from Figure 22-b as:

$$G_{pll}(s) = \frac{\hat{\theta}}{\theta} = \frac{\frac{V_{pcc\Delta}}{s}(k_{plf} + \frac{k_{ilf}}{s})}{1 + \frac{V_{pcc\Delta}}{s}(k_{plf} + \frac{k_{ilf}}{s})} = \frac{V_{pcc\Delta}(sk_{plf} + k_{ilf})}{s^2 + sV_{pcc\Delta}k_{plf} + V_{pcc\Delta}k_{ilf}} \tag{47}$$

which can be normalized as second order system. Hence, the controller parameters for PLL with bandwidth of α_{pll} tuned as:

$$\begin{aligned} k_{plf} &= \frac{2\xi\alpha_{pll}}{V_{pcc\Delta}} \\ k_{ilf} &= \frac{\alpha_{pll}^2}{V_{pcc\Delta}} \end{aligned} \tag{48}$$

where ξ is a damping factor and setting it to $1/\sqrt{2}$ would provide most favourable selection between overshoot and settling time [25].

3.8 Modulation and individual submodule capacitor voltage balancing

The reference signals generated by current controller are fed to the modulator to generate gate switching signals to obtain desired converter output voltage as close as possible

to the sinusoidal waveform. Moreover, this block performs the balancing of each individual submodule voltage based on sorting algorithm. In the following subchapters the operation principle of the given techniques explained in detail.

3.8.1 Nearest Level pulse Width Modulation (NL-PWM)

The modulation techniques applicable to multilevel converters can be divided into two main groups [16][19]:

- High Switching Frequency Modulation
- Fundamental Switching Frequency Modulation

Methods that utilize the switching frequency greater than 1 kHz and have many commutations of the power semiconductors during one period of the fundamental output voltage are high frequency switching frequency modulation techniques. Several high frequency modulation techniques that are based on well-known carrier-based sinusoidal Pulse Width Modulation (PWM) developed for application in multilevel converter applications. Examples of these methods are Phase-Shifter PWM, Level-Shifted PWM.

Fundamental frequency modulation techniques have the switching frequency such that PEDs have one or two commutation during one full cycle of the fundamental output voltage and generate stepwise output voltage waveform. Examples of these methods are Selective Harmonic Elimination, Nearest Vector Modulation and Nearest Level Modulation (NLM). In multilevel converter with high number of submodules the application of NLM has advantage of being conceptually simple and easiness to implement [19].

The operation principle of NLM based on approximation the output voltage to the desired voltage step wisely to the nearest possible voltage level. The output voltage approximated based on the following formula:

$$V_{VSC} = round(\frac{V_{DES}}{V_{dc}})V_{dc} \tag{49}$$

where $round(x)$ is the function of rounding the nearest integer, V_{VSC} and V_{DES} are correspondingly converter output and desired voltages, and V_{dc} is the DC-link capacitor voltage of the single submodule. The staircase voltage building may lead to capacitor-voltage unbalance because of using lower levels longer than higher levels [15]. To avoid energy unbalance in the submodules, individual submodule DC voltage balancing based on sorting algorithm is used which is described in next subchapter.

For given STATCOM a hybrid modulation technique that is the combination of NLM and PWM, or namely Nearest Level PWM (NL-PWM) is applied. The operation principle of

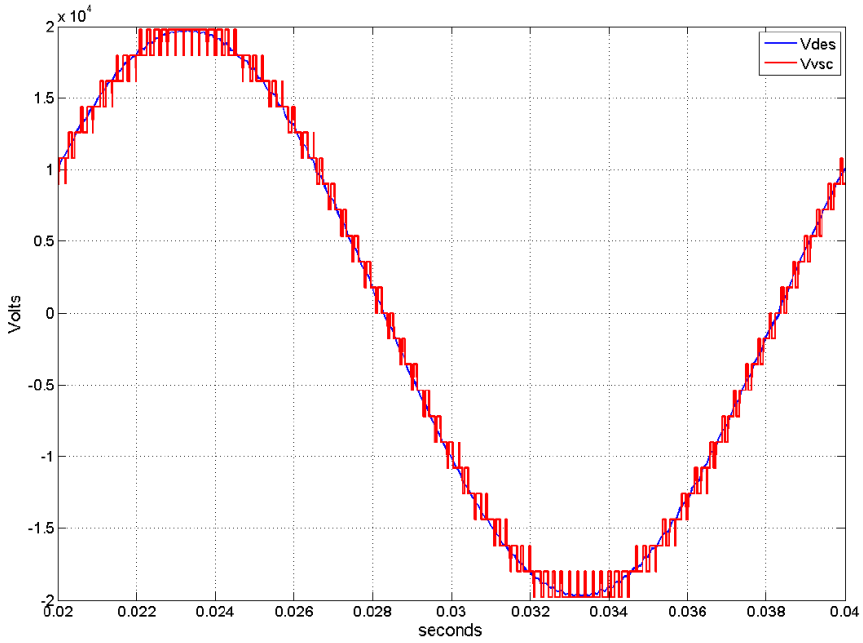

Figure 23. *Desired voltage and obtained converter output voltage waveforms with NL-PWM.*

the NL-PWM is same as NLM with the main exception that when voltage difference between the desired voltage V_{DES} and the converter output voltage V_{VSC} expressed by:

$$V_{diff} = V_{DES} - V_{VSC} \tag{50}$$

at k^{th} submodule is less than the capacitor voltage V_{dc}, k^{th} submodule is used in PWM. As result, the output voltage V_{VSC} becomes much closer to the sine wave. Figure 23 depicts the desired voltage and resulting converter output voltage waveforms when NL-PWM is applied.

3.8.2 Individual submodule capacitor voltage balancing

In previous calculations it was assumed that all capacitors are identical; hence, active power is equally shared among the submodules. However, small variations in capacitor characteristics will result in divergence of the DC-link voltages from their reference value. Hence, to keep capacitor voltages as close as possible to average value a control method to balance the capacitor energies is required. For this STATCOM voltage sorting strategy utilized to perform the individual submodule capacitor voltage balancing.

The sorting algorithm updates the state of each submodule with some f_{upd} frequency and depending on active power flow direction sorts these submodules according to their capacitor voltage in ascending or descending order. For example, when STATCOM absorbs active power from the grid the submodules are sorted in ascending order so that

the most discharged submodules switched on first, and the submodules sorted in descending order to discharge them first when STATCOM injects active power to the grid. By doing so, sorting control algorithm keeps the capacitor voltages close to the reference value without any extra control loop.

Even though use of sorting algorithm with NL-PWM may cause the increase in the average switching frequency due to constant submodules' state update and change of the submodule order, this method is very easy to implement and does not require separate control loop for each submodule.

3.9 Double Decoupled SRF-PLL (DDSRF-PLL)

Under ideal conditions which were assumed until now, the system voltage is stable and balanced. However, system voltage may be distorted by huge harmonic content and may be unbalanced due to i.e. fault. For STATCOM it is important to be able to track the positive sequence voltage magnitude and angle for reference frame transformation, synchronization etc. Moreover, the separation of positive and negative sequences makes it possible to control the positive- and negative-sequence currents independently.

Under unbalanced conditions SRF-PLL exhibits poor dynamics; hence, a method to be able accurately detect phase angle and extract positive and negative sequences is needed. This is possible using Double Decoupled SRF-PLL (DDSRF-PLL) [26]. DDSRF-PLL is an improved variant of SRF-PLL that has a decoupling network possible to detect and separate the positive and negative sequences and can quickly perform fast and accurate synchronization to positive sequence component under distorted and unbalanced system voltage conditions.

Under unbalanced conditions the positive and negative components of the system voltage in stationary reference frame can be expressed as:

$$\boldsymbol{v}^s = \begin{bmatrix} v_\alpha \\ v_\beta \end{bmatrix} = v_{\alpha\beta}^{+} + v_{\alpha\beta}^{-} = V^{+} \begin{bmatrix} \cos(\omega t + \varphi_{+}) \\ \sin(\omega t + \varphi_{+}) \end{bmatrix} + V^{-} \begin{bmatrix} \cos(-\omega t + \varphi_{-}) \\ \sin(-\omega t + \varphi_{-}) \end{bmatrix} \tag{51}$$

where V^+ and V^- are the correspondingly magnitudes of the positive and negative sequence voltage vectors, ω is the fundamental synchronous frequency and φ is the initial angle. It is obvious from the equation (51) $v_{\alpha\beta}^{+}$ rotates counter clockwise direction with angular frequency ω, and $v_{\alpha\beta}^{-}$, rotates clockwise direction with angular frequency ω.

Hence, in *dq*-domain the positive and negative sequence voltage components can be expressed as two rotating reference axes:

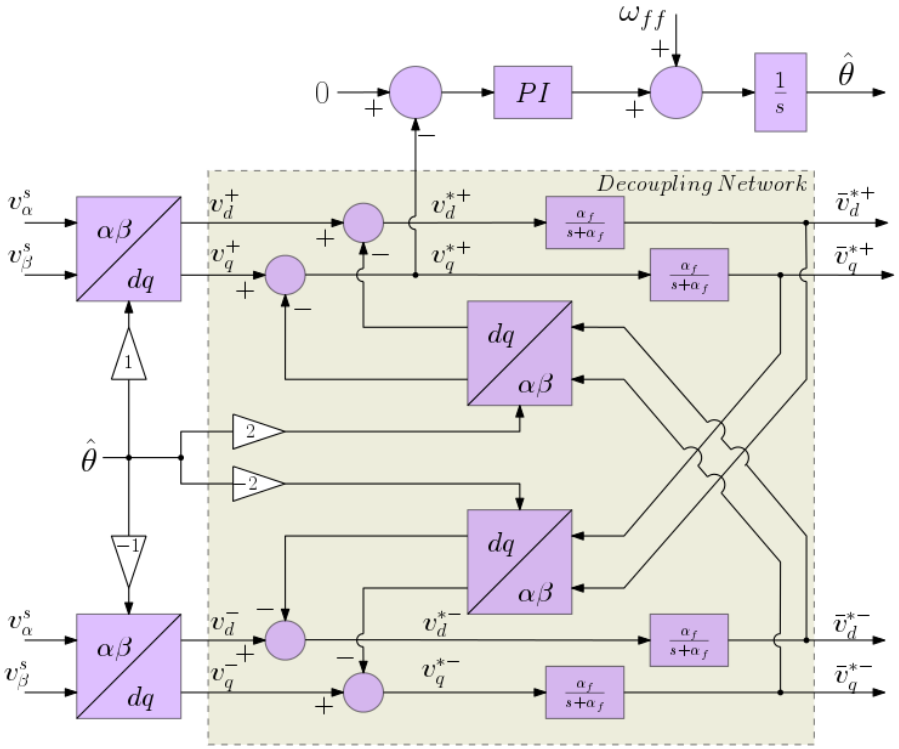

Figure 24. *Block diagram of DDSRF-PLL.*

$$\boldsymbol{v}_{dq}^{+} = \begin{bmatrix} v_d^+ \\ v_q^+ \end{bmatrix} = \left[T_{dq}^{+}\right]\begin{bmatrix} v_\alpha^+ \\ v_\beta^+ \end{bmatrix} = V^+\begin{bmatrix} 1 \\ 0 \end{bmatrix} + V^-\begin{bmatrix} \cos(-2\omega t) \\ \sin(-2\omega t) \end{bmatrix}$$
$$\boldsymbol{v}_{dq}^{-} = \begin{bmatrix} v_d^- \\ v_q^- \end{bmatrix} = \left[T_{dq}^{-}\right]\begin{bmatrix} v_\alpha^- \\ v_\beta^- \end{bmatrix} = V^+\begin{bmatrix} \cos(2\omega t) \\ \sin(2\omega t) \end{bmatrix} + V^-\begin{bmatrix} 1 \\ 0 \end{bmatrix} \quad (52)$$

where the transformation matrix T for an angle ωt is:

$$\left[T_{dq}^{+}\right] = \left[T_{dq}^{-}\right]^T = \begin{bmatrix} \cos(\omega t) & \sin(\omega t) \\ -\sin(\omega t) & \cos(\omega t) \end{bmatrix} \quad (53)$$

From equation (52) it is clear that positive and negative sequences are cross-coupled between each other in the *dq*-frame. This cross-coupling results in appearance of the positive sequence as AC component oscillating with 2ω frequency in dq^- and the negative sequence oscillates with -2ω frequency in dq^+. Therefore, a decoupling network is used to remove oscillating components and to extract the fundamental frequency positive and negative sequence voltage components as DC values.

The combination of the SRF-PLL and decoupling network along with Low Pass Filter (LPF) is depicted in the Figure 24. The calculated value of the v_q^{*+} is fed as input to SRF-PLL to synchronize the system to the positive sequence voltage and to detect the positive sequence voltage angle. The LPF is used to filter out quadruple frequency components that exist in decoupling network outputs and represents a simple low pass filter with bandwidth of α_f:

$$\mathrm{LPF(s)} = \frac{\alpha_f}{s+\alpha_f} \tag{54}$$

Thus, the transfer function of the measured positive and negative sequence components are:

$$\begin{aligned}
\overline{\boldsymbol{v}}_{dq}^{*+} &= \begin{bmatrix}\bar{v}_d^{*+}\\ \bar{v}_q^{*+}\end{bmatrix} = \begin{bmatrix}\frac{\alpha_f}{s+\alpha_f} & 0\\ 0 & \frac{\alpha_f}{s+\alpha_f}\end{bmatrix}\left\{\begin{bmatrix}v_d^{+}\\ v_q^{+}\end{bmatrix} - \begin{bmatrix}\cos(2\omega t) & \sin(2\omega t)\\ -\sin(2\omega t) & \cos(2\omega t)\end{bmatrix}\begin{bmatrix}\bar{v}_d^{*-}\\ \bar{v}_q^{*-}\end{bmatrix}\right\}\\
\overline{\boldsymbol{v}}_{dq}^{*-} &= \begin{bmatrix}\bar{v}_d^{*-}\\ \bar{v}_q^{*-}\end{bmatrix} = \begin{bmatrix}\frac{\alpha_f}{s+\alpha_f} & 0\\ 0 & \frac{\alpha_f}{s+\alpha_f}\end{bmatrix}\left\{\begin{bmatrix}v_d^{-}\\ v_q^{-}\end{bmatrix} - \begin{bmatrix}\cos(2\omega t) & -\sin(2\omega t)\\ \sin(2\omega t) & \cos(2\omega t)\end{bmatrix}\begin{bmatrix}\bar{v}_d^{*+}\\ \bar{v}_q^{*+}\end{bmatrix}\right\}
\end{aligned} \tag{55}$$

3.10 Zero Sequence Current Injection (ZSCI) under unbalanced conditions

The operation of STATCOM in unbalanced grid conditions will cause the flow of the negative sequence current inside its branches. Since MMC STATCOM does not have a common DC capacitor, the flow of the negative sequence current will lead to unequal active power distribution among the phases. This unequal active power distribution will result in deviation of the DC-link capacitor voltages. Hence, to prevent the asymmetrical active power distribution in phases and to keep the DC capacitor voltage balance, a method to control the negative sequence current is required. For MMC STATCOM the strategy to balance the phase active power based on injection of zero sequence component is used [21][27]. For delta connected configuration a method called Zero Sequence Current Injection (ZSCI) applied, which injects zero sequence current circulating inside delta branch to regulate the negative sequence current.

For system given in Figure 15 if unbalanced grid conditions assumed the phasors of the STATCOM phase voltages and currents with zero-sequence current injection can be given as:

$$\begin{aligned}
&\vec{V}_{stab} = \hat{V}^{+}\angle\theta_v^{+} + \hat{V}^{-}\angle\theta_v^{-}\\
&\vec{V}_{stbc} = \hat{V}^{+}\angle(\theta_v^{+} - \tfrac{2\pi}{3}) + \hat{V}^{-}\angle(\theta_v^{-} + \tfrac{2\pi}{3})\\
&\vec{V}_{stca} = \hat{V}^{+}\angle(\theta_v^{+} + \tfrac{2\pi}{3}) + \hat{V}^{-}\angle(\theta_v^{-} - \tfrac{2\pi}{3})\\
&\vec{I}_{ab} = \hat{I}^{+}\angle\delta_i^{+} + \hat{I}^{-}\angle\delta_i^{-} + \hat{I}^{0}\angle\alpha_0\\
&\vec{I}_{bc} = \hat{I}^{+}\angle(\delta_i^{+} - \tfrac{2\pi}{3}) + \hat{I}^{-}\angle(\delta_i^{-} + \tfrac{2\pi}{3}) + \hat{I}^{0}\angle\alpha_0\\
&\vec{I}_{ca} = \hat{I}^{+}\angle(\delta_i^{+} + \tfrac{2\pi}{3}) + \hat{I}^{-}\angle(\delta_i^{-} - \tfrac{2\pi}{3}) + \hat{I}^{0}\angle\alpha_0
\end{aligned} \tag{56}$$

where $\hat{V}^{+}$ and $\hat{V}^{-}$ are respectively rms magnitudes of the positive- and negative-sequence STATCOM voltage phasors, $\hat{I}^{+}$ and $\hat{I}^{-}$ rms magnitudes of the positive- and

negative-sequence STATCOM current phasors and $\hat{I}^0\angle\alpha_0$ is the phasor of the zero current phasor circulating inside delta branches.

Under normal conditions the zero-sequence components are equal to zero; however, by injecting zero-sequence current it is possible to control negative-sequence current. ZSCI method provides two degrees of freedom in terms of the injected zero current amplitude $\hat{I}^0$ and angle α_0. Hence, the purpose is to obtain the values of the zero-sequence such that it will remove the unequal active power distribution due to interaction of the between sequences. The average active power in phases *a* and *b* for unbalanced case with zero-sequence current injection expressed as:

$$P_a = Re\left(\vec{V}_{stab}\vec{I}^*_{ab}\right) = \hat{V}^+\hat{I}^+\cos(\theta_v^+ - \delta_i^+) + \hat{V}^-\hat{I}^-\cos(\theta_v^- - \delta_i^-) + \hat{V}^+\hat{I}^-\cos(\theta_v^+ - \delta_i^-) + \hat{V}^-\hat{I}^+\cos(\theta_v^- - \delta_i^+) + \hat{V}^+\hat{I}^0\cos(\theta_v^+ - \alpha_0) + \hat{V}^-\hat{I}^0\cos(\theta_v^- - \alpha_0) \quad (57)$$

$$P_b = Re\left(\vec{V}_{stbc}\vec{I}^*_{bc}\right) = \hat{V}^+\hat{I}^+\cos(\theta_v^+ - \delta_i^+) + \hat{V}^-\hat{I}^-\cos(\theta_v^- - \delta_i^-) + \hat{V}^+\hat{I}^-\cos\left(\theta_v^+ - \delta_i^- - \frac{4\pi}{3}\right) + \hat{V}^-\hat{I}^+\cos\left(\theta_v^- - \delta_i^+ + \frac{4\pi}{3}\right) + \hat{V}^+\hat{I}^0\cos\left(\theta_v^+ - \alpha_0 - \frac{2\pi}{3}\right) + \hat{V}^-\hat{I}^0\cos(\theta_v^- - \alpha_0 + \frac{2\pi}{3}) \quad (58)$$

the first two terms in equations (57) and (58) are the expressions for the positive and negative sequence active power which can be controlled by common DC-link voltage controller. The third and fourth terms in the equations (57) and (58) that consists of combination of positive and negative-sequence components stand for active power, which lead to unequal active power distortion among the phases. The last two terms represent the active power generated by zero sequence current, which are used to eliminate the active power distortion caused by sequence interaction. Hence, if the items $\hat{V}^+\hat{I}^+$ and $\hat{V}^-\hat{I}^-$ omitted, then the equations (57) and (58) after some trigonometrical manipulations can be written as [27]:

$$\hat{I}^0 k_1 cos\alpha_0 + \hat{I}^0 k_2 sin\alpha_0 = -k_3 \quad (59)$$

$$\hat{I}^0 k_4 cos\alpha_0 + \hat{I}^0 k_5 sin\alpha_0 = -k_6 \quad (60)$$

where

$$k_1 = \hat{V}^+\cos\theta_v^+ + \hat{V}^-\cos\theta_v^- \quad (61)$$

$$k_2 = \hat{V}^+\sin\theta_v^+ + \hat{V}^-\sin\theta_v^- \quad (62)$$

$$k_3 = \hat{V}^+\hat{I}^-\cos(\theta_v^+ - \delta_i^-) + \hat{V}^-\hat{I}^+\cos(\theta_v^- - \delta_i^+) \quad (63)$$

$$k_4 = \hat{V}^+\cos(\theta_v^+ - \frac{2\pi}{3}) + \hat{V}^-\cos(\theta_v^- + \frac{2\pi}{3}) \quad (64)$$

$$k_5 = \hat{V}^+\sin(\theta_v^+ - \frac{2\pi}{3}) + \hat{V}^-\sin(\theta_v^- + \frac{2\pi}{3}) \quad (65)$$

$$k_6 = \hat{V}^+\hat{I}^-\cos\left(\theta_v^+ - \delta_i^- - \frac{4\pi}{3}\right) + \hat{V}^-\hat{I}^+\cos\left(\theta_v^- - \delta_i^+ + \frac{4\pi}{3}\right) \quad (66)$$

Thus, by solving the equations (59) and (60) the phase angle and amplitude of the required zero-sequence current obtained as:

$$\alpha_0 = \tan^{-1}\left(\frac{k_1 k_6 - k_3 k_4}{k_3 k_5 - k_2 k_6}\right) \quad (67)$$

$$\hat{I}^0 = \frac{-k_3}{k_1 cos\alpha_0 + k_2 sin\alpha_0} = \frac{-k_6}{k_4 cos\alpha_0 + k_5 sin\alpha_0} \quad (68)$$

4. MMC STATCOM OPERATION IN WEAK GRID

4.1 Introduction

Power system's ability to maintain its voltage during disturbance (i.e. fault or fluctuation in supply or demand) is determined by system strength. The system strength is usually expressed by the short circuit capacity, the maximum amount of the current a grid can provide at a given point when three-phase to ground fault happens. Short circuit capacity measured in MVA and is a product of fault current with the pre-fault voltage [28]. Short circuit capacity of the system is inversely proportional to the Thevenin equivalent impedance and for any given bus i can be calculated as:

$$S_{SC,i} = \frac{V_i^2}{Z_{th,i}} \tag{68}$$

where $S_{SC,i}$ is short circuit capacity, V_i is the voltage and $Z_{th,i}$ is the equivalent Thevenin impedance at bus *i* respectively. Sometimes grid strength is quantified as Short Circuit Ratio (SRC), the ratio of the available short circuit power at the particular bus to the power rating of the interconnecting equipment (i.e. generator, load, FACTS or HVDC converters).

Depending on strength grids are classified as strong or "stiff" and weak grid. Strong grid is a type of grid with many synchronous machines that provide high short circuit capacity. This means if fault happens at any bus in strong grid, it is capable to maintain the voltage at other buses within its limits. Weak grid on the other hand has low short circuit capacity and can be modelled as connection to the source via high impedance. Grid with $SCR < 3$ considered to be weak and grids $SCR < 2$ are very weak grids [29].

Most of the power electronic equipment does not contribute to system strength as much as synchronous generation [30]. Therefore, high penetration of power electronic devices with no increase or decrease in synchronous generation decreases the system strength thus brings the challenge to the system [30]. In case of weak grid this challenge expressed in terms of voltage transients and variations, voltage stability and system stability. Overall the challenges of the VSC operation in weak grid can be divided into two categories:

- Deterioration of the weak grid stability due to VSC operation. The voltage stability impaired due to high dV/dQ sensitivity of the weak grid, integration of power electronic equipment with fast dynamic response to voltage change may lead to un-

damped voltage oscillations. Due to limited power transfer capabilities the power exchange between grid and VSC is also limited [31][32][33].

- Negative impact of the weak grid on the VSC performance. The interaction of the high grid impedance with the inner control dynamics of the degrades the stability of the VSC. VSC designed to operate in strong grid has very good performance and its outer loop controllers keep excellent tracking of the power and voltage references. However, in weak grids with the initial gains outer loop controllers become faster than inner loop controller which lead to instability. Another major issue is the performance of the SRF-PLL in the weak grid that brings poor synchronization which will be explained in more details in the next subchapter. PLL dynamics influence the performance of the current controllers [34] and DC link controller [35].

4.2 PLL Self-synchronization in weak grid

VSC proper waveform generation relies on the grid, hence, synchronization is important for stable operation. SRF-PLL explained in the previous chapters provides very robust synchronization to the grid voltages when operated in strong grids. However, under weak grid conditions the dynamics of the SRF-PLL are impaired which impacts the control system stability. Interaction of the PLL with the high grid impedance lead to self-synchronization of the PLL [36][37].

Figure 25 depicts single line diagram of the VSC utilizing PLL operating in the weak grid. Weak grid is represented by its Thevenin equivalent model where ideal voltage source $\boldsymbol{V_g}$ is connected in series with high grid impedance Z_g. Due to complex dynamics the terminal voltage V_t consists of two components:

$$\boldsymbol{V}_t = \boldsymbol{V}_g + R_g \boldsymbol{I}_c + L_g \frac{d\boldsymbol{I}_c}{d(\omega_0 t)} \tag{69}$$

where R_g and $L_g$are respectively grid resistance and inductance, $\boldsymbol{I}_c$ is converter output current and $\omega_0$is the angular speed of the grid. In the weak grid as it can be observed from this equation the terminal voltage is highly influenced by the converter output current.

The output current dynamics determined by the current references controlled by current controller and PLL. Since the bandwidth of the current controller is higher than PLL's bandwidth, current controller dynamics can be neglected. Therefore, converter output current in the stationary reference frame can be expressed as:

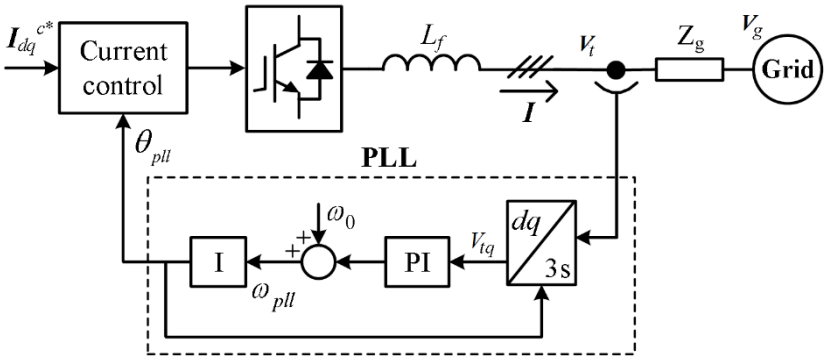

Figure 25. *Equivalent model of VSC connected to weak grid. Adapted from [37].*

$$\boldsymbol{I}_c = \left(i_{cd}^* + ji_{cq}^*\right)e^{j\theta_{pll}} \tag{70}$$

where θ_{pll} is the PLL measured angle. Based on (70) converter can be modelled as the constant current source with the output current affected by the PLL dynamics.

By combining equations (69) and (70) the terminal voltage can be expressed as:

$$\boldsymbol{V}_t = V_g + (R_g + j\frac{\omega_{pll}}{\omega_0}X_g)I_c \tag{71}$$

where ω_{pll} is the instantaneous rotational speed of PLL.

Due to high grid impedance current injected by converter will introduce “self-synchronization” loop to the PLL synchronization process as it can be observed from the Figure 26. From the Figure 26 it is obvious that PLL measured angle θ_{pll} is dependent on the sensed *q* component of the terminal voltage in the PLL reference frame V_{tq}^c. By use of the inverse Park’s transformation V_{tq}^c can be expressed as:

$$V_{tq}^c = Imag(V_t e^{-j\theta_{pll}}) \tag{72}$$

The equation (71) in stationary reference frame can be written as:

$$V_t = V_g e^{j\theta_g} + (R_g + j\frac{\omega_{pll}}{\omega_0}X_g)\left(i_{cd}^* + ji_{cq}^*\right)e^{j\theta_{pll}} \tag{73}$$

Combination of (72) and (73) will give the following:

$$V_{tq}^c = X_g i_{cd}^* \frac{\omega_{pll}}{\omega_0} + R_g i_{cq}^* + V_g \sin(\theta_g - \theta_{pll}) \tag{74}$$

As it is seen from the equation (74) converter sensed *q*-component of the terminal voltage V_{tq}^c is influenced by grid impedance and converter output current. Sensed *q*-component in equation (74) is not same as in equation (45) thus linearization as in equation

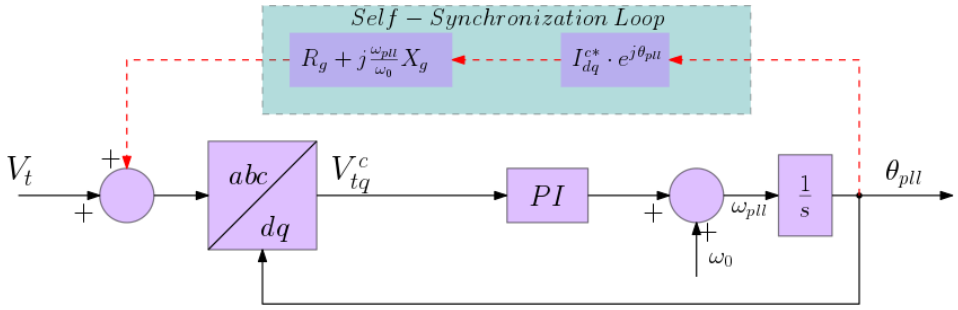

Figure 26. *SRF-PLL synchronization process in weak grid.*

(46) does not hold anymore. Therefore, it can be concluded that PLL measured angle is influenced by the converter output current. Consequently, during VSC operation in the weak grid due to interaction with the grid impedance converter loses the synchronization with the grid. To reduce the negative effects of the high grid impedance and to remove the self-synchronization effect of the PLL some methods are proposed. The reduction of the PLL bandwidth makes PLL slower; hence, its performance is less prone to large angle changes [32]. Another method that is proposed is to measure the grid impedance and compensation of this measured grid impedance removes the effect of the self-synchronization loop and provides synchronization to stronger point of the grid [38][39][40]. Finally, a method based on current error compensation for the PLL and voltage measurements for VSC operating in the grid conditions is suggested in [41].

Equation (74) shows that exchange of active power between grid and converter leads towards the self-synchronization. However, in case of STATCOM there is only reactive power exchange between the grid and converter. Since R_g is usually small compared to X_g hence it can be neglected, equation (74) can be simplified as:

$$V_{tq}^c \approx V_g \sin(\theta_g - \theta_{pll}) \tag{75}$$

Based on the equation (75) it can be concluded that STATCOM operation in the weak grid should not cause any PLL self-synchronization issues. Therefore, during operation in weak grid the PLL should not erode the control performance of the STATCOM. To prove this and explore any other factors that affect the STATCOM operation in the weak grid, STATCOM model will be simulated in weak grid conditions in the Matlab/Simulink environment. Next subchapter will present simulation model and model parameters.

4.3 STATCOM weak grid simulation model

To investigate the operating limits and the control system behavior of the STATCOM in the weak grid conditions the model implemented in the MATLAB/Simulink environment was simulated. Since the purpose of the simulations was to test the control system of the STATCOM in the weak grid conditions Thevenin equivalent network model was used. Thevenin equivalent model consists of ideal voltage source and equivalent impedance which can be changed to vary Short Circuit Level (SCL). Single line diagram of the given system is depicted in the Figure 27 and the circuit parameters are provided in Table 1. MMC STATCOM with rating of 100 MVA and consisting of delta connected 40 submodules connected to weak grid via step-down transformer. A passive High Frequency (HF) filter with 7.7 MVA rated power to filter out 11^{th} harmonic is connected to medium voltage side. Since simulated grid cases were weak and very weak, HF filter rating had very great impact on the PCC voltage magnitude. Hence, for simulations depending on the SCL, the grid source voltage was adjusted so that PCC voltage was equal to $1.0\ pu$. The adjusted source voltage values are given in the Table 2.

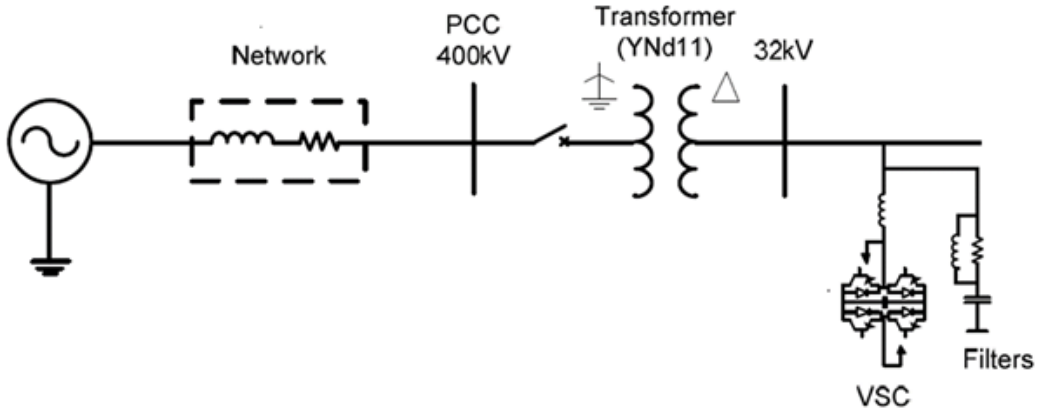

Figure 27. *Single line diagram of the simulated model.*

Since the purpose of the simulations was to study the effects of the weak grid on the STATCOM control performance, initially for SCLs given in the Table 2 STATCOM operating as constant current source was performed. STATCOM operating limits and factors limiting stable operation in the weak grid were identified. A possible solution for given issues was provided. Next STATCOM for the same SCLs was simulated in voltage regulation mode. Likewise, the limiting factors were identified, and solution was proposed. Finally, STATCOM response and control system performance during the faults were simulated. Chapter 5 presents the simulation results.

Table 1. *Simulated grid and STATCOM parameters.*

Parameter	**Value**
Grid	
Voltage, line-to-line	400 kV (rms)
Frequency	50 Hz
X/R ratio	14
Transformer	
Rating	225 MVA
Secondary side voltage	32 kV (rms)
Configuration	YNd11
Leakage reactance	0.0925 pu
HF Filter	
Rating	7.7 MVAr
Tuned frequency	550 Hz
STATCOM	
Rating	100 MVA
Number of submodules	40

Table 2. *Normalized source voltage corresponding to each simulated SCL.*

SCL (MVA)	400	350	300	250	200	150	100	75	50	35
Source Voltage (pu)	0.982	0.979	0.976	0.972	0.965	0.953	0.929	0.9055	0.858	0.797

5. SIMULATION RESULTS

5.1 Introduction

This chapter provides simulation results of the STATCOM model presented in Chapter 4 operating in the weak and very weak grid conditions. The simulation consists of 3 parts; 1) STATCOM constant current operation mode, 2) STATCOM operation in voltage regulation mode and 3) STATCOM operation performance during faults.

In the initial case STATCOM was simulated in constant current mode and the operation limits for capacitive and inductive mode were obtained. The effect of the weak grid on STATCOM stability was studied and solution to enhance the operation limits were suggested. In the same way factors that restrict the STATCOM operation in voltage regulation mode were investigated. It was found out that HF filter has significant impact on the STATCOM operation and at some SCLs resonance happens. Finally, STATCOM control system's behavior during symmetrical and asymmetrical faults in weak grid conditions was explored.

5.2 STATCOM operation as constant current source

In this case the purpose was to study the stability of the STATCOM operating as a constant current source in weak and very weak grid conditions, to obtain the factors that limit the STATCOM operation in weak grid and to identify possible solution for these issues. In the constant current mode voltage controller of the STATCOM is switched off and there is no feedback to regulate the grid voltage. Therefore, in this mode of operation STATCOM will supply the amount of reactive power that is manually pre-set irrespective of the grid voltage magnitude. Constant current mode simulations consist of two parts; STATCOM operation as 1) a constant capacitive current source and 2) a constant inductive current source.

5.2.1 Constant capacitive current mode

In the given case STATCOM was simulated as constant current source for each of the SCL given in the Table 2. For each of these SCLs Figure 28 depicts the maximum amount of the capacitive current STATCOM is capable to supply to the grid without causing any stability issues. As it can be observed from the given figure for grids with SCL

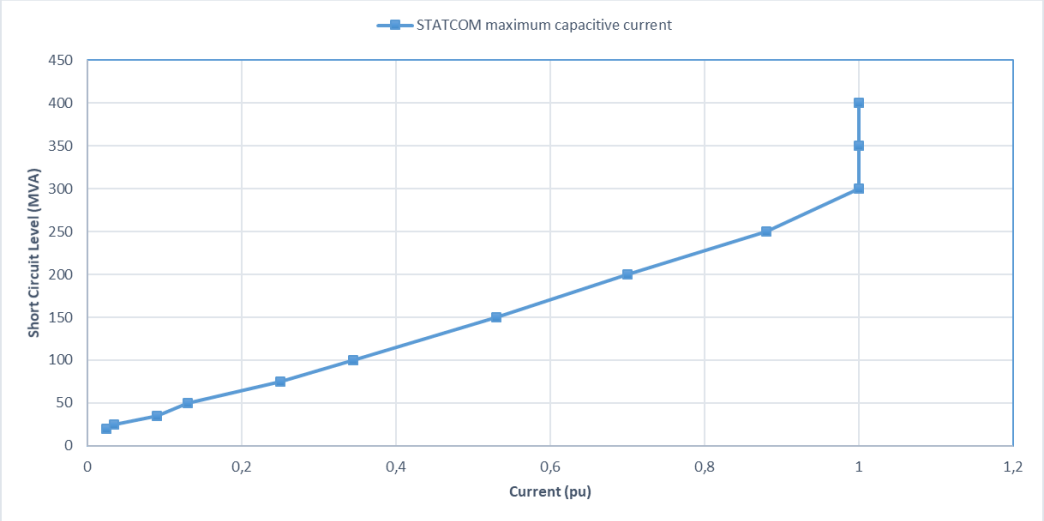

Figure 28. *Maximum capacitive current STATCOM capable to supply versus grid strength.*

lower than 300 MVA STATCOM is not capable to supply full rated current to the grid. Also, the lowest SCL STATCOM capable to operate without any stability issues was found to be 20 MVA. For SCL below 20 MVA the initial connection of the STATCOM to the grid and charge of the capacitors results in synchronization loss and overall system instability. DDSRF-PLL measurements for SCL = 15 MVA of the grid voltage *dq*-components and instantaneous HV voltage waveforms are depicted in the Figure 29. As it can be observed from these waveforms when the STATCOM is initially connected at time $t = 0.2\ sec$ the overall system becomes unstable and the grid voltage becomes distorted.

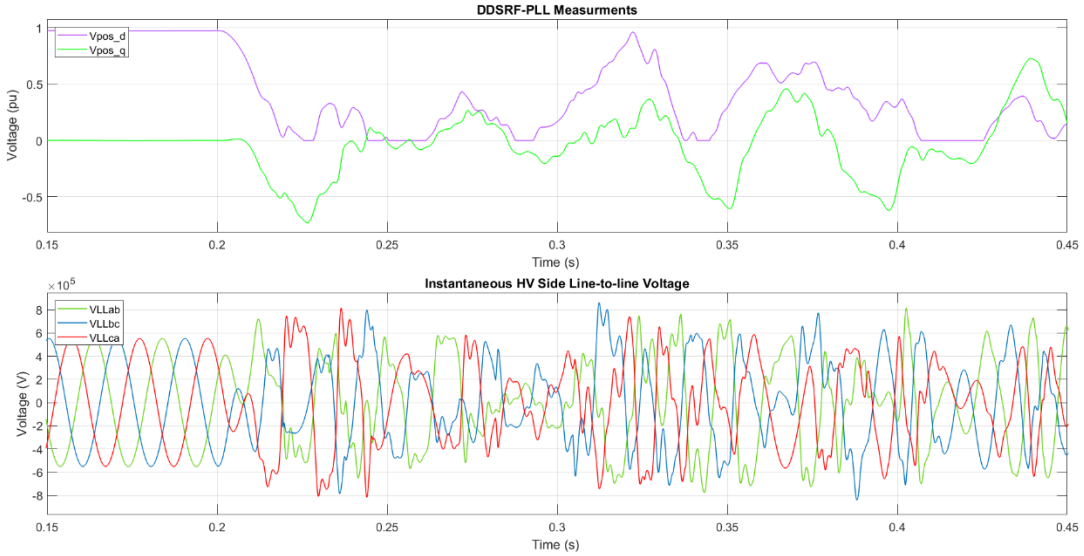

Figure 29. *Estimated positive and negative sequence components of the grid voltage and HV side line-to-line voltage waveforms for SCL = 15 MVA.*

Simulations showed that for SCLs below 300 MVA STATCOM is not capable to supply fully rated power to the system. If the supplied current was above the limit mentioned in Figure 28, the harmonic content would appear in the grid voltage and the voltage waveform becomes distorted. To demonstrate the effect of the high capacitive current on the voltage waveforms, a case when STATCOM provides $0.85\ pu$ capacitive current to the grid with strength of 200 MVA was simulated. Figure 30 illustrates the estimated fundamental frequency positive and negative sequence components of the grid voltage and grid voltage waveforms. From these waveforms it is obvious that high current supplied by STATCOM during $0.2\ sec \leq t \leq 0.45\ sec$ time interval causes the grid voltage distortion.

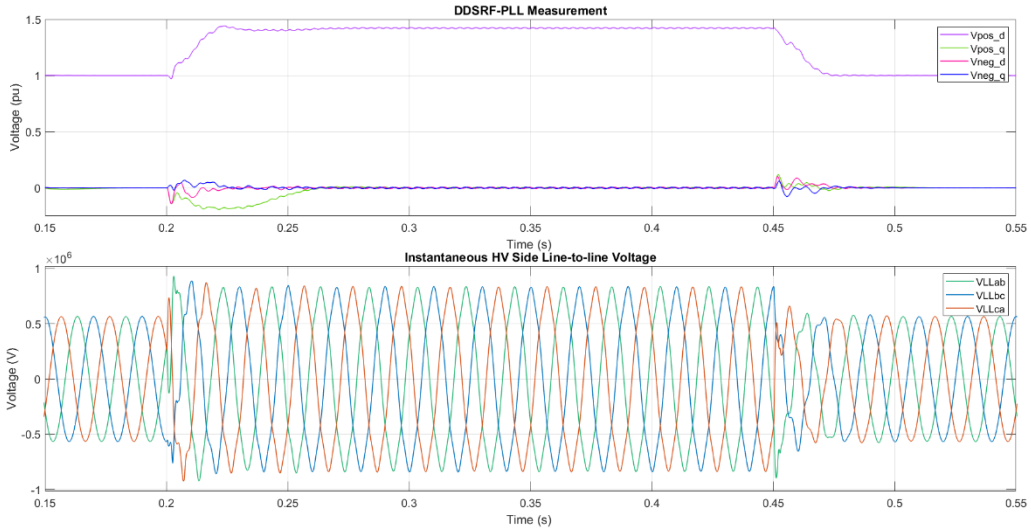

Figure 30. *Estimated positive and negative sequence components of the grid voltage and HV side line-to-line voltage waveforms for 0.85 pu capacitive current supply in 200 MVA grid.*

During the simulations it was noticed that in capacitive mode grid voltages start to deviate from the ideal sinusoidal whenever the magnitude of the grid voltage at PCC exceeds $1.352\ pu$. The explanation behind this issue is the DC link capacitor voltage available which is limited by the amount of the available submodules. When the STATCOM operates in the weak grid and supplies high amount of the reactive power PCC voltage rises significantly. Since the output voltage of the converter is created from the DC link capacitor voltage and simply can be expressed as:

$$V_c = mV_{DCref} \tag{76}$$

where V_c is converter output voltage, m is modulation index and V_{DCref} is the charged capacitor voltage level which in our case is equal to $1.352\ pu$. Hence, for grid voltage rise above $1.352\ pu$ value, STATCOM is not capable to generate sinusoidal waveforms

and as result it generates distorted waveforms consequently supplying harmonics to the grid as it is depicted in Figure 30.

Figure 31 shows DC link voltage level, STATCOM modulator created reference voltage waveforms $V_{ref}$and the resulting converter output voltages. As it can be observed from the figure during the STATCOM operation modulator generated voltage V_{ref} exceeds the DC link voltage level. However, STATCOM does not have enough DC link voltage to create the output voltage with the correct peak value. Thus, STATCOM cannot generate sinusoidal voltage waveforms and this results in harmonic injection to the system.

In the next simulation case the DC link voltage was increased to $1.5\ pu$ and STATCOM was simulated in very weak grid with SCL equal to 150 MVA and STATCOM supplied $0.6\ pu$ capacitive current to the grid $0.2\ sec \leq t \leq 0.45\ sec$ time interval. With the original parameters the maximum amount of current STATCOM is capable to supply to the grid with this strength is equal to $0.53\ pu$ as it can be checked from the Figure 28. Figure 32 depicts the DC link voltage level, modulator generated V_{ref} reference voltages and grid voltages for case with higher DC link voltage reference. Since there is enough DC voltage available, modulator generated voltage references does not exceed it. Consequently, STATCOM is capable to supply higher current without any grid voltage distortion as it can be observed from Figure 32. Therefore, DC link voltage level plays critical in the capacitive mode operation and for proper operation STATCOM must avoid the rising of the PCC voltage above this level.

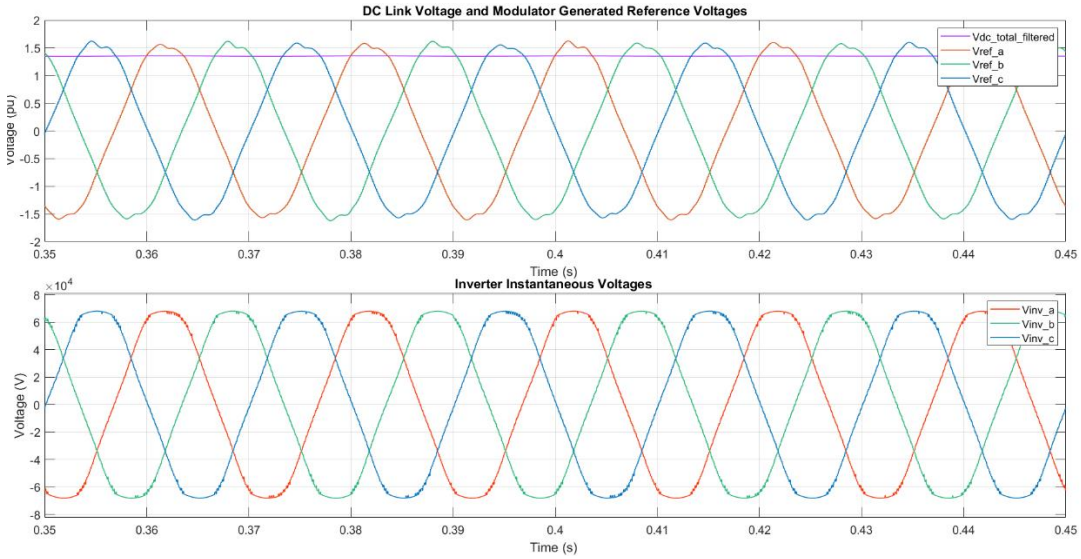

Figure 31. *DC link voltage, modulator reference voltages and corresponding VSC output voltages for 0.85 pu capacitive current supply in 200 MVA grid.*

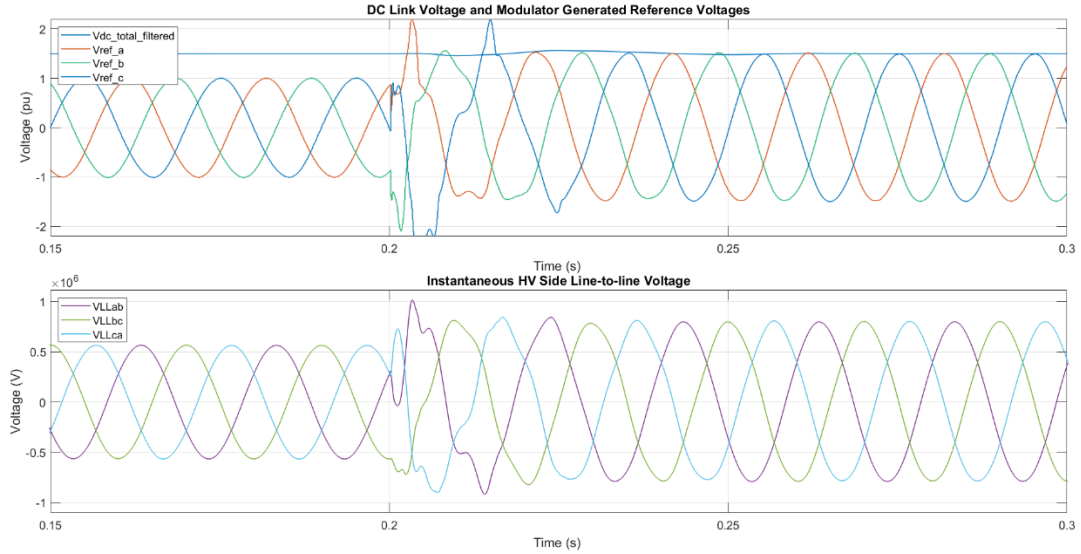

Figure 32. *DC link voltage, modulator reference voltages and HV line-to-line voltages for STATCOM supplying 0.6 pu capacitive current in 150 MVA grid, V_{dc} = 1.5 pu.*

However, high voltage rise due capacitive current supply should not be an issue for the STATCOM as its task is to maintain the system voltage typically in range of $0.9\,pu \leq V_{pcc} \leq 1.1\,pu$. Thus, in case of large voltage drop, STATCOM is capable to supply full rated power to the grid to bring voltage back to the safe operation range.

A case when large voltage dip occurs in grid with 200 MVA SCL was simulated, to show that STATCOM without any DC link voltage modifications is capable to supply full rated

power to the grid. In the given case the system voltage during $0.15\ sec \leq t \leq 0.45\ sec$ time interval drops to 0.75 pu and STATCOM is switched on during $0.2\ sec \leq t \leq 0.45\ sec$ time interval and supplies full rated capacitive current to the grid. Figure 33 shows the resulting grid line-to-line voltage and line current waveforms. As it is depicted in this figure, the grid voltage drops at time $t = 0.15\ sec$ to 0.75 value and during $0.2\ sec \leq t \leq 0.4\ sec$ time interval STATCOM supplies full rated power. Since the STATCOM is operated in the constant current mode there is no feedback to control the voltage. Consequently, high initial current supply at $t = 0.2\ sec$ creates voltage distortion and some time is required for transient to disappear and grid voltages to settle.

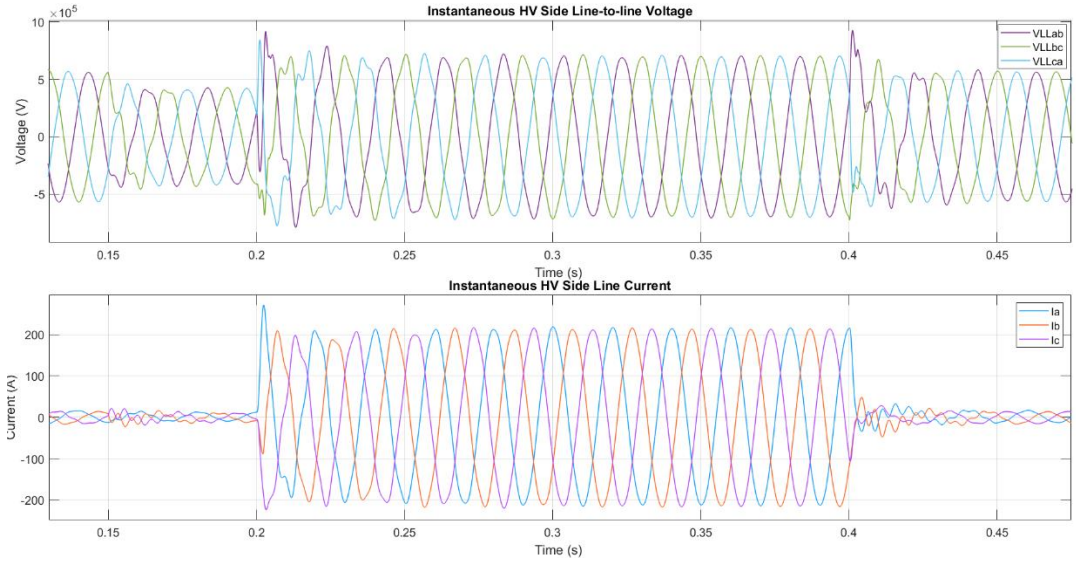

Figure 33. *HV side line-to-line voltage and line current waveforms for STATCOM supplying 1 pu capacitive current to 200 MVA grid.*

Figure 34 depicts the estimated voltage *dq* components and frequency measurements, DC link voltages and current references generated by the current controller. Measured grid voltage *dq*-components show that after transient the grid voltage settles at $1.24\ pu$ value. DC link controller operates normally as it can be observed from DC link voltage waveforms. When the STATCOM starts to supply current, the current quadrature reference I_{q_ref} as it can be observed from the current reference graph in Figure 34 is limited and as a result this limitation causes some distortion in the grid voltage waveforms. This limitation is caused by high zero sequence I_0current requirement by STATCOM to balance its branches due to initial voltage disturbance. To limit total STATCOM current supply below $1\ pu$, the required I_0 is subtracted from the I_{q_ref}. Once the STATCOM phase branches are balanced, which happens at time at $t \approx 0.28\ sec$, the full rated current is supplied to the grid and grid voltages stabilize at $1.24\ pu$ value as depicted in Figure 33 and Figure 34.

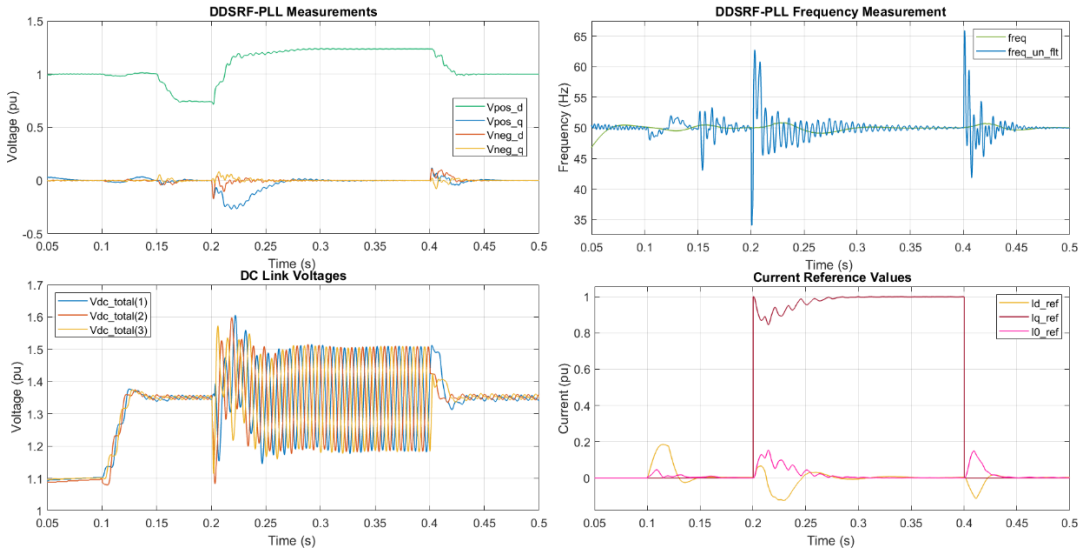

Figure 34. *DDSRF-PLL voltage and frequency measurements, DC link voltages and generated current references for STATCOM supplying 1 pu capacitive current to 200 MVA grid.*

Hence, based on the previous simulations it is possible to conclude that STATCOM is capable to supply full rated reactive power to weak and very weak grids without any issues to the system stability as long as the grid voltage does not exceed DC link voltage level. Therefore, in case of fault in weak grid STATCOM is capable to support the system with injecting reactive power.

Another aspect that needs to be considered during weak grid operation is the impact of the passive HF filter to the PCC voltage level and voltage transients during initial current injection by STATCOM. With the decrease of the grid strength the voltage rise due to HF filter reactive power contribution increases significantly. A case to show the impact of the HF filter on the PCC voltage in very weak grid when source voltage is not normalized and equal to $Vs = 1.0\,pu$ was simulated. In this case STATCOM operates in 100 MVA grid and supplies $0.1\,pu$ current and Figure 35 illustrates the estimated *dq*-components of the grid voltage and grid voltage waveforms. When STATCOM was in idle mode the voltage at PCC due to relatively high reactive power supply by HF filter rises to $V_{PCC} = 1.08\,pu$ and further rises when STATCOM starts to supply current to unstable levelsfrom control point of view. Moreover, as it can be observed from the given waveforms time required for transient to disappear when STATCOM starts and stops to supply reactive power is more. Also, the grid voltage distortion during these transients is higher and for lower SCLs it gets more severe.

Figure 36 shows measurements of positive sequence *d* component of the grid voltage for two cases when the STATCOM was supplying $0.1\,pu$ and $0.15\,pu$ capacitive current to the 75 MVA grid. As it can be observed from these measurements the time required

to clear out the transient is getting greater and higher current injection causes more harmonic content to appear and consequently higher amplitude of the transient.

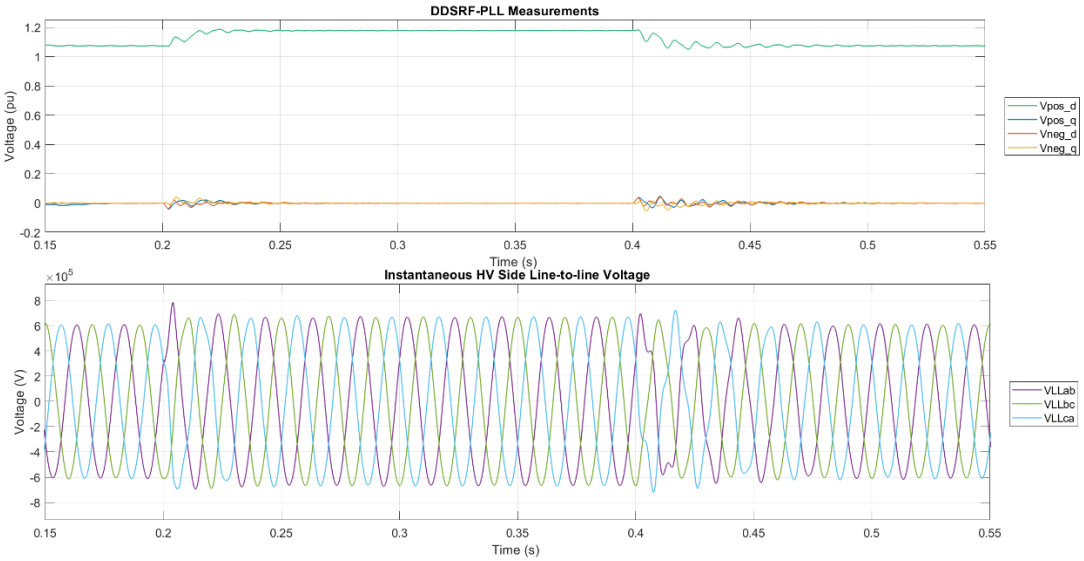

Figure 35. *DDSRF-PLL measurements and HV side line-to-line voltage waveforms for STATCOM supplying 0.1 pu capacitive current in 100 MVA grid, Vs= 1.0 pu.*

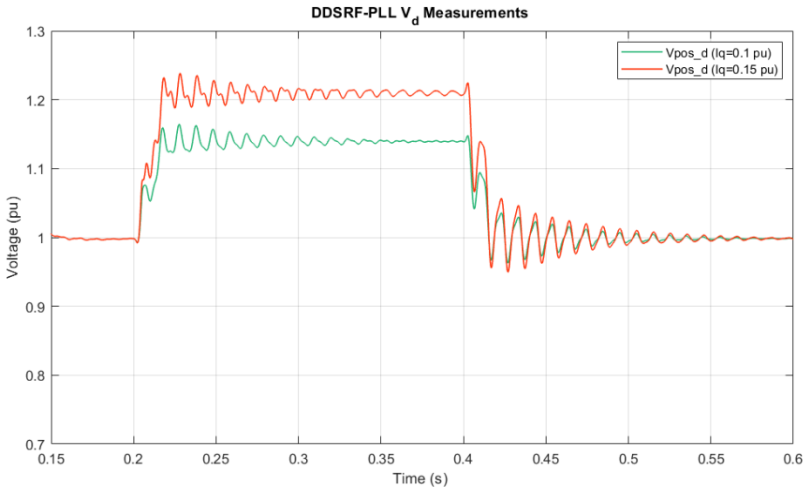

Figure 36. *V_d measurements for STATCOM supplying 0.1 pu and 0.15 pu capacitive current to 75 MVA grid.*

5.2.2 Constant inductive current mode

In the given case STATCOM was simulated as constant inductive current sink to obtain the maximum amount of the inductive power STATCOM is capable to absorb from the without losing stability. STATCOM was simulated for the same SCLs given in Table 2 and Figure 37 shows the STATCOM stable operating limits corresponding for each SCL.

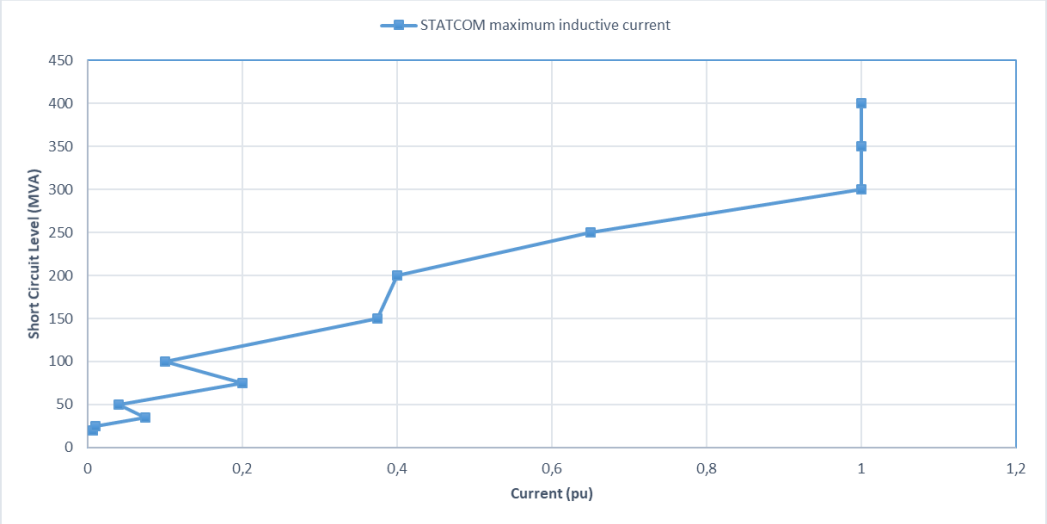

Figure 37. *Maximum inductive current STATCOM capable to absorb versus grid strength.*

During the simulations it was observed that in inductive mode STATCOM tends to supply harmonics to the system which are reflected as periodic oscillations in the estimated *dq* components of the grid voltage. The frequency of these oscillations changes depending on the SCL of the grid. STATCOM was simulated in five grids with different strength and Table 3 shows the measured ripple frequency in the detected positive and negative sequence components of the grid voltage. From the table is it obvious that with the grid strength decrease, the oscillation frequency decreases as well. Figure 38 illustrates the estimated positive sequence *d*-component of the grid voltage for these grids and as it can be observed from these waveforms the amplitude of these increases with the decrease of the SCL. Moreover, the amplitude of the oscillations also increases with the increase of the supplied current magnitude and, consequently, the time required to settle down is higher. Two cases with STATCOM absorbing $0.25\ pu$ and $0.35\ pu$ inductive current from the 150 MVA grid were simulated to show the increase of the ripple amplitude. Measured positive and negative sequence *dq*-components of the grid voltage and grid voltage phase *ab* waveforms are depicted in Figure 39. From these waveforms it is obvious that in case of $0.35\ pu$ current absorption ripple amplitude is higher and voltage waveforms are more distorted and, consequently in this case more time required for voltages to settle.

Also, during inductive mode of operation, it was observed that at some SCLs resonance happens and as a result STATCOM becomes unstable at lower current values. As it can be observed from Figure 37 resonance happens at 50 MVA and 100 MVA SCLs. Detailed information about resonance nature will be provided in subchapter 5.3.

Table 3. *Ripple frequency measured for inductive mode operating STATCOM in five different SCL.*

SCL (MVA)	Current Reference Value (pu)	Ripple Frequency (Hz)
300	- 1.00	210
250	- 0.65	171
200	- 0.40	165
150	- 0.35	130
100	- 0.10	112.5

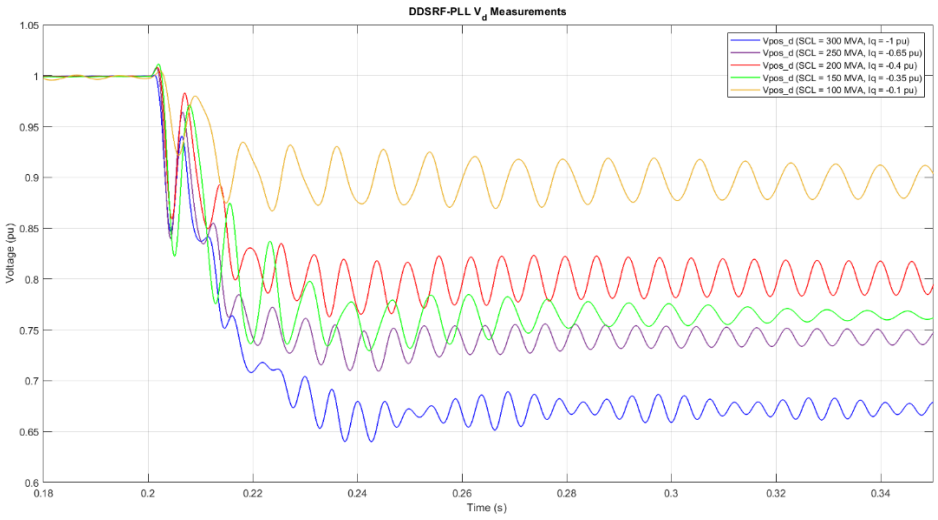

Figure 38. *Estimated grid voltage d-component for STATCOM operating in five different grids.*

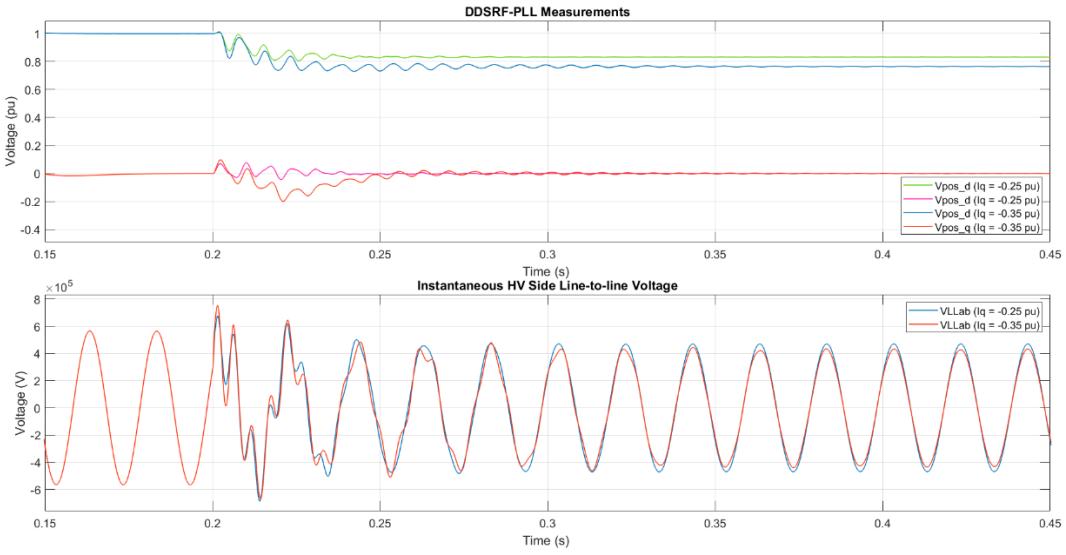

Figure 39. *DDSRF-PLL measurements and HV side voltage waveforms for STATCOM absorbing 0.25 pu and 0.35 pu inductive current in 150 MVA grid.*

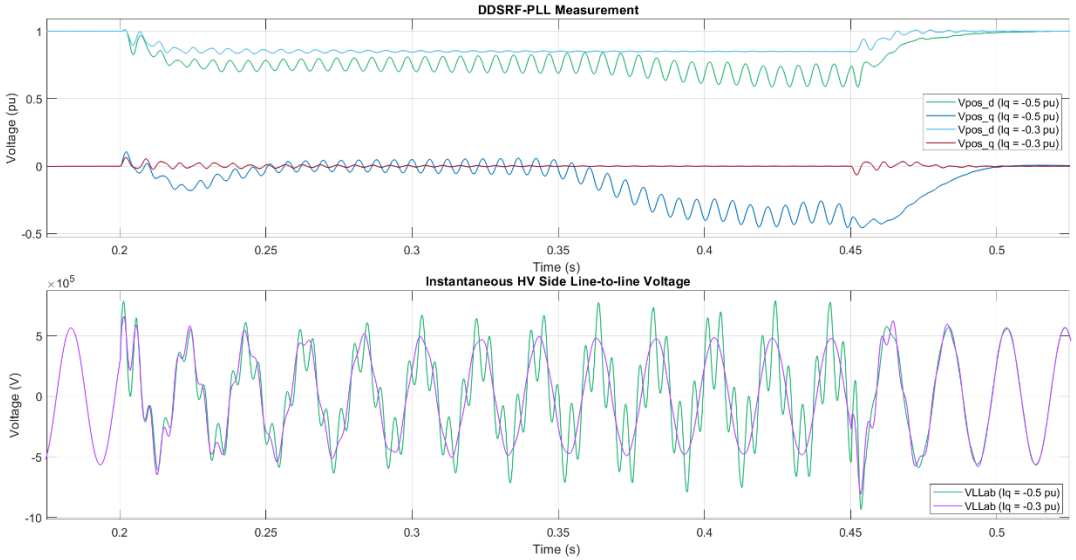

Figure 40. *DDSRF-PLL measurements and HV side phase ab voltage waveforms for STATCOM absorbing 0.5 pu and 0.3 pu inductive current in 200 MVA grid.*

If the current reference value is set above the stability limit, STATCOM operation causes the system to lose synchronization. This opposes the capacitive mode case where operation above limits does not cause synchronization issues. To elaborate the effect of the STATCOM's high inductive current absorption on the grid, two cases were run in 200 MVA grid. In these simulations inductive current reference values were set to $Iq = 0.5\,pu$ and $Iq = 0.3\,pu$ which consequently are the values above and below operation limit for this SCL (as it can be observed from Figure 37). Figure 40 depicts the resulting grid voltage's positive and negative sequence *dq*-components and grid voltage waveforms. As it can be observed from the DDSRF-PLL measurements for case when the STATCOM current reference values is set above the limit, system becomes unstable and becomes stable once STATCOM stops current supply at time at $t = 0.45\,sec$. In both cases ripple exists in the measured grid voltages; however, for $Iq = 0.3\,pu$ case this ripple is small and after some time disappears whereas for $Iq = 0.5\,pu$ case the initial amplitude of the ripple is higher and increases with the time. Moreover, after time $t \approx 0.35\,sec$ the STATCOM completely losses the synchronization with the grid voltage as it can be seen from the DDSRF-PLL measurements. Harmonic content in the grid voltage in unstable case increases throughout the STATCOM operation. STATCOM is capable to restore synchronization only after it stops to absorb inductive current.

The loss of synchronization that leads to the system instability is caused by the fast PLL operation, which due to high dV/dQ sensitivity of the weak grid results in high error in the detected angle. Figure 41 shows PLL sensed angles and STATCOM modulator generated V_{ref} voltage reference waveforms. As it can be observed from these waveforms

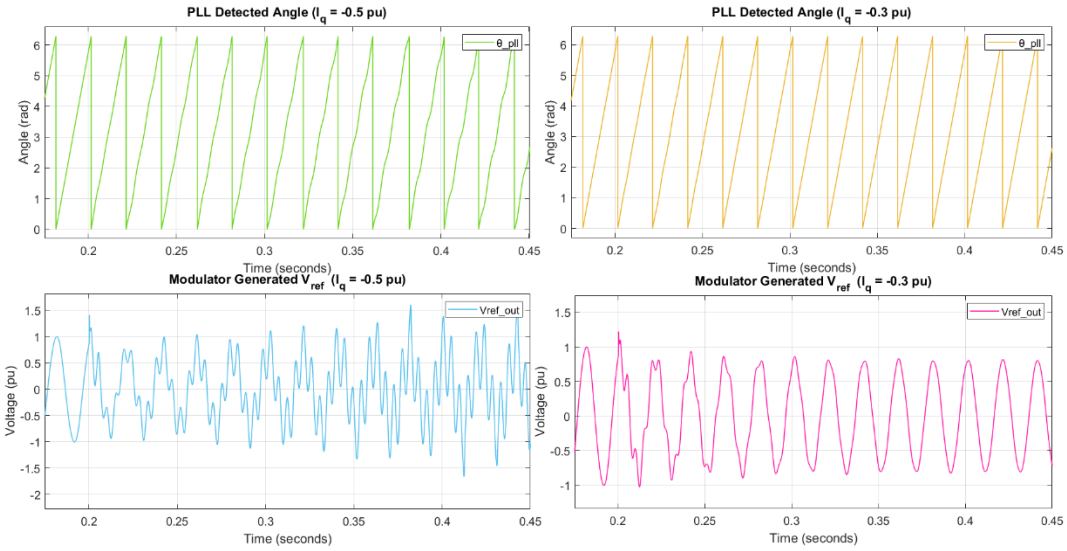

Figure 41. *PLL detected grid angles and modulator generated V_{ref} waveforms for STATCOM absorbing 0.5 pu and 0.3 pu inductive current in 200 MVA grid.*

when the current reference value is set below operational limit value, the error in the detected angle is small and, as a result, the reference voltage V_{ref} does not exhibit high amount of harmonic content and after couple of cycles the error is cleared out and reference voltage waveform becomes pure sinusoidal. However, when the current reference value exceeds the maximum stability limit, initial error in the detected angle is high which in return cause harmonics injection to the system by STATCOM distorting the grid voltage waveforms. Distorted grid voltages result in further increase of the error in the detected angle by PLL, causing avalanche effect on the reference voltage V_{ref} waveforms making them even more distorted until synchronization is completely lost.

Since the synchronization loss happens due to fast PLL operation, gains of the PLL were reduced as it was suggested [32]. To investigate the impact of the slower PLL on the system stability STATCOM was simulated in a grid with 200 MVA and the current reference value was set $I_q = 0.5\ pu$, a value which cause unstable operation with the original PLL. Figure 42 presents the resulting estimated positive and negative sequence *dq* components of the grid voltage and HV side line-to-line voltage waveforms. From these waveforms it is obvious that PLL modification makes the system operation more stable for previously unstable current reference value. As it can be observed from the DDSRF-PLL measurements during $0.2\ sec \leq t \leq 0.4\ sec$ time interval the voltage drops to 0.75 pu, the ripple disappeared and the STATCOM synchronized to the grid without any issues which can be observed from the grid voltage waveforms as well. Therefore, it can be concluded that PLL parameters do influence the STATCOM synchronization in weak grid operation.

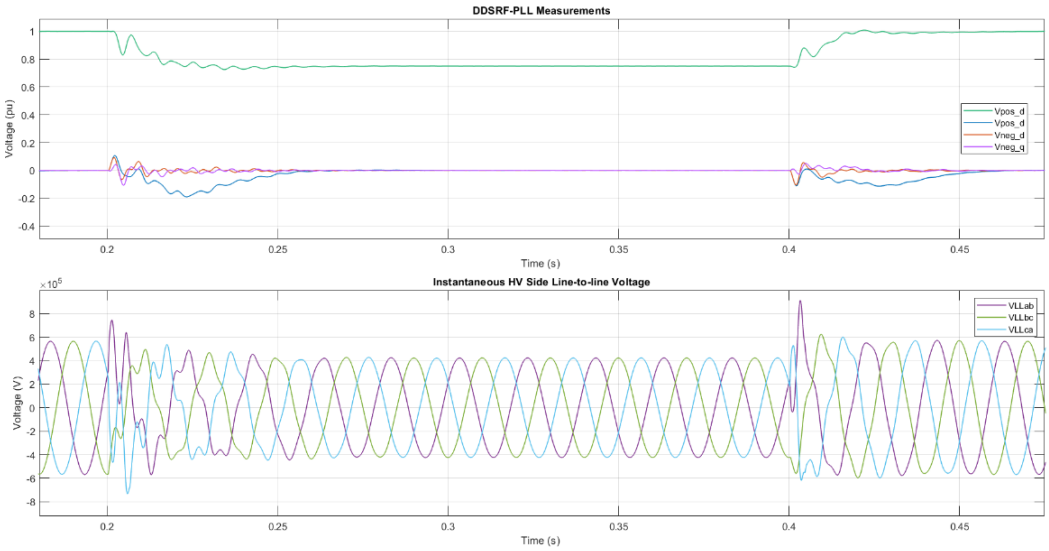

Figure 42. *DDSRF-PLL measurements and grid voltage waveforms for STATCOM with modified PLL absorbing 0.5 pu inductive current in 200 MVA grid.*

However, even though PLL modification improves the STATCOM synchronization performance, the PLL modification has dramatic effect on the DC link voltage controller. Figure 43 illustrates DC side voltage waveforms and current reference values generated by STATCOM. During normal operation conditions of the STATCOM with the original parameters there is no active power exchange between the grid and STATCOM, except for very small amount of the active power consumed to compensate the losses which is equal to $I_d = 0.002\,pu$ as it can be observed from the Figure 34. However, with the modified PLL as it can be observed from the DC link voltage waveforms in the Figure 43, during the STATCOM operation interval DC link voltages deviates from their reference value and stabilize at lower level. Since the error between the V_{dc_ref} and $V_{dc\_feedback}$ is high, STATCOM is generating the I_{d_ref} equal to 0.043 pu a value that is 21 times greater the nominal value. Based on this it can be concluded that STATCOM is absorbing more active power than it is capable to dissipate. Since given STATCOM does not have any energy storage connected on DC side this is not correct.

Based on the waveforms it is obvious that DC voltage controller does not operate properly and active power is dissipated somewhere. The reason standing behind DC voltage controller's improper operation may be that the overall plant transfer function changes due to PLL parameters modification. When PLL parameters changed the transfer function also changed. Since the PLL transfer function is the part of the plant transfer function of the DC voltage control process, any modification will result in the new plant transfer function for which the controller parameters designed with original PLL parameters may not have enough phase margin, gain margin etc. Hence, the PLL parameters modification means the retuning or even re-design of the DC voltage controller.

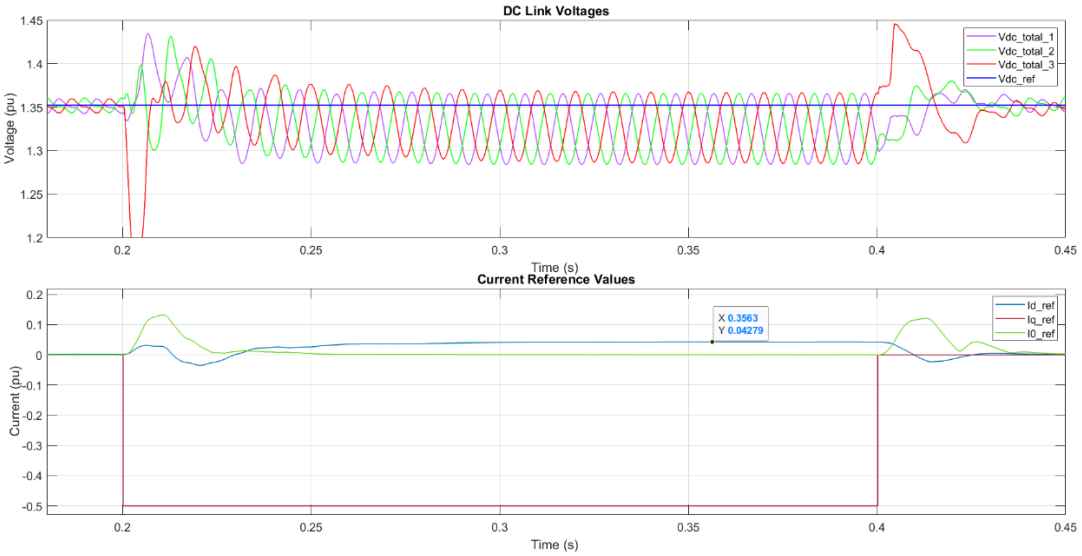

Figure 43. *DC link voltages and generated current references for STATCOM with modified PLL absorbing 0.5 pu inductive current in 200 MVA grid.*

In the next simulation the DC link voltage controller parameters were retuned, and the proportional gain of the controller was increased to twice the original value. Figure 44 shows the resulting DC link voltage waveforms and the current reference values generated by the controllers. It was possible to decrease the amount of the absorbed active current almost twice; however, the resulting value still greater than initial value. Further increase of the gain will result the higher DC link voltage level and consequently the current will be negative which means the STATCOM is supplying the active power to the grid which should not happen. This means that DC link controller should be modified to be able to operate normally with the modified PLL parameters.

In order to achieve ordinary active current reference value, DC link voltage controller was modified. Modification consists of the integral controller addition and tuning the parameters. STATCOM was again simulated in 200 MVA grid absorbing 0.5 pu inductive current from the grid. The resulting DC link voltage waveforms and generated current reference values for modified DC link voltage controller are shown in the Figure 45 and these results are very close to the normal operation results. The DC link voltages are very close to the reference level and generated active current reference value $I_{d\_ref} = 0.005\ pu$ is low, which can be brought to 0.002 pu with further tuning of the proportional gain. The settling time during step changes takes a bit longer time but this could be improved by better controller tuning.

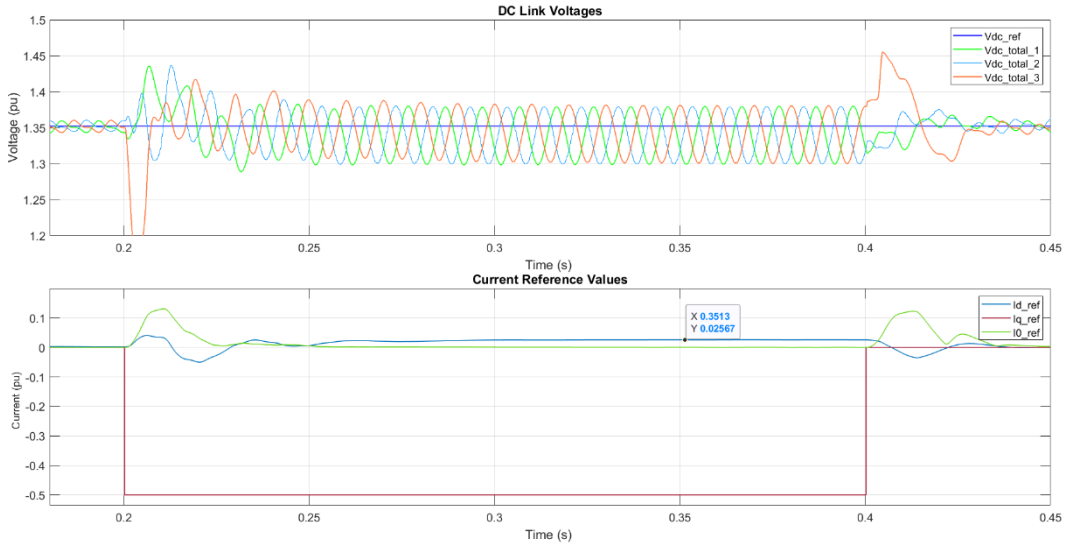

Figure 44. *DC link voltages and generated current references for STATCOM with modified PLL and retuned DC link voltage controller absorbing 0.5 pu inductive current in 200 MVA grid.*

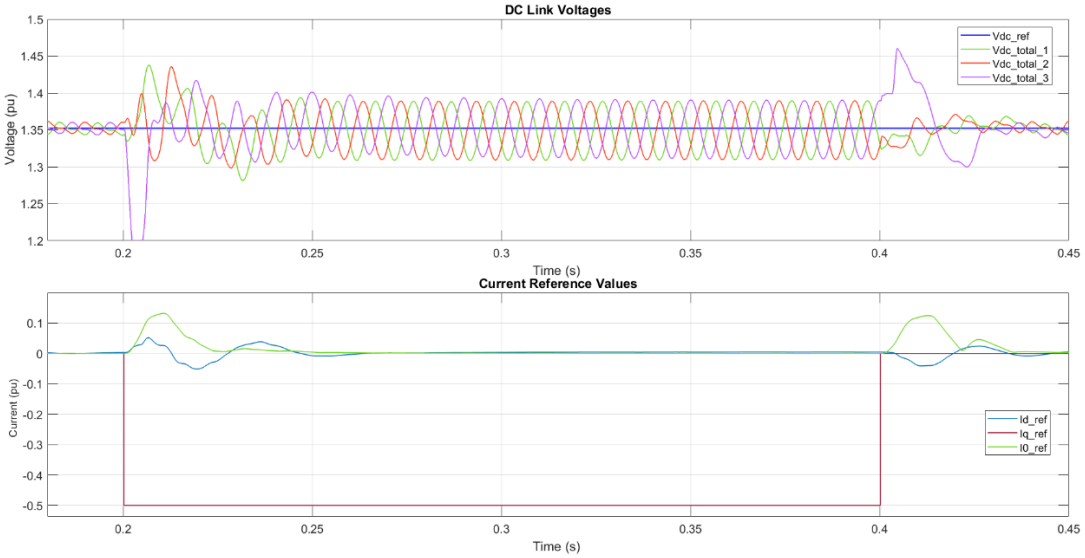

Figure 45. *DC link voltages and generated current references for STATCOM with modified PLL and DC link voltage controller absorbing 0.5 pu inductive current in 200 MVA grid.*

However, when the STATCOM with modified PLL and DC link voltage controllers is run in 150 MVA grid and absorbs $0.4\ pu$ reactive power from the grid the DC link voltages did not stabilized around the reference value as it supposed to. Figure 46 shows the resulting grid voltage, DDSRF-PLL measurements, DC link voltage waveforms and the generated current reference values. As it can be observed from these waveforms the PLL modification same as in 200 MVA case improved the grid voltage waveforms and removed the ripple. However, the DC link voltage controller malfunctions here and the

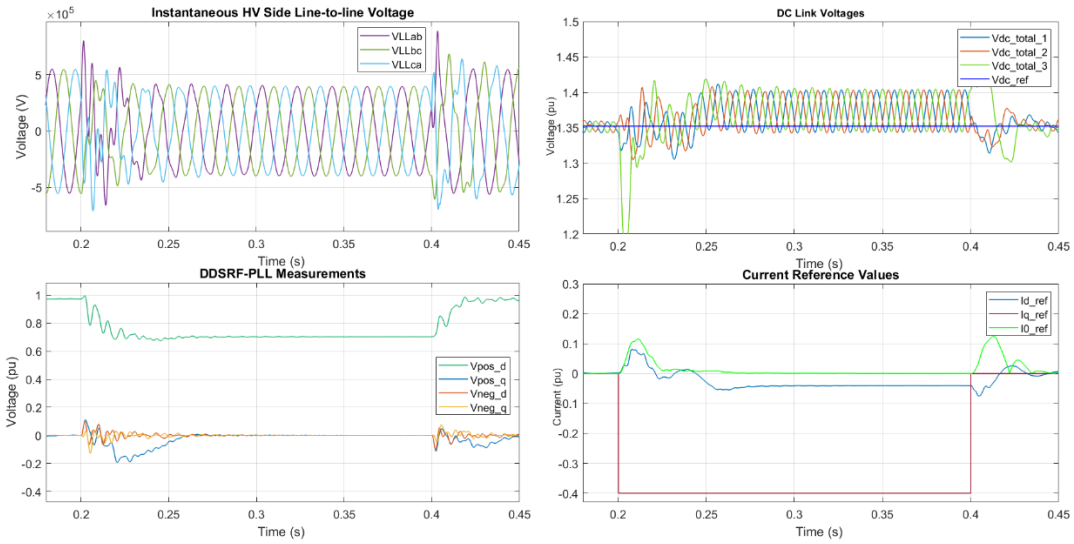

Figure 46. *Grid voltages, DDSRF-PLL measurements, DC link voltages and generated current references for STATCOM with modified PLL and DC link voltage controller absorbing 0.4 pu inductive current in 150 MVA grid.*

resulting active current reference value is negative meaning the active power supply to the grid by the STATCOM. Therefore, the DC link controller parameters should be modified for given SCL. It can be concluded that the interaction of the PLL, DC link controller and grid strength is more complex, and it should be further elaborated to design better DC link voltage controller.

However, for STATCOM the main task is not decreasing the grid voltage to very low levels but is just the opposite keeping it around $1.0\ pu$. Hence, proposed modification for the inductive mode of operation might not be needed since the factors that affect STATCOM operation in constant current mode may not appear in voltage regulation mode.

5.2.3 Constant current mode summary

STATCOM was simulated in the weak grid conditions in the constant current control mode to investigate the factors affecting the normal operation. STATCOM was run as current source supplying or absorbing the reactive current. The minimum SCL where the STATCOM with reduced output current can operate and capable to supply limited amount of the reactive was found out to be 20 MVA.

In capacitive mode the main limiting factor for the normal STATCOM operation was the DC link voltage level, where high amount of the reactive power flow to the grid causes voltage rise above this DC link voltage which in turn generates harmonics due to distorted reference voltage generation by the STATCOM. In inductive mode operation the weak grid operation causes the ripple appearance in the grid voltage which increases

with the amount of the absorbed current and the frequency of this ripple changes depending on the SCL STATCOM operating, decreasing from high to lower. The modification of the PLL has removed this ripple and improved the voltage waveforms; however, the DC link voltage controller operation was affected. The modification of the DC link voltage controller improves the DC link voltage controller performance, but it needs to be designed properly in order to operate at various SCL without any further tuning.

Overall, the STATCOM has some limitations in the weak grid and these limitations depending on the mode of operation can be resolved or may be left without any attention. For example, STATCOM will not be operated as a constant inductive current source to reduce grid voltage below $0.9\ pu$ since this may lead to voltage instability.

Moreover, since STATCOM operation as constant current source does not regulate PCC voltage it can be stated that it operates in open loop mode. Hence, it might be the STATCOM is open loop unstable in the weak grid and closed loop stable. Thus, to elaborate this, STATCOM in voltage regulation mode in the weak grid needs to be studied and observed whether the factors noted in this section also affects in the voltage regulation mode.

5.3 STATCOM operation in Voltage Regulation (VR) mode

In this case STATCOM was operating in the Voltage Regulation (VR) which means STATCOM was regulating PCC voltage to $1.0\ pu$ reference value. Same as in the constant current mode the purpose was to obtain the stability limits of the STATCOM operating in weak and very grid conditions, the limiting factors and possible solutions to extend the operation region of the STATCOM are presented. STATCOM voltage regulation mode simulations consist of three parts; 1) operation with the original parameters, 2) operation with notch filter added to DDSRF-PLL and 3) obtaining maximum and minimum operating limits with notch filter added limiting factors.

In the VR mode voltage controller that was bypassed in the previous cases was switched on. Since the grid impedance is part of the plant transfer function the voltage controller, proportional and integral gains of this controller were modified to keep the voltage controller bandwidth smaller than the current controller.

5.3.1 STATCOM VR mode operation with the original parameters

In this case STATCOM was simulated with the original parameters to obtain the factors affecting its operation in the weak and very weak grid conditions. The weak grid simulations showed that when the STATCOM starts to regulate the grid voltage to the reference

value a ripple will appear in the grid voltage. From the simulations it was obtained that the frequency of this ripple changes and the weaker grid gets the lower ripple frequency gets. Table 4 presents the measured ripple frequency for each the simulated SCLs. The amplitude of the oscillations increases with the increase of the STATCOM supplying/absorbing current magnitude.

Table 4. *Measured ripple frequency to each SCL STATCOM operating.*

SCL (MVA)	Ripple Frequency (Hz)
300	210
250	171
200	165
150	150
100	115
75	99
50	69

Figure 47 illustrates the estimated fundamental frequency positive and negative sequence components of the grid voltage and grid voltage waveforms for two voltage dip cases. In these two cases 150 MVA grid voltage drops to $0.9\,pu$ and $0.8\,pu$ for $0.2\ secs$ and STATCOM operates to bring voltage back to $1.0\,pu$. As it can be observed from the measured dq-components of the grid voltages in both cases the STATCOM

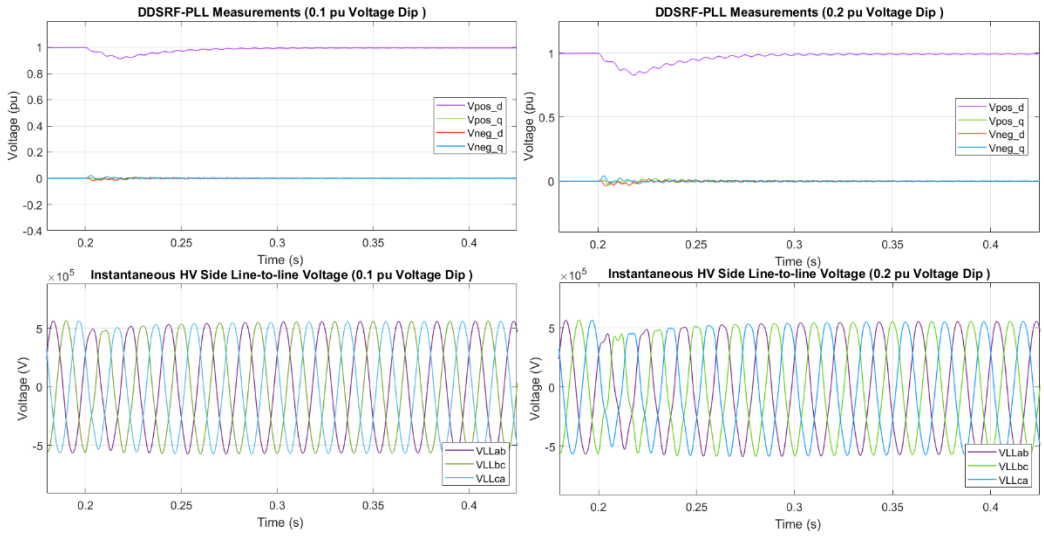

(a) *(b)*

Figure 47. *Estimated fundamental frequency positive and negative sequences of the grid voltage and grid voltage waveforms for STATCOM with original parameters during (a) 0.1 pu voltage dip and (b) 0.2 pu voltage dip in 150 MVA grid.*

regulation starting at $t = 0.2\ sec$ time introduces the ripple to the grid voltage. In both cases STATCOM successfully regulates the voltage to $1.0\ pu$ and clears out the ripple.

However, in case of $0.2\ pu$ voltage dip the magnitude of the oscillations is higher compared to $0.1\ pu$ dip case and consequently it takes more time to clear it out. Moreover, it should be noted that current reference I_q generated by voltage controller exhibits the same ripple as can be observed from Figure 48, and it is further fed to the grid. Therefore, if the voltage dip gets higher the resulting amplitude of the oscillations will get high as well. Thus, at some point amplitude of the oscillations will reach a value above which control system is not capable to damp it. Consequently, the high amplitude oscillations will result in further harmonic injection to the grid voltage via current controller.

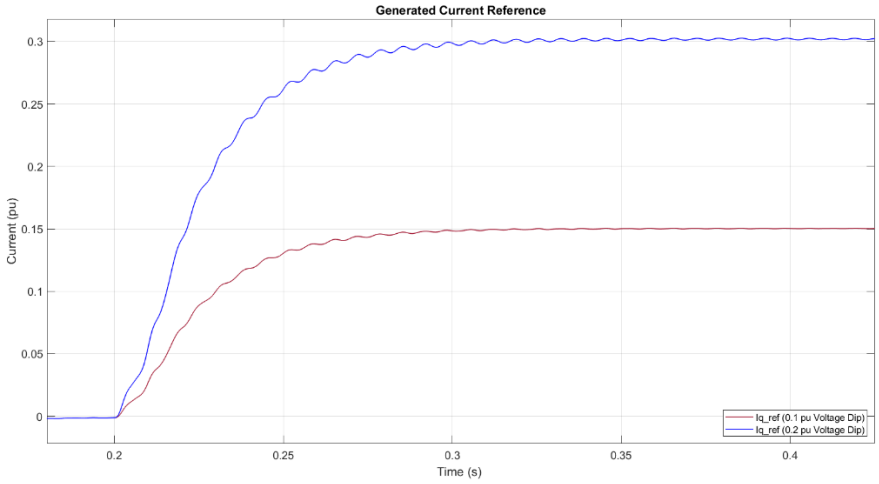

Figure 48. *Voltage controller generated I_q references for STATCOM with original parameters during 0.1 pu and 0.2 pu voltage dips in 150 MVA grid.*

In addition, the amplitude of ripple also increases with decrease of the grid strength. Figure 49 depicts the estimated fundamental frequency positive and negative sequence components of the grid voltage and grid voltage waveforms for a STATCOM operating in 100 MVA grid. In this simulation case the grid voltage maintained at its reference value 1 pu and no dip happens on the grid side thus the STATCOM is in idle mode. However, the initial connection of the STATCOM to the grid at $t = 0.1\ sec$ causes ripple to the grid voltage. Since the stability margin of the system is small it is not capable to damp the initial high ripple amplitude and the system becomes unstable. This results in harmonics injection by the STATCOM and overall grid voltage distortion as it can be observed from Figure 49. It can be concluded that in weak grid conditions it is possible to operate the STATCOM. However, for very weak grid conditions and severe fault conditions STATCOM operation becomes unstable. Hence, in order to operate safely, the ripple appearing during STATCOM operations needs to be removed.

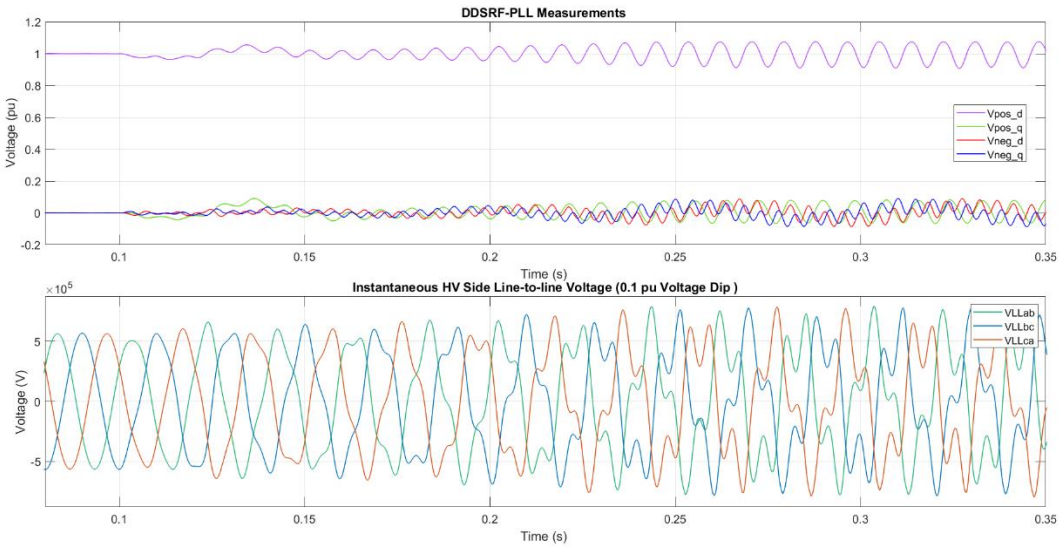

Figure 49. *Estimated fundamental frequency positive and negative sequences of the grid voltage and grid voltage waveforms for STATCOM with original parameters operating in 100 MVA grid.*

5.3.2 STATCOM VR mode operation with the notch filter added

The operation of the STATCOM with the original parameters showed that during STATCOM operation a ripple appears in the grid voltage and it further emerges in the generated current references. Hence, for stable operation a method to remove this ripple from the measurements is required. Since the ripple appears in the measured fundamental frequency positive and negative sequence components of the grid voltage as it can be observed from Figures 47 and 49 it is possible to remove these oscillations by adding a notch filter to the DDSRF-PLL voltage measurement outputs. The block diagram of the modified DDSRF-PLL is shown in the Figure 50. As it can be observed from this figure it is just the addition of an extra filter to each voltage sequence output of the DDSRF-PLL in the Figure 24. Notch filter rejects all the signals with the frequency it is tuned to.

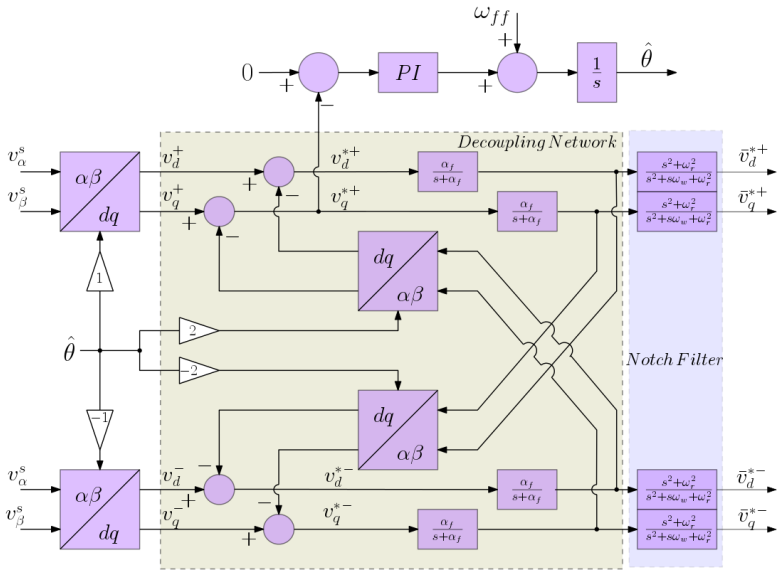

Figure 50. *Modified DDSRF-PLL with notch filter added.*

The addition of the notch filter successfully removes the ripple and STATCOM operation becomes stable. Two simulation cases to show the performance of the STATCOM with notch filter representing voltage rise to $1.2\ pu$ and voltage dip to $0.8\ pu$ of the grid voltage in 150 MVA grid were run. Figure 51 illustrates the DDSRF-PLL measured fundamental frequency positive and negative sequence components of the grid voltage and grid voltage waveforms. For both simulation cases a sudden grid voltage change happens during $0.2\ sec \leq t \leq 0.4\ sec$ time interval and then voltage returns back to normal value. As it can be observed from the Figure 51 notch filter successfully removed the ripple from the *dq* components measurements of the grid voltage and STATCOM regulates the grid voltage to its nominal value during the fault.

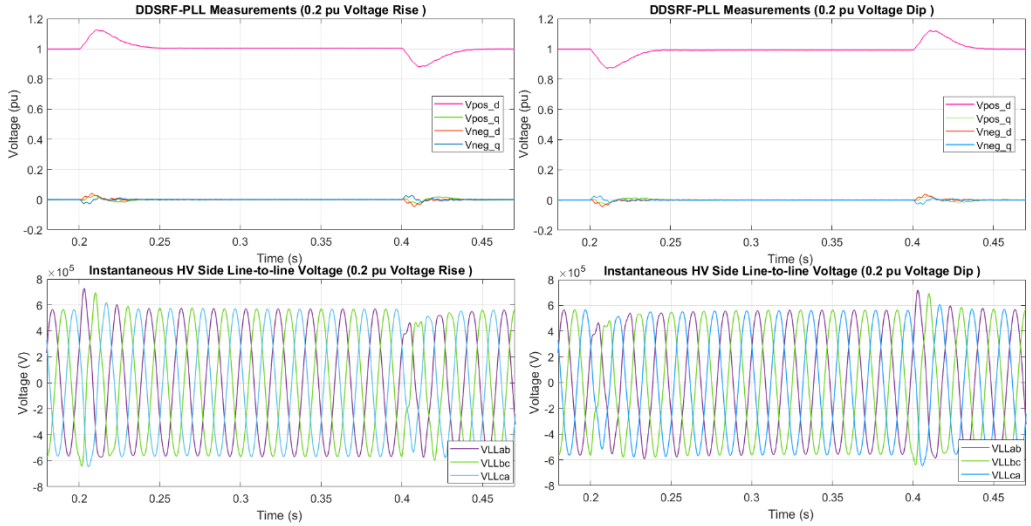

(a) *(b)*

Figure 51. *Estimated fundamental frequency positive and negative sequences of the grid voltage and grid voltage waveforms for STATCOM with notch filter during (a) 0.2 pu voltage rise and (b) 0.2 pu voltage dip in 150 MVA grid.*

Figure 52 shows the current references I_{d_ref}, I_{q_ref} and I_{0_ref} generated by the STATCOM and DC link voltage waveforms and from these waveforms it is obvious that the STATCOM is operating normally. In contrast to the simulation case with the original parameters, the ripple in the current reference has been successfully removed.

Hence, the notch filter clears out the ripple in the measured sequences and consequently significantly improves the STATCOM performance in the weak grid. However, the major drawback of the given method is the requirement to tune the notch filter's parameters according to the ripple frequency appearing in each SCL STATCOM is run as it shown in the Table 4. The filter parameters can be stored in look-up table and based on the operating SCL, STATCOM could update filter parameters from this table. However, in practice this would require constant and accurate grid strength measurement.

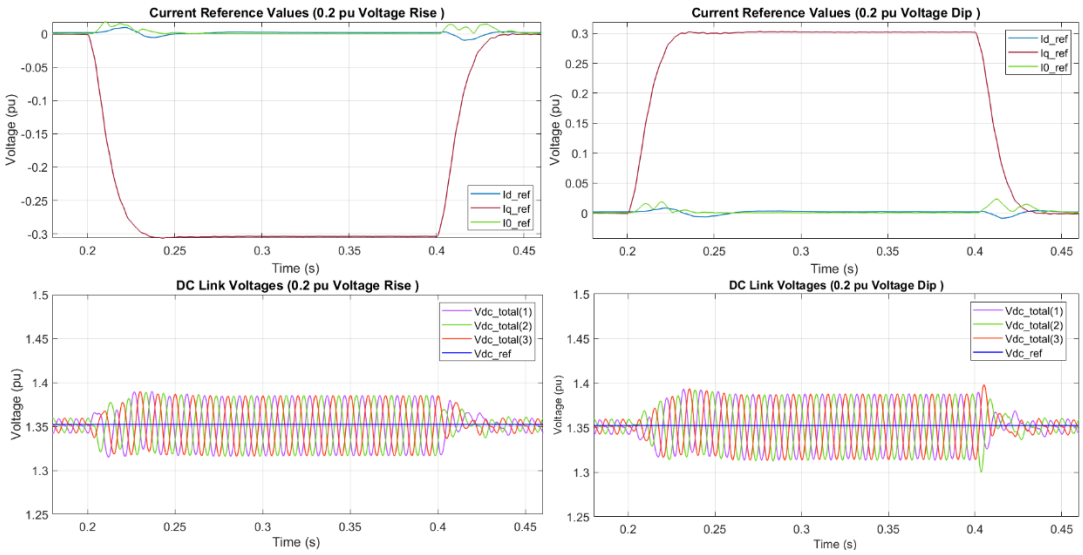

(a) *(b)*

Figure 52. *Voltage controller generated I_q references and DC link voltage waveforms for STATCOM with notch filter during (a) 0.2 pu voltage rise and (b) 0.2 pu voltage dip in 150 MVA grid.*

5.3.3 STATCOM operating limits in VR mode with notch filter added

To obtain the maximum and minimum voltage range within which STATCOM is capable to operate without causing any issues to the system, STATCOM was run for each SCLs in the Table 2. These simulations consisted of two scenarios; in the first case the PCC voltage undergoes sudden voltage rise and the maximum grid voltage that STATCOM can regulate without stability loss is determined. Likewise, in the second case the voltage at PCC suddenly drops and lowest grid voltage at which STATCOM can operate is obtained. The settling time for which the STATCOM considered to be stable was chosen as 300 msec. Graphs in the Figure 53 represent the resulting voltage limits for STATCOM stable operation. As it can be observed from these graphs, STATCOM is capable to regulate the grid voltage without any stability issue in grid with SCL as low as 35 MVA. Simulations showed that as grid strengths weakened, the maximum PCC voltage deviation that STATCOM can handle decreases. As it can be observed from the graphs in the Figure 53, for the SCLs below 300 MVA the stable voltage operation range shrinks. It was found that at lower SCLs the interaction with HF cause the harmonic injection to the grid which distorts the voltage waveforms. Moreover, at 200 MVA and 100 MVA SCLs the resonance with the HF filter causes the bottleneck in the stable operation range.

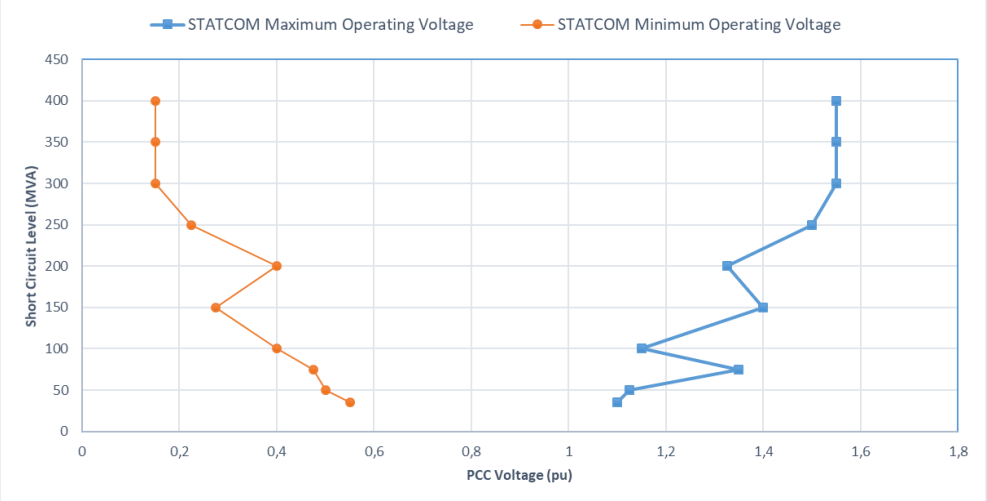

Figure 53. *Grid's maximum and minimum voltage levels STATCOM capable to operate versus grid strength.*

Figure 54 illustrates the estimated fundamental frequency components of the grid voltage and instantaneous grid voltage waveforms for two cases simulated with STATCOM operating in 150 MVA grid. In the first simulation case at time $t = 0.2\,sec$ grid voltage drops to $0.35\,pu$ and STATCOM starts to operate and injects the reactive power to the

system. However, high current interferes with HF filter current and this produces harmonics that are further injected to the grid. As it can be observed from the DDSRF-PLL measured *dq*-components of the grid voltage in Figure 54-a during the transient this interaction with the HF filter distorts the grid voltage waveforms. However, the system is capable to clear out these harmonics and grid voltage waveforms are restored to sinusoidal waveforms. If the voltage drop during the fault is high, the amplitude of the harmonics will be high as well and consequently required settling time will be higher. Therefore, if the settling time is chosen greater than $300\ msec$ the low voltage operation range given in the Figure 53 can be extended and vice versa can be decreased if the settling time chosen to be smaller than $300\ msec$.

In the second simulation case depicted in the Figure 54-b at time $t = 0.2\ sec$ grid voltage rises to $1.4\ pu$. As it can be observed from these waveforms STATCOM capable to regulate the voltage to its reference value and in contrast to the previous case there is no harmonic injection due to HF filter interaction in the measured grid voltage *dq*-components during transient. Therefore, based on these simulations it can be concluded that STATCOM is able to regulate the grid voltage during faults if the voltage limits given in the Figure 53 are not exceeded.

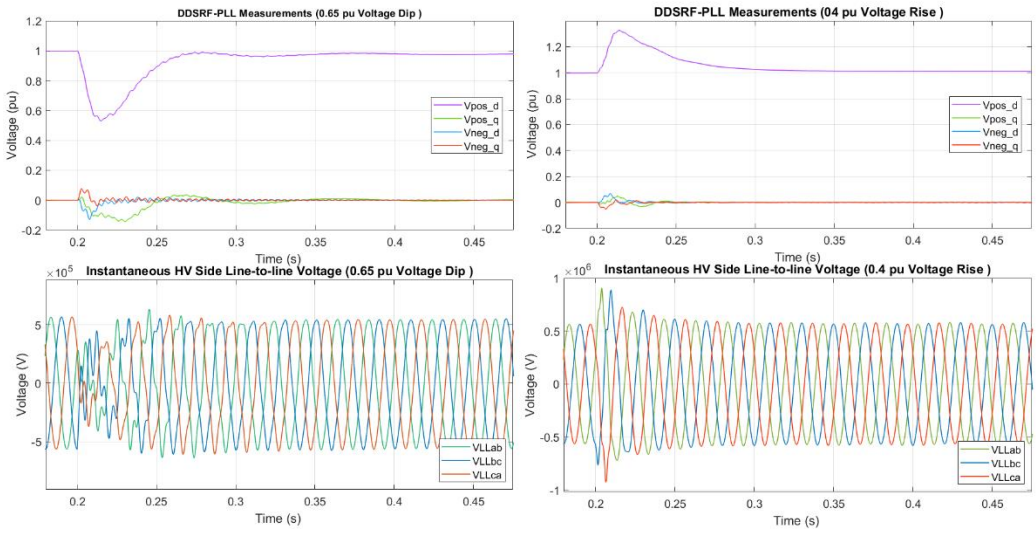

(a) *(b)*

Figure 54. *Estimated fundamental frequency positive and negative sequences of the grid voltage and grid voltage waveforms for STATCOM with notch filter with (a) 0.65 pu voltage dip and (b) 0.4 pu voltage rise faults in 150 MVA grid.*

However, if voltage variation exceeds safe operational boundaries indicated in the Figure 53 the grid voltage gets heavily distorted and STATCOM operation becomes unstable. The reason for distortion as it was mentioned earlier is due to the interaction with passive HF filter current. To illustrate the operation of the STATCOM in unstable region and the factors that affects the stability of the STATCOM operation two simulations cases were

run. In these cases, STATCOM operates in 200 MVA grid where resonance happens as it can be observed from graphs in the Figure 53.

Initially the fault representing the voltage dip is simulated at time $t = 0.2\ sec$ and the grid voltage drops to 32.5% of its original value which is below the stable operation for given SCL as it can be observed from the Figure 53. Figure 55 illustrates the measured fundamental frequency *dq* components of the grid voltage and instantaneous grid voltage waveforms. As it can be observed from the estimated grid voltage *dq* components the magnitude of the harmonics due to resonance with the HF is much larger compared to previous simulation case in 150 MVA. Therefore, the time for the system to damp the harmonics and to bring the voltage waveforms back to sinusoidal is greater than $300\ msec$ which makes, by the selected definition, the system unstable. However, if the time for voltage to settle selected is larger, then system can be expressed as stable for given case.

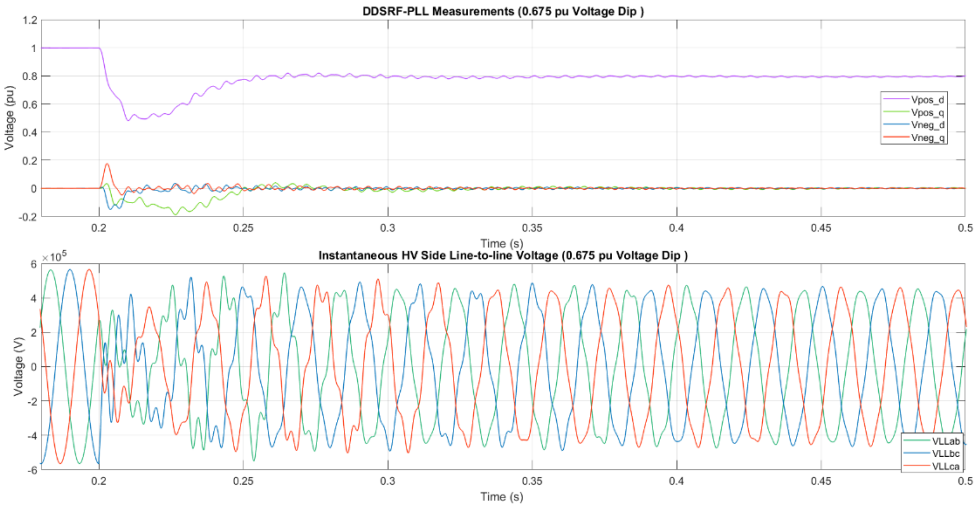

Figure 55. *Estimated fundamental frequency positive and negative sequences of the grid voltage and grid voltage waveforms for STATCOM with notch filter with 0.675 pu voltage dip in 200 MVA grid.*

In the second unstable simulation case at time $t = 0.2\ sec$ a fault resembling the grid voltage rise to $1.4\ pu$ value occurs, and Figure 56 shows the DDSRF-PLL measurements of the grid voltage's positive and negative sequence *dq* components and grid voltage waveforms. Both from the *dq* components and voltage waveforms it is obvious that the operation of STATCOM causes grid voltage distortion and overall system instability. In the estimated unfiltered *dq* components ripple is detected which increases over the time and the application of the notch filter is not capable to clear it out. The main reason for this ripple to appear is the interference of the STATCOM with the current of the HF filter

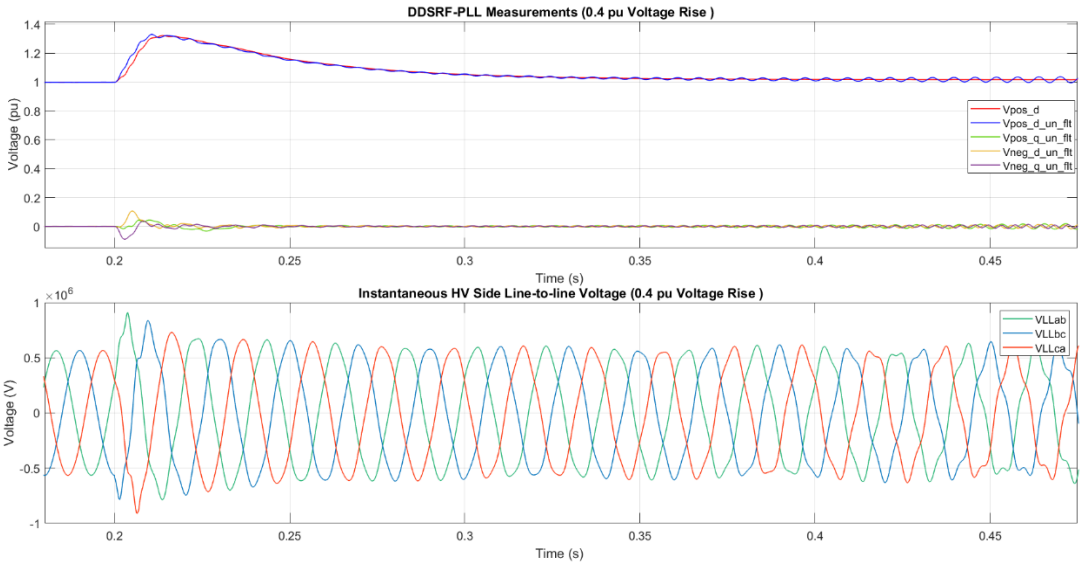

Figure 56. *Estimated fundamental frequency positive and negative sequences of the grid voltage and grid voltage waveforms for STATCOM with notch filter with 0.4 pu voltage rise in 200 MVA grid.*

which distorts the MV side current and consequently it distorts the grid voltage. The distorted voltage brings an error in the PLL's measured angle. Since initially measured angle has large error based on which the modulator generates voltage references with small distortion. These distorted STATCOM generated voltage waveforms further distort the grid voltage waveforms which increases the error in the measured angle. This results in avalanche effect and consequently leads to complete loss of the synchronization. Figure 57 depicts the measured instantaneous STATCOM current, MV side current and the modulator generated voltage reference waveforms. As it can be observed from these waveforms the MV side current becomes distorted over the time and likewise the voltage references are also distorted over time. Hence, it can be concluded that interference with HF filter causes the voltage distortion in the inductive mode. In the next simulation case HF filter parameters will be modified to observe if there are any changes in the system operation behavior.

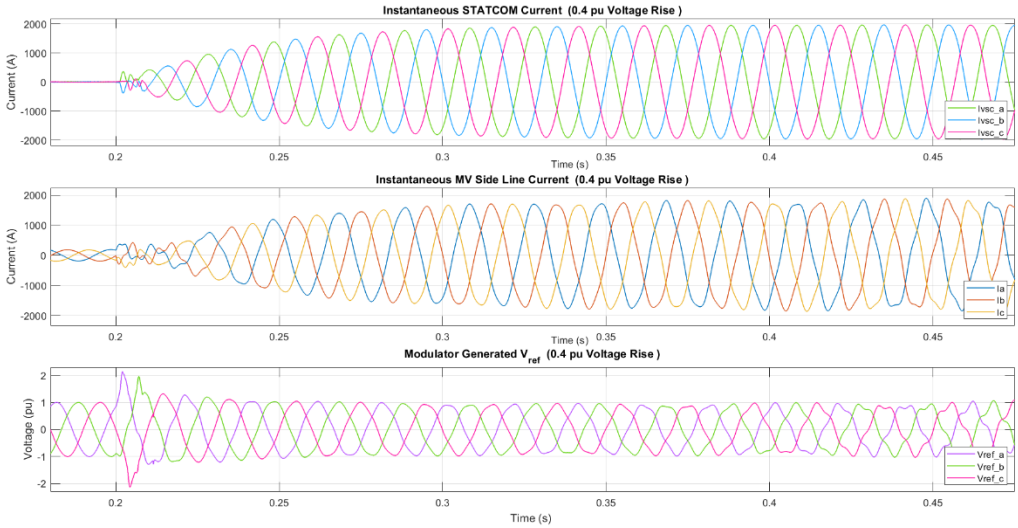

Figure 57. *STATCOM generated current, MV side line current and STATCOM modulator generated voltage reference waveforms during 0.4 pu voltage rise in 200 MVA grid.*

To reduce the effect of the HF filter during the STATCOM operation, HF filter parameters were modified HF filter reactive power rating decreased to 65% of the initial rating. With the given HF parameters previous two fault simulation cases of STATCOM operating in 200 MVA case were rerun. Figure 58 depicts the estimated fundamental frequency positive and negative sequence components of the grid voltage and grid voltage waveforms for both cases. As it can be observed from the waveforms the modification of the HF parameters improved the STATCOM operation for cases that initially were unstable.

The HF filter modification in STATCOM capacitive mode operation has significantly decreased the amount of the harmonics and as it can be observed from the measured *dq*-components of the grid voltage in Figure 58-a. The harmonic content with lower amplitude requires less time for control system to remove these oscillations. Hence, with modified HF filter the settling time for the grid voltage waveforms is lower compared with the original filter parameters.

In case STATCOM operates in inductive mode with modified HF filter, the interaction with the HF filter does not take place and therefore the ripple does not appear. This can be noticed from the DDSRF-PLL measurements in the Figure 58-b which shows that STATCOM operation is stable and grid voltage properly regulated to $1\ pu$.

The modification of the HF filter removes instability factors limiting STATCOM operation and enhances the STATCOM operation range. However, it is almost impossible to change the HF parameters after its installation as it would require scrapping of old components and installation new ones. Therefore, if during initial system studies the HF filter

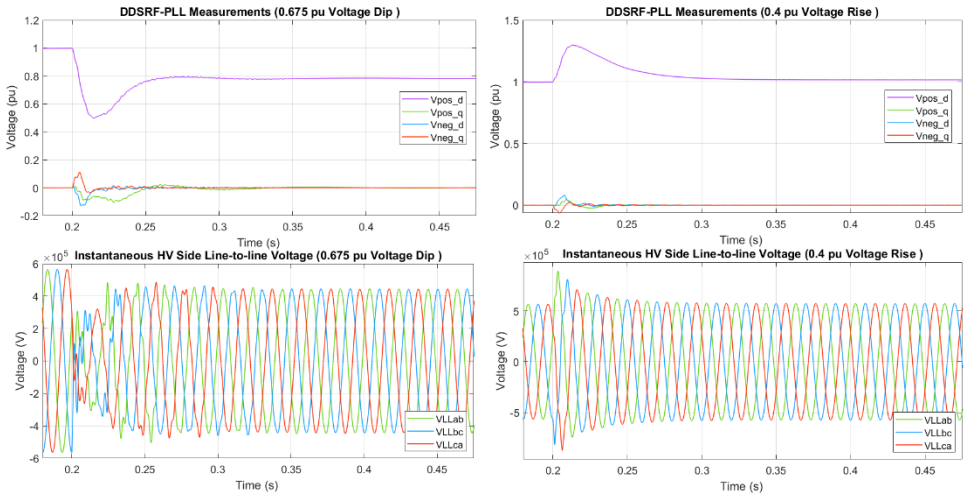

(a) *(b)*

Figure 58. *Estimated fundamental frequency positive and negative sequences of the grid voltage and grid voltage waveforms for STATCOM with notch filter and modified HF during (a) 0.675 pu voltage dip and (b) 0.4 pu voltage rise faults in 200 MVA grid.*

impact on the STATCOM operation in the weak grids is not considered, modification of the HF filter is not the best way to solve the instability issue.

If HF filter modification is not possible, extension of the STATCOM operation region in weak grid is achievable by modifying PLL. Since the instability especially in inductive mode is cause by PLL erroneous angle measurement which leads to synchronization loss, making PLL slower will remove the synchronization issue. To prove this STATCOM with decreased PLL bandwidth was simulated in 200 MVA grid with the same voltage deviations as in previous case. Figure 59 depicts the DDSRF-PLL measured positive and negative sequence *dq*-components of the grid voltage and grid voltage waveforms. From these waveforms it is clear that PLL modification makes system stable and in both fault cases the STATCOM regulates the voltage to its reference without much distortion to grid waveforms.

Hence, PLL modification removes the effects of the HF interaction and consequently the STATCOM operation becomes more stable. However, the modification degrades the DC link voltage controller performance and DC link voltage controller redesigning or parameters retuning required.

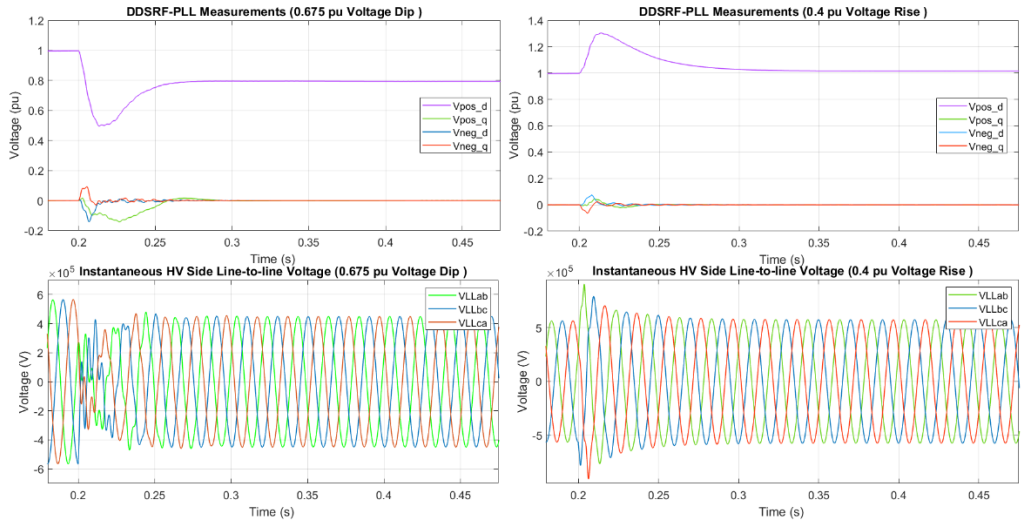

(a) *(b)*

Figure 59. *Estimated fundamental frequency positive and negative sequences of the grid voltage and grid voltage waveforms for STATCOM with notch filter and modified PLL during (a) 0.675 pu voltage dip and (b) 0.4 pu voltage rise faults in 200 MVA grid.*

5.3.4 VR mode summary

STATCOM operating in the voltage regulation mode was simulated in the weak grid conditions to investigate factors that limits its operation. It was found out that STATCOM operation with the original parameters results in the injection of the harmonics to the grid which are detected as a ripple in the measured positive and negative sequence *dq*-components of the grid voltage. The frequency of the injected harmonics changes with the grid strength, the weaker grid gets the lower is the ripple frequency. The magnitude of the ripple increases with amount of the supplied reactive power and at weaker grids ripple amplitude is higher than in the stronger ones.

Next a notch filter to remove the ripple in the measured *dq*-components of the grid voltage was added to the DDSRF-PLL voltage output. The notch filter cleared out the ripple and made voltage regulation much smoother and more stable. With the notch filter added the STATCOM is capable to regulate the voltage in very weak grids with grids strengths lower than 50 MVA and capable to deal with extreme voltage variations. However, in very weak grids the interaction with HF filter limits the operation range of the STATCOM and leads to instability. Moreover, at some SCLs the resonance with HF occurs that distorts the grid voltage and the system becomes unstable. HF filter modifications removed the resonance and decreased the interaction with the filter. Therefore, if the weak grid operation considered to be the part of the STATCOM operation it is very important

to include the effect of the resonance in the initial harmonic studies and component selection.

Finally, PLL parameters to reduce its speed were modified and STATCOM with modified PLL demonstrated stable operation. However, this modification also requires the tuning of the DC link controller to achieve stable DC link voltages.

There are several factors that limit STATCOM to supply or absorb full rated reactive power to/from the grid. Main factors that limit STATCOM operation in the weak grid are DC link voltage level, interference with the HF filter, loss of synchronization. Modification to the control parameters improves the system stability significantly. However, if initial system design studies consider the effects of the weak grid operation i.e. HF filter interference there would be less unpredictable factors which would require the control parameters modification.

Therefore, based on the investigations and simulations made it can be assumed that STATCOM is capable to operate in the weak grid with its rated power. To avoid synchronization loss the effects of the HF filter and DC voltage level during the system design stage should be considered.

5.4 STATCOM operation during faults

In this case symmetrical and asymmetrical faults were simulated when STATCOM was operating in the weak grid conditions. The purpose was to test control system performance and how STATCOM will react to different fault types. First, a symmetrical three-phase to ground fault was simulated and the behaviour of the control system was tested. In the second case two asymmetrical, single-phase to ground and phase-to-phase faults were simulated to test the control system behaviour in case of the unbalanced grid conditions.

During the fault conditions STATCOM control system performs as it is designated. In symmetrical case it will supply the rated reactive power to the grid to support the grid voltage. However, in case asymmetrical fault the grid voltage support will move to the second plan due to severe DC link voltage unbalance. The bulk of the STATCOM generated current will flow inside the delta branches as zero sequence current.

5.4.1 Three-phase to ground fault

To analyse STATCOM response during symmetrical fault in 200 MVA grid was simulated. In the given case at time $t = 0.2\ sec$ a fault that mirrors three-phase to ground fault in the grid that results in the $0.55\ pu$ voltage drop at PCC happens and it clears at time $t = 0.45\ sec$. Figure 60 illustrates the grid voltage waveforms and STATCOM supplied current waveforms. From this figure it is clear that when fault happens STATCOM starts to supply rated current to the grid until the fault is cleared. Once fault clears after short transient STATCOM stops supplying the current to the grid and as it can be observed from the current waveforms in the Figure 60 current reduced to zero.

Figure 61 depicts the DDSRF-PLL estimated positive and negative sequence *dq*-components and frequency measurements, DC link voltage waveforms and generated current references in *dq*-domain. These graphs reflect the control system's response to the fault. It is obvious from the DDSRF-PLL measurements that synchronization is robust and after fault happens PLL quickly restores the synchronization. During the fault DC link voltage controller keeps the DC voltages close to reference values. Since the fault is symmetrical the generated current consists only *q*-component as it can be observed from the generated current references. Overall, in case of symmetrical fault STATCOM does not lose the synchronization with the grid and it is capable to supply rated current to the grid to support grid voltage. Even though the grid voltage during the fault drops below $0.5\ pu$, control system of the STATCOM does not face any issues.

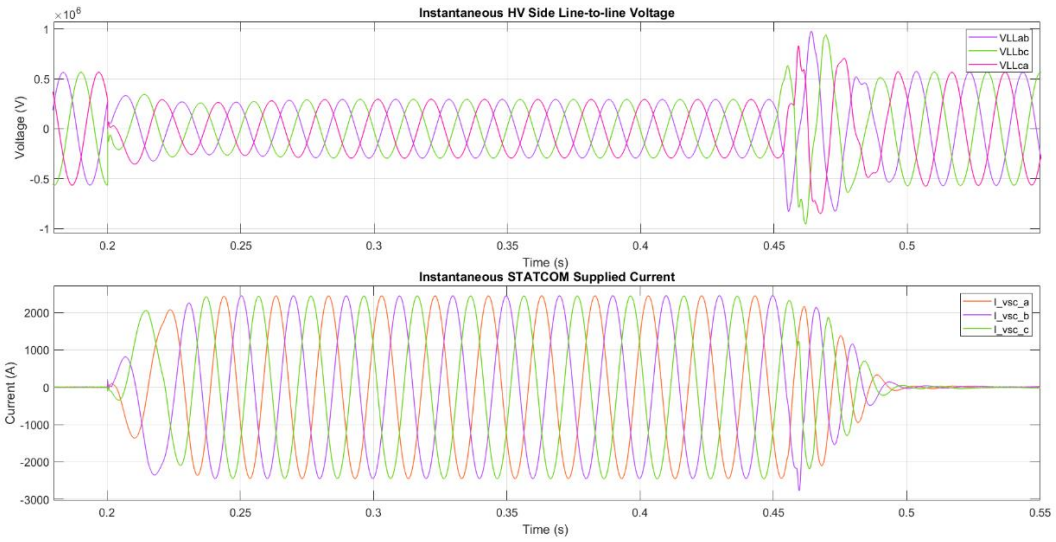

Figure 60. *Grid voltage waveforms and STATCOM supplied current during three-phase to ground fault in 200 MVA grid.*

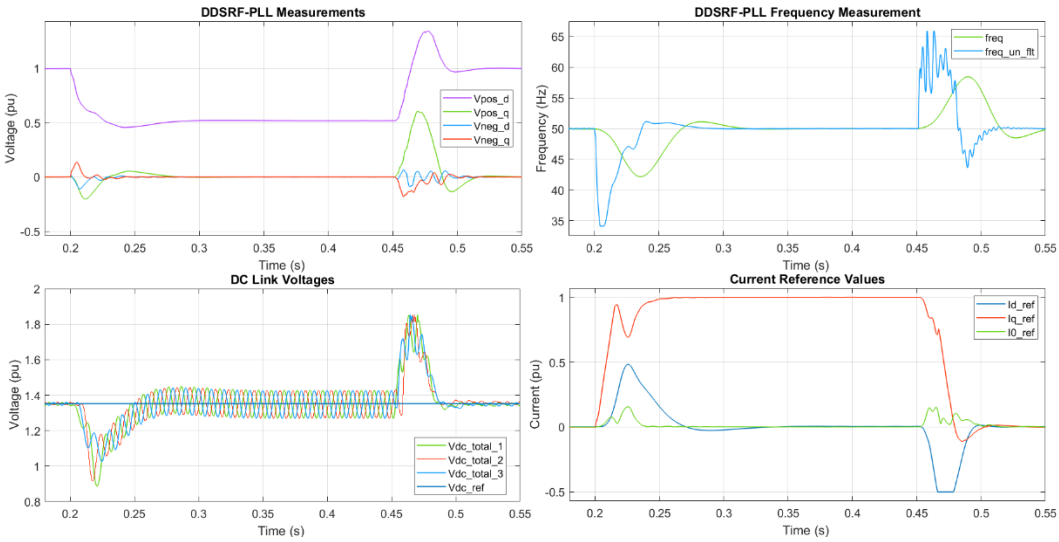

Figure 61. *DDSRF-PLL voltage and frequency measurements, DC link voltages and generated current references during three-phase to ground fault in 200 MVA grid.*

5.4.2 Single-phase to ground fault

In this case STATCOM's response to asymmetrical fault in 200 MVA grid was investigated. In the given case at time $t = 0.2\ sec$ a single-phase to ground that results in 50% voltage drop in phase *a* occurs and fault is cleared at $t = 0.45\ sec$. STATCOM responses immediately to the fault as it can be observed from the Figure 62 which depicts grid voltage waveforms and STATCOM supplied current waveforms. Since the grid voltages are unbalanced injected capacitive current will create the overvoltage in the unaffected lines as it can be observed from grid voltage waveforms. Compared to symmetrical case STATCOM does not supply fully rated current to the grid as it can be observed from the Figure 62. This happens due to unbalanced grid voltages which requires ZSCI controller to inject zero sequence current to balance the DC link voltage waveforms and to prevent inequal power dissipation in STATCOM branches.

Figure 63 represents the estimated positive and negative sequence of the grid voltages, measured frequency, DC link voltages and generated current references. DDSRF-PLL voltage measurements shows that decoupling network separated positive and negative sequence components and PLL locked to the positive sequence network *d* component. Unbalanced grid voltage results in the deviation of the DC link voltages from their reference value when fault occurs which successfully regulated to their reference value by ZSCI as it is depicted in Figure 63. Since the required zero sequence current for DC link

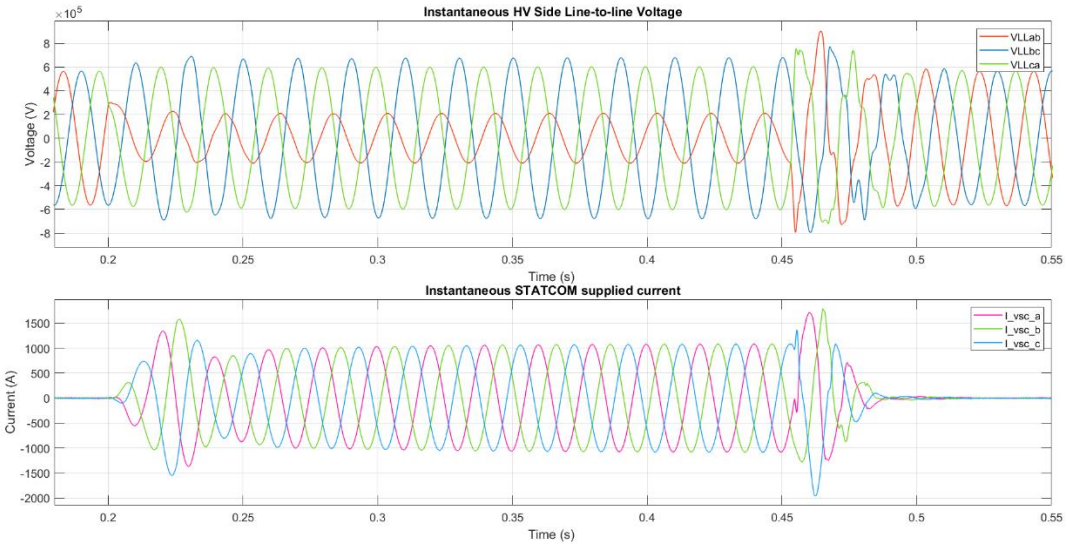

Figure 62. *Grid voltage waveforms and STATCOM supplied current during single-phase to ground fault in 200 MVA grid.*

voltage balancing is high as it can be observed from the generated current references it will limit the amount of the available current quadrature component. Hence, this will result in the limited amount of the available reactive current at STATCOM output as it seen in Figure 62.

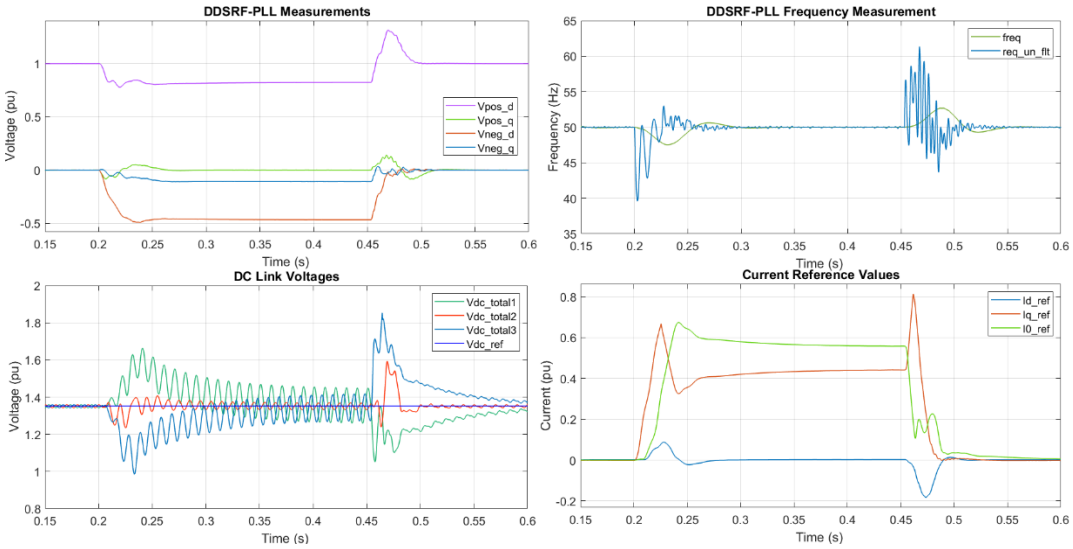

Figure 63. *DDSRF-PLL voltage and frequency measurements, DC link voltages and generated current references during single-phase to ground fault in 200 MVA grid.*

5.4.3 Phase-phase to ground fault

The final fault that was simulated was phase-to-phase with fault resistance of 75 ohm in the 200 MVA grid. Same as in previous cases fault occurs at time $t = 0.2\,sec$ and clears at $t = 0.45\,sec$. The resulting grid voltage, STATCOM supplied current and STACOM branch current waveforms depicted in Figure 64. In contrast to the previous fault cases STATCOM does not supply reactive power to the grid to support the grid voltages as it can be observed from the STATCOM output current waveforms. Voltage unbalance is heavier compared to the previous case; hence, the voltage DC link balancing requires more zero sequence current which makes up the STATCOM branch current as it can be observed from the Figure 64.

Figure 65 represents the estimated positive and negative sequence of the grid voltages, measured frequency, DC link voltages and generated current references. As it can be observed from the DDSRF-PLL measurements the amount of the negative current is higher compared to single-phase to ground fault. Consequently, DC link voltage deviation from their reference is high as it can be observed from DC link voltage waveforms. Thus, required zero sequence current for balancing and time needed to reach reference value is higher. As it can be observed from the current references STATCOM current consists only of the zero sequence component thus no capacitive current is supplied to the grid as it can be observed from the Figure 64.

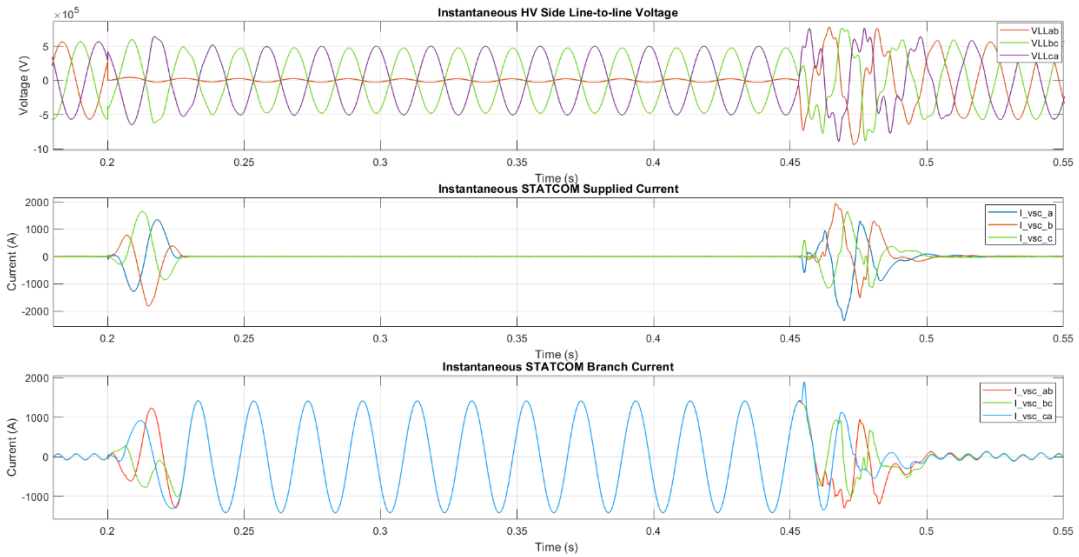

Figure 64. *Grid voltage waveforms and STATCOM supplied current during phase-to-phase fault in 200 MVA grid.*

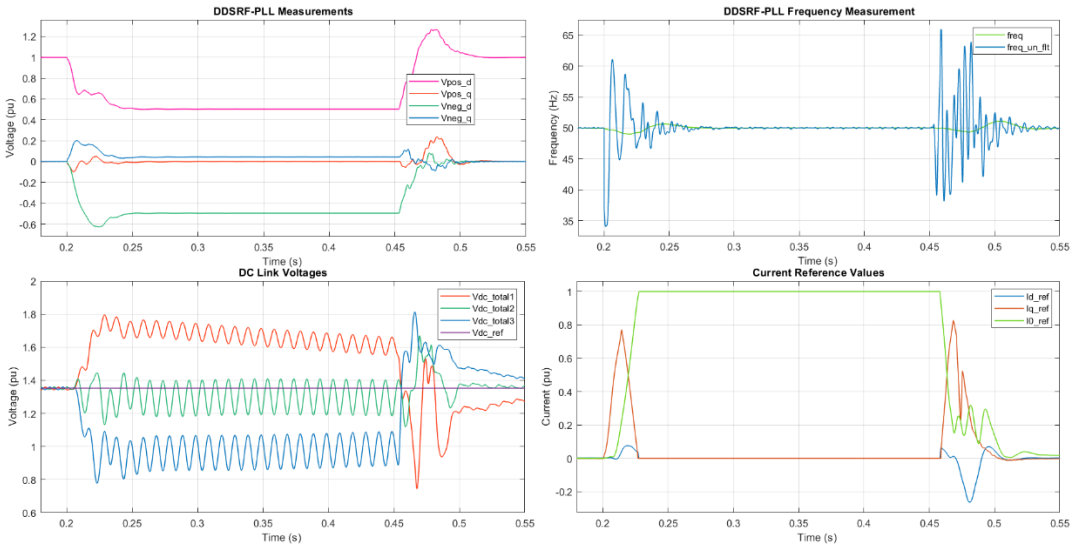

Figure 65. *DDSRF-PLL voltage and frequency measurements, DC link voltages and generated current references during phase-to-phase fault in 200 MVA grid.*

6. CONCLUSIONS AND FUTURE WORK

The purpose of this thesis was to study the effect of the weak grid operation on the STATCOM control system. Integration of the VSC devices to the weak grid is challenging due to high dV/dQ sensitivity and high grid impedance. One of the major issues that limits the integration of the power electronic converters utilizing SRF-PLL in weak grid conditions is the synchronization loss. Synchronization loss happens due to interaction with the high grid impedance which deteriorates PLL operation. To investigate the impact of the weak grid on STATCOM operation three different cases were simulated.

First, STATCOM operating as constant current source was simulated in weak grid conditions to obtain the factors that impact STATCOM stability. In this mode STATCOM is capable to operate at extremely weak grid conditions; however, the amount of the reactive power will be limited. It was found out that in capacitive mode main limiting factor that restricts normal operation is amount of the available DC voltage level. Due to high sensitivity of the grid voltage in the weak grid to the amount of injected reactive power, high amounts of the reactive power will cause the voltage rise above the available DC link voltage level. DC link voltage exceeding will result in the harmonics injection by STATCOM. Inductive mode simulations showed that in weak grid conditions STATCOM operation will result in appearance of high frequency oscillations in the grid voltage. It was noticed that the ripple frequency decreases with the decrease of the system strength. High amount of the current absorption will increase the amplitude of the ripple that due to fast PLL synchronization will lead control system instability. PLL bandwidth reduction has improved the synchronization; however, this modification made DC link voltage controller operation erroneous. Hence, with modification of the PLL parameters DC link voltage controller also needs to be retuned. In addition, HF filter has a huge impact in terms of the voltage rise and voltage distortion during the transients.

Next, STATCOM operating in VR mode was simulated in weak grid conditions and it was observed that during voltage regulation grid voltage exhibits ripple in the grid voltage. Same as in constant current mode case the frequency decreased with the SCL. To remove these high frequency oscillations, a notch filter tuned to the ripple frequency was added to the DDSRF-PLL voltage measurement output. This modification significantly improved the STATCOM performance. With notch filter added the operational limits for various grid conditions were obtained. In capacitive mode it was noticed that STATCOM is capable to support grid voltage for very high voltage drops. However, in inductive mode it was noticed that addition of the notch filter cannot clear the ripple if the limits exceeded.

Moreover, at some SCL resonance happens and the operation range is lower compared to adjacent SCLs. Further elaboration revealed that in inductive mode interaction of the STATCOM supplied current with the HF filter causes grid voltage distortion and STATCOM instability. Reduction of the HF filter rating decreased the negative effect of the HF filter. Another proposed suggestion was to decrease PLL bandwidth to make PLL less sensitive to errors; however, this method would require DC link voltage controller modification.

Finally, weak grid with STATCOM connected was subjected to symmetrical and asymmetrical faults. In all cases STATCOM control system performed without any issues. In case of symmetrical fault STATCOM supplied the rated reactive power to the grid. While in case of asymmetrical faults due to unbalanced grid voltages the bulk of the STATCOM current was supplied to balance DC link voltage waveforms.

Under scope of studies in the simulations cases STATCOM's control system's performance was tested in the weak grid conditions under varying SCLs and voltage levels. Even though the simulation results for studied cases showed promising results for STATCOM application in weak grid conditions, control system performance was not tested for cases where grid exhibits high harmonic distortion or frequency variation happens. These topics were excluded from the scope of the present work due to of lack time and can be included in the future studies.

As a first step in the future work controls of STATCOM can be tested with the same ideal source connected weak grid model but for varying conditions. Frequency variation studies can be further expanded to cases where the ideal source is substituted with real generator model. Same test as in this thesis can be simulated to verify the STATCOM operability for varying frequency conditions.

Another interesting topic that could be investigated in the future studies is the energisation of the STATCOM in weak grid conditions. This study can be extended to study where STATCOM is used to support grid voltage during the black start.

REFERENCES

[1] International Energy Agency, World Energy Outlook 2018, https://www.iea.org/weo/ accessed Dec. 05, 2018, 2018.

[2] REN21, Renewables 2018: Global Status Report, http://www.ren21.net/wp-content/uploads/2018/06/17-8652_GSR2018_FullReport_web_final_.pdf, accessed Dec. 05, 2018, 2018.

[3] Y. Qiu, C. Dai and R. Jin, "Impact of power electronic device development on power grids," *2016 28th International Symposium on Power Semiconductor Devices and ICs (ISPSD)*, Prague, 2016, pp. 9-14

[4] J.M. Maza-Ortega, E. Acha, S. García and A. Gomez-Exposito, "Overview of power electronics technology and applications in power generation transmission and distribution, " *Journal of Modern Power Systems and Clean Energy*, 2017.

[5] Breuer, W., et al. "Role of HVDC and FACTS in future Power Systems." CIGER Symposium, Shang Hai, 2004.

[6] X. P. Zhang, C. Rehtanz, and B. Pal, *Flexible AC Transmission Systems Modelling and Control*, Springer, 2006.

[7] GE Grid Solutions, "*Flexible AC Transmission Systems*", http://www.gegridsolutions.com/products/brochures/powerd_vtf/STATCOM_GEA31986_HR.pdf, accessed Dec. 05, 2018, 2016.

[8] D. P. Kothari and I. J. Nagrath, *Modern power system analysis* (3rd ed), New Delhi: Tata McGraw-Hill Pub. Co, 2003, pp 694.

[9] J. Dixon, L. Moran, J. Rodriguez, and R. Domke, "Reactive Power Compensation Technologies: State-of-the-Art Review," in *Proceedings of the IEEE*, vol. 93, no. 12, pp. 2144-2164, Dec. 2005.

[10] C. A. Bharadwaj and S. Maiti, "Modular multilevel STATCOM with energy storage," *2016 11th International Conference on Industrial and Information Systems (ICIIS),* Roorkee, 2016, pp. 730-735.

[11] A. Virtanen, H. Tuusa and J. Aho, "Performance analysis of conventional STATCOMs and STATCOMs with energy storage in electric arc furnace applications," *2013 Twenty-Eighth Annual IEEE Applied Power Electronics Conference and Exposition (APEC)*, Long Beach, CA, 2013, pp. 1623-1629.

[12] P. Maibach, J. Wernli, P. Jones and M. Obad, "STATCOM technology for wind parks to meet grid code requirements." *Proceedings of EWEC*, 2007.

[13] S. Castagno, R. D. Curry and E. Loree, "Analysis and Comparison of a Fast Turn-On Series IGBT Stack and High-Voltage-Rated Commercial IGBTS," in *IEEE Transactions on Plasma Science*, vol. 34, no. 5, pp. 1692-1696, Oct. 2006.

[14] J. Rabkowski, D. Peftitsis, and H. P. Nee, "Silicon carbide power transistors: A new era in power electronics is initiated^," *IEEE Industrial Electronics Magazine*, 6(2):17–26, June 2012.

[15] K. Sharifabadi, L. Harnefors,H.-P. Nee, S. Norrga, R. Teodorescu, *Design, control, and application of modular multilevel converters for HVDC transmission systems*, Wiley-IEEE press, 2016. 386 p.

[16] J. Rodriguez, J.-S. Lai and F. Z. Peng, "Multilevel inverters: a survey of topologies, controls, and applications," in *IEEE Transactions on Industrial Electronics*, vol. 49, no. 4, pp. 724-738, Aug. 2002.

[17] M. A. Perez, S. Bernet, J. Rodriguez, S. Kouro and R. Lizana, "Circuit Topologies, Modeling, Control Schemes, and Applications of Modular Multilevel Converters," in *IEEE Transactions on Power Electronics*, vol. 30, no. 1, pp. 4-17, Jan. 2015.

[18] A. Dekka, B. Wu, R. L. Fuentes, M. Perez and N. R. Zargari, "Evolution of Topologies, Modeling, Control Schemes, and Applications of Modular Multilevel Converters," in *IEEE Journal of Emerging and Selected Topics in Power Electronics*, vol. 5, no. 4, pp. 1631-1656, Dec. 2017.

[19] J. Rodriguez *et al*., "Multilevel Converters: An Enabling Technology for High-Power Applications," in *Proceedings of the IEEE*, vol. 97, no. 11, pp. 1786-1817, Nov. 2009.

[20] H. Akagi, "Classification, Terminology, and Application of the Modular Multilevel Cascade Converter (MMCC)," in *IEEE Transactions on Power Electronics*, vol. 26, no. 11, pp. 3119-3130, Nov. 2011.

[21] E. Behrouzian, "On control of cascaded H-bridge converters for STATCOM applications, " Ph.D. Thesis, Department of Electrical Engineering, Chalmers University of Technology, Sweden, 2017.

[22] J. H. Vivas, G. Bergna and M. Boyra, "Comparison of multilevel converter-based STATCOMs," *Proceedings of the 2011 14th European Conference on Power Electronics and Applications*, Birmingham, 2011, pp. 1-10.

[23] A. Yazdani and R. Iravani, *Voltage-Sourced Converters in Power Systems: Modeling, Control, and Applications*, Wiley-IEEE press, 2010, 451 p.

[24] F. Shahnia, S. Rajakaruna and A. Ghosh, *Static Compensators (STATCOMs) in Power Systems,* Singapore:Springer-Verlag 2015.

[25] T. Suntio, T. Messo and J. Puukko, *Power Electronic Converters: Dynamics and Control in Conventional and Renewable Energy Applications*, Wiley-VCH press, 2018, 702 p.

[26] P. Rodriguez, J. Pou, J. Bergas, J. I. Candela, R. P. Burgos and D. Boroyevich, "Decoupled Double Synchronous Reference Frame PLL for Power Converters Control," in *IEEE Transactions on Power Electronics*, vol. 22, no. 2, pp. 584-592, March 2007.

[27] R. Betz and T. Summers, “Introduction to symmetrical components and their use in statcom applications,” University of Newcastle, Australia, School of Electrical Engineering and Computer Science, Tech. Rep., November 2009.

[28] C. L. Wadhwa, *Electrical Power Systems* (7th ed), Kent: New Academic Science, 2017, pp 984.

[29] IEEE Guide for Planning DC Links Terminating at AC Locations Having Low Short-Circuit Capacities," in *IEEE Std 1204-1997* , vol., no., pp.1-216, 21 Jan. 1997

[30] D. Stenclik, et al, " Oahu Distributed PV Grid Stability Study, Part 3: Grid Strength," Hawaii Natural Energy Institute, Jul., 2016. Accessed on: Aug.19, 2019. Available: https://www.hnei.hawaii.edu/sites/www.hnei.hawaii.edu/files/Oahu%20DPV%20Grid%20Stability%20Report%20Pt3.pdf

[31] A. Egea-Alvarez, C. Barker, F. Hassan and O. Gomis-Bellmunt, "Capability curves of a VSC-HVDC connected to a weak AC grid considering stability and power limits," *11th IET International Conference on AC and DC Power Transmission*, Birmingham, 2015, pp. 1-5.

[32] J. Z. Zhou and A. M. Gole, "VSC transmission limitations imposed by AC system strength and AC impedance characteristics," *10th IET International Conference on AC and DC Power Transmission (ACDC 2012)*, Birmingham, 2012, pp. 1-6.

[33] S. Grunau and F.W. Fuchs, “Effect of wind-energy power injection into weak grids,” European Wind Energy Conference and Exhibition 2012, EWEC 2012.

[34] T. Midtsund, J. A. Suul and T. Undeland, "Evaluation of current controller performance and stability for voltage source converters connected to a weak grid," *The 2nd International Symposium on Power Electronics for Distributed Generation Systems*, Hefei, 2010, pp. 382-388.

[35] P. Zhou, X. Yuan, J. Hu and Y. Huang, "Stability of DC-link voltage as affected by phase locked loop in VSC when attached to weak grid," *2014 IEEE PES General Meeting | Conference & Exposition*, National Harbor, MD, 2014, pp. 1-5.

[36] D. Dong, B. Wen, D. Boroyevich, P. Mattavelli and Y. Xue, "Analysis of Phase-Locked Loop Low-Frequency Stability in Three-Phase Grid-Connected Power

Converters Considering Impedance Interactions," in *IEEE Transactions on Industrial Electronics*, vol. 62, no. 1, pp. 310-321, Jan. 2015.

[37] Q. Hu, L. Fu, F. Ma and F. Ji, "Large Signal Synchronizing Instability of PLL-Based VSC Connected to Weak AC Grid," in *IEEE Transactions on Power Systems*.

[38] K. Lentijo and D. F. Opila, "Minimizing inverter self-synchronization due to reactive power injection on weak grids," *2015 IEEE Energy Conversion Congress and Exposition (ECCE)*, Montreal, QC, 2015, pp. 1136-1142.

[39] J. A. Suul, S. D'Arco, P. Rodríguez and M. Molinas, "Impedance-compensated grid synchronisation for extending the stability range of weak grids with voltage source converters," in *IET Generation, Transmission & Distribution*, vol. 10, no. 6, pp. 1315-1326, 21 4 2016.

[40] M. F. M. Arani and Y. A. I. Mohamed, "Voltage source converter connected to very weak grids under disturbances," *2017 IEEE Power & Energy Society Innovative Smart Grid Technologies Conference (ISGT)*, Washington, DC, 2017, pp. 1-5.

[41] K. Givaki, D. Chen and L. Xu, "Current Error Based Compensations for VSC Current Control in Weak Grids for Wind Farm Applications," in *IEEE Transactions on Sustainable Energy*, vol. 10, no. 1, pp. 26-35, Jan. 2019.